Mechanistic Investigation into *Saccharomyces cerevisiae* Ferulic Acid Decarboxylase, a Prenylated FMN-dependent Decarboxylase

by

April K. Kaneshiro

A dissertation submitted in partial fulfillment
of the requirements for the degree of
Doctorate of Philosophy
(Biological Chemistry)
in the University of Michigan
2023

Doctoral Committee:

        Professor E. Neil G. Marsh, Chair
        Assistant Professor Markos Koutmos
        Associate Professor Bruce A. Palfey
        Professor Stephen W. Ragsdale
        Associate Professor Raymond C. Trievel

April K. Kaneshiro

kaneshia@umich.edu

ORCID iD: 0000-0002-7560-9895

Dedication

This dissertation is dedicated to my parents Ken and Teresa, my brother Ian, and my spouse Joel. Thank you for all your love and support throughout this endeavor.

Acknowledgements

I would first like to thank my advisor Prof. E. Neil G. Marsh for his guidance and mentorship throughout my graduate studies. I have learned a tremendous amount from him, not just in terms of enzymology and experimental design and conduct but also in maintaining the bigger picture of my work and the purpose behind writing. Your guidance has helped me to become a better scientist. Thank you for being supportive and patient with me as I jumped from population genetics in bats to the protein sciences.

I would also like to thank my previous and current committee members, Prof. Markos Koutmos, Prof. Nina Lin, Prof. Bruce Palfey, Prof. Stephen Ragsdale, and Prof. Raymond Trievel, for all their feedback and advice on my thesis work. I also thank my collaborators, Dr. Chunyi Zhao, Prof. Brandon Ruotolo, Dr. Nick Miller, Prof. Roseanne Sension, Dr. Kazuhiro Yamada, Dr. Leena Mallik, Prof. Markos Koutmos, Prof. Bruce Palfey, and Prof. David Ballou, for their hard work and for teaching me about their areas of expertise.

I thank the past and present members of the Marsh lab, Dr. Kyle Ferguson, Dr. Nattapol Arunrattanamook, Dr. Marie Hoarau, Dr. Ajitha Cristie-David, Dr. Soumi Ghosh, Dr. Arti Dumbrepatil, Dr. Kelsey Diffley, Dr. Takunda Chazovachii, Dr. Hannah Chia, Dr. Ayesha Patel, Dr. Tim Grunkenmeyer, Dr. Karl Koebke, Prathamesh Datar, Srijoni Majhi, Victor Rivera-Santana, Katherine Hunter, and Daniel DiRocco, for all their support, advice, and wonderful discussions throughout the years. Thank you for all the knowledge and wisdom you've shared with me as well as all the wonderful times both in and outside of lab. I will miss our coffee breaks, breakroom snacks, and after-lab get-togethers. I also want to thank my Biochem friends,

Table of Contents

List of Tables

List of Figures

List of Abbreviations

ADH   Alcohol dehydrogenase

ATP   Adenosine triphosphate

CAR   Carboxylic acid reductase

CID   Collision-induced dissociation

DFT   Density functional theory

DMAP(P)   Dimethylallyl(pyro)phosphate

EDTA   Ethylenediaminetetraactetic acid

EPR   Electron paramagnetic resonance

FDC   Ferulic acid decarboxylase

FMN   Flavin mononucleotide

FNVB   2-Fluoro-2-nitro-vinylbenzene

GMP   Geranyl monophosphate

HFCD   Homo-oligomeric flavin-binding cysteine decarboxylase

HMF   Hydroxymethylfurfural

IM-MS   Ion mobility-mass spectrometry

IMP   Isopentenyl monophosphate

IPTG   Isopropyl-β-D-1-thiogalactopyranoside

KIE   Kinetic isotope effect

LC-MS   Liquid chromatography-mass spectrometry

LC-ESI-MS   Liquid chromatography-electrospray ionization-mass spectrometry

MS   Mass spectrometry

NADPH   Nicotinamide adenine dinucleotide phosphate

nESI   Nano-electrospray ionization

PAD1   Phenylacrylic acid decarboxylase

PAE   Phthalic acid esters

PAL   Phenylalanine ammonia lyase

PCA   Phenazine-1-carboxylic acid

PLP   Pyridoxal phosphate

prFMN   Prenylated flavin mononucleotide

Q-IM-ToF MS   Quadrupole-ion-mobility-time-of-flight mass spectrometer

SAXS   Small-angle X-ray scattering

SVD   Singular value decomposition

tPAD1   Truncated PAD1 (mitochondrial-targeting sequence removed)

TPP   Thiamine pyrophosphate

UPLC/ESI-Q-ToF-MS   Ultra performance liquid chromatography/electrospray ionization-

quadrupole-time-of-flight-mass spectrometry

Abstract

The UbiD family of decarboxylase enzymes uses a recently discovered, prenylated flavin mononucleotide (prFMN) as a cofactor. The best-studied UbiD enzyme is ferulic acid decarboxylase (FDC) from yeast. FDC catalyzes the reversible decarboxylation of phenylacrylic acids into their corresponding styrenes. Prior studies of FDC suggest that the mechanism involves an unprecedented 1,3-dipolar cycloaddition in which cycloadducts are formed between prFMN and substrate. Previous mechanistic studies have proposed that the rate-determining step of the reaction is cycloelimination of the styrene-prFMN cycloadduct instead of decarboxylation. However, prior to my studies, no substrate-prFMN adducts had been characterized and the pre-steady state kinetics of FDC had not been investigated.

This dissertation describes the characterization of the reaction catalyzed by FDC using a combination of U.V.-visible spectroscopy, native MS, and stopped-flow absorption spectroscopy. Native MS experiments established that the styrene-prFMN cycloadduct accumulates in FDC upon reaction with either phenylacrylic acid or styrene, providing additional support that the cycloelimination step is rate-limiting. To gain further insight into the formation and breakdown of reaction intermediates, the pre-steady state kinetics of FDC reacting with both phenylacrylate and styrene were investigated.

FDC exhibited surprisingly complex kinetic behavior. Reaction with either substrate resulted in loss of the prFMN iminium species monitored at 380 nm and the appearance of a broad peak at 460 nm, due to the styrene-prFMN cycloadduct. For the reaction of phenylacrylate, up to four kinetic phases could be discerned. The concentration-dependence of the amplitudes of

the slower phases were directly related to substrate concentration, whereas the faster phases were relatively unaffected. This kinetic behavior suggested a half-of-sites reactivity model, a form of negative cooperativity. Global analysis of these data supported a model in which one active site of the FDC homodimer reacts rapidly with phenylacrylate in a kinetically competent manner (i.e., faster than $k_{cat} = 11.3$ s^{-1}), whereas the second active site reacts too slowly to be kinetically competent.

However, a more extensive series of measurements using both phenylacrylate and styrene supports a different model. The reaction of styrene, which forms a dead-end complex, is described by three phases and is consistent with half-of-sites reactivity. For both substrates, the slower phases are no longer apparent when substrate:enzyme ratio is below 0.5, indicating one active site has a much higher affinity than the other. Although the data proved too complex to model quantitatively, they can be explained qualitatively by a "two-stroke" kinetic model in which negative cooperativity arises through catalytically relevant domain motions that have been recently proposed in the UbiD family.

In this model, the high-affinity active site binds phenylacrylate and catalyzes decarboxylation to form the styrene-prFMN cycloadduct. Next, the low-affinity active site binds phenylacrylate, resulting in a conformational change that switches the affinities of the active sites. This conversion allows the energetically favorable cycloaddition and decarboxylation of phenylacrylate in the second site to be coupled to the rate-limiting cycloelimination step that releases styrene in the first site. The model is supported by the observation that the low-affinity site reacts with phenylacrylate with an observed rate constant, $k_{obs} \sim 8$ s^{-1}, similar to k_{cat}.

While additional experiments are necessary to fully understand the kinetics of FDC and determine the how it performs catalysis, this dissertation describes the first pre-steady state

kinetic investigations into a prFMN-dependent enzyme and provides a template for future kinetic

studies.

Chapter 1 Introduction

The fungal enzyme ferulic acid decarboxylase (FDC) has emerged as an enzyme of interest for both industry and the flavin enzymology field. FDC catalyzes the reversible decarboxylation of antimicrobial phenylacrylic acids as a detoxification pathway in yeast, producing the corresponding styrene products. FDC belongs to the UbiD family, which is named after its first member: UbiD, a bacterial decarboxylase involved in ubiquinone biosynthesis.[1] Members of the UbiD family have been found in all three domains of the microbial world[2] and catalyze the decarboxylation of various α,β-unsaturated carboxylic acids, many of which are otherwise chemically unreactive. In this chapter, I will discuss the history of the UbiX/UbiD system; the discovery of a new flavin cofactor utilized by the UbiD family; the structure of FDC and how the enzyme performs its reaction; the biosynthesis and maturation of the cofactor; and the current understanding of the UbiD family.

1.1 The PAD1/FDC and UbiX/UbiD System

UbiD is named for its role in the bacterial ubiquinone biosynthesis pathway in which it catalyzes the decarboxylation of 4-hydroxy-3-octaprenylbenzoate to 2-octaprenylphenol.[1, 3] However, at the time of UbiD's discovery, it was believed that bacteria possessed a separate but isofunctional decarboxylase. This was due to *ΔubiD* strains producing ~20% of the normal level of ubiquinone, suggesting that another decarboxylase was present.[1] However, these strains did have a buildup of 4-hydroxy-3-octaprenylbenzoate and no decarboxylase activity could be detected in *ΔubiD* cell extracts. UbiX, another enzyme implicated in ubiquinone biosynthesis, was initially considered to be this redundant enzyme.[4, 5]

Genetic studies of the genes *ubiX* and *ubiD* revealed that there are over 100 homologues of both genes distributed throughout all three domains of the microbial world.[2] In some organisms, these homologous genes were implicated as putative decarboxylases of various hydroxybenzoate compounds. Interestingly, in a few microbes, a small third gene was present in the gene cluster containing the *ubiX* and *ubiD* homologues and this gene appeared to be necessary for decarboxylase activity.

The yeast homologue of UbiX is phenylacrylic acid decarboxylase (PAD1), which exhibits 50% amino acid sequence identity. The *PAD1* gene was found to confer resistance to the food preservative cinnamic acid, although the gene product was not tested for decarboxylase activity *in vitro*.[6] In addition, due to the sequence homology of PAD1 and UbiX, PAD1 was thought to be involved in ubiquinone biosynthesis in yeast. However, we now know that yeast diverge from bacteria at the decarboxylation step. Specifically, while in bacteria 4-hydroxy-3-polyprenylbenzoate is decarboxylated, in yeast this intermediate undergoes further ring modifications before being decarboxylated by an unrelated enzyme.[4] Nevertheless, there was evidence that UbiX and PAD1 performed a similar reaction. In one study, a *ΔubiX Escherichia coli* strain was rescued by the expression of PAD1.[7] Specifically, the *ΔubiX* strains had low ubiquinone levels and accumulated 4-hydroxy-3-octaprenylbenzoate. Expression of UbiX in this strain restored ubiquinone levels and significantly reduced the level of 4-hydroxy-3-octaprenylbenzoate. Similarly, expression of PAD1 in the *ΔubiX* strain resulted in the strain producing 67% of the normal levels of ubiquinone, although there was still an accumulation of 4-hydroxy-3-octaprenylbenzoate, suggesting PAD1 was not as efficient as UbiX itself.

FDC, the yeast homologue of UbiD (25% amino acid sequence identity), was determined to decarboxylate ferulic acid.[8] Sake yeast, which lack the ability to decarboxylate ferulic acid,

gained this ability when *FDC1* from a wine yeast was introduced. The *FDC1* and *PAD1* genes are located in close proximity to each other on chromosome 4 of *Saccharomyces cerevisiae*. This fact, coupled with the sequence similarities of PAD1 and FDC to UbiX and UbiD respectively, led to the belief that PAD1 and FDC were isofunctional decarboxylases. However, a genetic knockout study provided strong evidence that this assumption was wrong.[8] Three yeast strains were produced: *ΔFDC1* which lacked FDC, *ΔPAD1* which lacked PAD1, and *ΔPAD1ΔFDC1* which lacked both enzymes. While the wild-type strain decarboxylated phenylacrylic acids, none of the three knockout strains possessed decarboxylase activity *in vivo* or in cell-free extracts. Importantly, decarboxylase activity was observed when the cell-free extracts of *ΔPAD1* and *ΔFDC1* were combined. Taken together, these data demonstrated that neither enzyme alone could perform decarboxylation and that PAD1 and FDC together were needed for this activity.

1.2 Early Crystal Structures of UbiX and UbiD Family Members

To determine the roles of PAD1 and FDC, the enzymes needed to be studied *in vitro* but attempts to purify active enzymes were often unsuccessful. However, X-ray crystallography provided important insights into the UbiX and UbiD families.

The first UbiX family member to be crystallized was Pad1 from the enterohemorrhagic *E. coli* strain O157:H7.[9] This *E. coli* strain possesses UbiX as well as a paralog named Pad1 (EcPad1) which is more than 52% identical to *E. coli* UbiX (EcUbiX) and *S. cerevisiae* PAD1. Purified EcPad1 was yellow in color and had an absorbance spectrum with maxima at 382 nm and 460 nm, suggesting the presence of a flavin. However, purified EcPad1 as well as crude *E. coli* lysates containing EcPad1 did not possess decarboxylase activity against any of the tested phenylacrylic acids. The crystal structure of EcPad1 revealed that EcPad1 was a dodecameric protein and this was supported by dynamic light scattering measurements. Each EcPad1

monomer was ~23 kDa and possessed a Rossmann fold, commonly found in flavin-binding proteins. Additionally, there was clear electron density that matched well with flavin mononucleotide (FMN). Each FMN molecule was located in a tunnel at the interface between two monomers and was partially solvent-exposed. The overall structure of EcPad1 matches well with the structures of two members of the homo-oligomeric flavin-binding cysteine decarboxylase (HFCD) family: EpiD from *Staphylococcus epidermidis*[10] and MrsD from *Bacillus sp.*[11] All three enzymes exist as dodecamers although the basic unit of EcPad1 is dimeric whereas the basic unit for both EpiD and MrsD is trimeric. In addition, despite the low amino acid sequence homology of the three enzymes, their monomeric structures are remarkably similar. Nevertheless, the location of the flavin-binding pockets does differ between EcPad1 and the HFCD members. In EcPad1, the FMN molecules are located on the solvent-exposed faces of the protein, whereas the flavins in EpiD and MrsD are located near the center of the dodecamer and are accessible through a large tunnel. Together, these data indicated that while EcPad1 has similarities to the HFCD family, EcPad1 is likely part of a separate family.

The second crystal structure of a UbiX family member was of PA4019, the UbiX homologue in *Pseudomonas aeruginosa* (PaUbiX).[12] PaUbiX shared many characteristics with EcPad1. Purified PaUbiX was yellow and had absorption maxima at 380 nm and 460 nm, indicating the enzyme bound flavin. PaUbiX is a dodecamer composed of 25 kDa monomers, each of which possessed a Rossmann fold. In addition, FMN molecules were located in hydrophilic pockets created by the interactions of two neighboring monomers. However, these FMN molecules were occluded from solvent. Interestingly, there was a notable hydrophilic cavity located above the isoalloxazine ring where a substrate could bind. This cavity was formed through interactions between side chains from three adjacent monomers and was also closed off

from solvent. It was thus proposed that conformational changes of these side chains would be necessary for substrates to enter the cavity. The presence of a sulfate ion in this cavity suggested that these motions were possible. Interestingly, loss of FMN did not greatly alter the structure of PaUbiX on either the monomeric or dodecameric level. As previously found with EcPad1, the structure of PaUbiX was similar to members of the HFCD family including EpiD and MrsD, even though there is little amino acid sequence identity. Conversely, PaUbiX and EcPad1 are 40% identical in sequence. Unfortunately, decarboxylase activity against phenylacrylic acids was not detected for PaUbiX. This lack of decarboxylase activity for purified UbiX family members provided additional support to the emerging hypothesis that decarboxylation required both a UbiX family member and a UbiD family member.[7, 8]

In 2015, the first crystal structure of *S. cerevisiae* FDC was solved by Bhuiya and coworkers.[13] Although not noted at the time of publication, this crystal structure was of apo-FDC; nevertheless, this structure did provide valuable insights into FDC. The crystal structure revealed that FDC is a dimer (Figure 1.3A). Each FDC monomer was comprised of an N-terminal domain and a C-terminal domain which contained a flexible loop that ended in a final α helix. FDC dimerized through interactions mostly between the C-terminal domains of the two monomers, resulting in a "U-shaped" dimer with the N-terminal domains at the ends of the "U". The structure of FDC was compared with two published UbiD-like proteins: PA0254 (HudA) from *P. aeruginosa*[14] and UbiD from *E. coli* (EcUbiD, PDB entry 4IDB)[13]. FDC shares 39% sequence identity with HudA and 25% with UbiD. Interestingly, while the monomers of all three enzymes share a similar structure, FDC and HudA both form dimers and EcUbiD is a hexamer. Additionally, the FDC crystal structure possessed electron density in both monomers that matched well with 4-vinylphenol. Since 4-hydroxyphenylacrylic acid was present in the

crystallization solution, it was proposed that FDC had decarboxylated this molecule before crystallization had occurred. 4-vinylphenol was located in a large hydrophobic pocket in the N-terminal domain which suggested that this pocket was the enzyme's active site. The active site residue E285 was proposed to be involved in catalysis due to its position near the 4-vinylphenol molecule and the fact that purified WT FDC possessed decarboxylase activity against 4-hydroxyphenylacrylic acid and 4-hydroxy-3-methoxy-phenylacrylic acid while the E285A variant was inactive. Importantly, this glutamic acid residue is conserved in HudA and is substituted for an aspartic acid in EcUbiD, suggesting an important role for an acidic residue in catalysis. The authors also noted that R175, conserved among all three proteins, positioned E285 in the active site.

1.3 The Discovery of the Prenylated FMN Cofactor

In 2015, the relationship between PAD1 and FDC was finally elucidated. Lin and coworkers successfully purified holo-FDC after recombinant expression in *E. coli* BL21 which contains an endogenous UbiX enzyme (EcUbiX).[15] Importantly, the authors observed that dialyzing purified FDC resulted in loss of activity, even when using a 3.5 kDa membrane cutoff. This suggested that FDC required a dialyzable cofactor. In addition, this cofactor would be lost in the presence of EDTA. Decarboxylase activity could be restored to dialyzed FDC through incubation with cell-free extracts from *E. coli* BL21. In contrast, FDC purified from a BL21 strain that lacked EcUbiX (*ΔubiX* BL21 strain) was inactive and incubation of dialyzed FDC with the cell-free extracts of this strain did not confer activity. However, FDC purified from the *ΔubiX* BL21 strain could be activated using lysates of wild-type *E. coli* BL21 as well as by *ΔubiX* BL21 strain lysates containing purified PAD1. Interestingly, FDC could be activated without direct interactions with PAD1 or EcUbiX, indicating that FDC bound its cofactor

without additional help. Surprisingly, incubating dialyzed FDC with a variety of known cofactors, including flavins, did not restore activity. Altogether, these data confirmed that UbiX and PAD1 performed the same reaction and that this reaction likely generated a small, uncommon cofactor needed by FDC.

Agreeing with previous studies on UbiX family members[9, 12], purified truncated PAD1 (tPAD1; lacking the first 58 residues which encode a mitochondrial-targeting sequence) was yellow in color and possessed an absorption spectrum with maxima at 384 nm and 458 nm. However, it was noted that the absorption peak at 384 nm was more intense than the 458 nm peak, which is contrary to typical oxidized FMN spectra. The identity of the flavin was confirmed to be FMN through liquid chromatography electrospray ionization mass spectrometry (LC-ESI-MS).

Finally, holo-FDC was produced by co-expressing FDC and tPAD1 in *E. coli* BL21. The holoenzyme had a pale yellow color as well as an ~8-fold increase in specific activity compared to singly-expressed FDC. Surprisingly, the absorption spectrum of holo-FDC displayed a single maximum at 342 nm, which matches better with the spectra of reduced flavins. However, FDC did not require anaerobic conditions for stability or activity. Attempts to identify the cofactor were ultimately unsuccessful. Nevertheless, LC-MS of base-treated holo-FDC did detect a peak at $(m+H^+)/z = 457.1$ which corresponds to FMN. This along with the previous data suggested that the cofactor was a form of modified FMN produced by PAD1/UbiX.

Shortly afterwards, the identity of the cofactor was determined. Crystal structures of holo-FDC from *Aspergillus niger* (AnFDC), *S. cerevisiae*, and *Candida dublinienis* (CdFDC) were solved.[16] All three enzymes were co-expressed with overexpressed EcUbiX as the authors had also observed distinct differences in singly-expressed FDC compared to FDC co-expressed

with EcUbiX. All three enzyme species possessed electron density for a highly modified FMN

cofactor. The electron density revealed the isoalloxazine moiety had modifications at both the N5

and C6 positions. Due to the high resolution achieved for AnFDC, the modification could be

further determined to be an addition of an isopentyl group that spanned the N5 and C6 positions

resulting in a fourth 6-membered ring (Figure 1.1). Thus, this modified FMN cofactor was

named prenylated FMN (prFMN). The production of prFMN by PaUbiX was described in an

accompanying paper by the same group[17] and will be discussed later in this chapter.
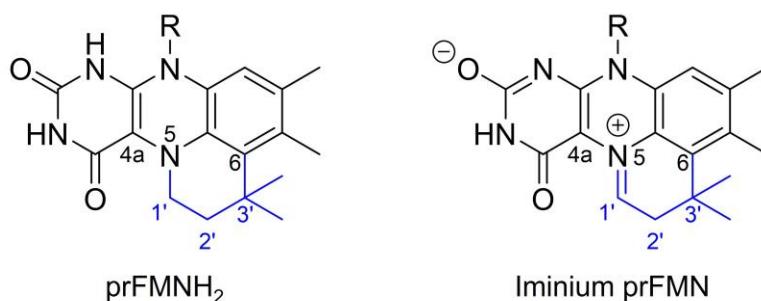
Figure 1.1: Structures of reduced prFMN (prFMNH₂) and the active iminium prFMN species.

Based on high-resolution mass spectrometry, the catalytically relevant species of the

prFMN cofactor was determined to be an oxidized state referred to as the iminium species

(Figure 1.1). This oxidized state was further supported by the inactivation of holo-FDC with the

reducing agent sodium cyanoborohydride. Holo-FDC possessed a single absorption maximum at

~380 nm (Figure 1.3C).
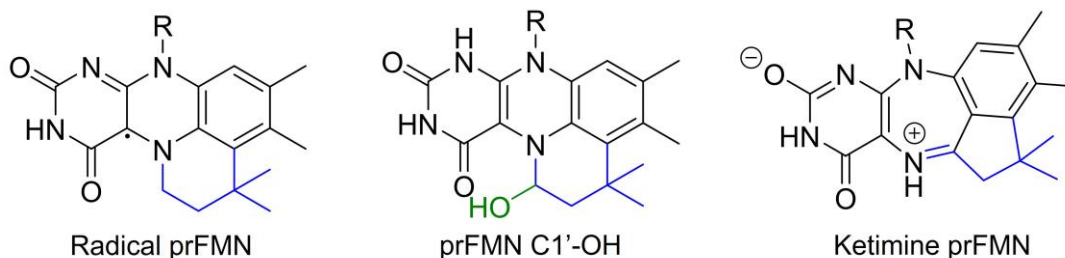
Figure 1.2: Structures of radical prFMN, prFMN C1'-OH, and ketimine prFMN.

Three additional species of prFMN were observed in this study. Reduced holo-FDC that was re-oxidized in air turned purple in color but remained inactive. The species of prFMN was determined to be a radical species through electron paramagnetic resonance (EPR) and its absorption spectrum possessed a peak at ~550 nm (Figure 1.2). Another species was observed in older AnFDC crystals in which the prFMN had been hydroxylated at the C1' position (prFMN C1'-OH, see Figure 1.2). This species was likely produced through hydrolysis of the N5=C1' bond. The final species was markedly different in structure from the other observed prFMN species. Named the ketimine species, the prenyl C1' had been incorporated into the central ring of the isoalloxazine structure resulting in a seven-membered central ring with the N5 existing as a secondary ketimine (Figure 1.2). However, neither the prFMN C1'-OH species nor the ketimine prFMN species was observed in crystal structures of FDC from *S. cerevisiae* or *C. dubliniensis*, indicating that these species were not catalytically relevant.

1.4 Structure of FDC

The detailed crystal structures of holo-FDC from three different fungi allowed for important structural insights into the enzyme. The FDC monomer can be divided into three sections: an N-terminal prFMN-binding domain, an oligomerization domain, and a C-terminal α-helical region (Figure 1.3B).[16, 18] We now know that this general structure of the monomer is highly conserved within the UbiD family and is often referred to as the UbiD-like fold.[18] All three species of holo-FDC form a dimer through interactions between the oligomerization domains as well as interactions between one monomer's C-terminal helical region and the neighboring subunit's prFMN-binding domain (Figure 1.3A).

The active site is formed at the interface of the prFMN-binding domain and the oligomerization domain. The prFMN-binding domain also contains the sequence motif

$RX_nEX_4(E/D)$. This motif is highly conserved throughout the UbiD family and in FDC, is necessary for catalysis and proper oxidative maturation of the prFMN cofactor.[19] The arginine (R175 in *S. cerevisiae* FDC) and first glutamic acid (E277) form a conserved salt bridge interaction and R175 is implicated in prFMN maturation. The second, catalytic glutamic acid (E285) has been found to adopt a variety of conformations in crystal structures. Many of these conformations interact with R175, suggesting that R175 may assist in positioning E285. Similarly, R175 and the backbone of E285 appear to position the substrate carboxyl group directly above the prFMN C1' through hydrogen bond interactions, allowing for catalysis to occur.
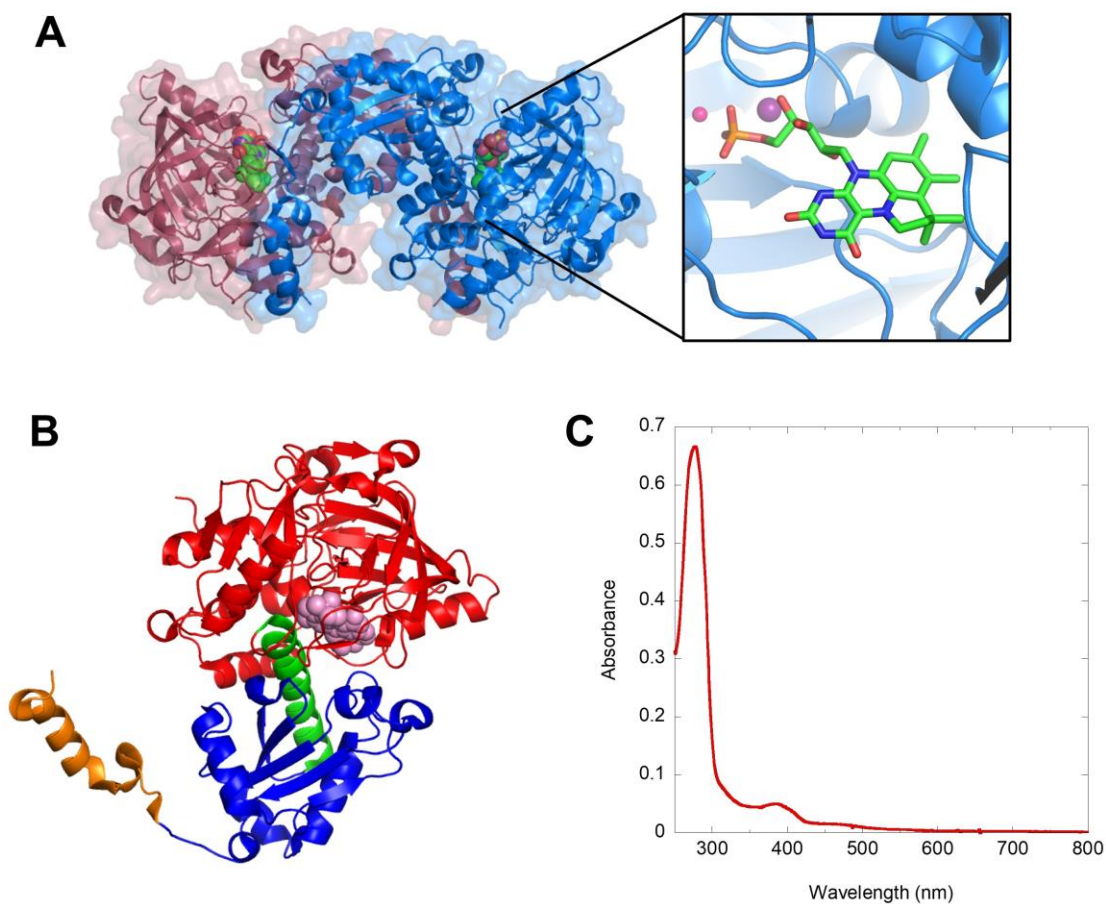
Figure 1.3: Structure and U.V.-visible spectrum of *S. cerevisiae* holo-FDC. A) Holo-FDC dimer (PDB: 4ZAC). The active site of FDC is shown in the outlined box, showing the prFMN as well as the Mn^{2+} and K^+ ions displayed in pink and purple respectively. FDC is in the "closed" conformation. **B)** Domain organization of FDC. prFMN-

binding domain is shown in red, oligomerization domain is shown in blue, and C-terminal helical region is shown in orange. The α-helix that links the prFMN-binding domain to the oligomerization domain is shown in green. The prFMN cofactor is shown in pink spheres. **C)** Representative spectrum of 12 μM holo-FDC. The absorbance peak at 380 nm represents bound iminium prFMN cofactor.

The prFMN cofactor is bound in the active site through coordination of its phosphate group to a Mn^{2+} ion and a K^+ ion (Figure 1.3A). These ions were identified through their electron density in crystal structures and by EPR spectroscopy for Mn^{2+}.[16] This metal-binding potential had been previously suggested for both EcUbiD[3] and HudA.[14] In particular, for EcUbiD, the authors determined that both Mn^{2+} and an unidentified, heat-stable cofactor were needed for decarboxylase activity.[3] Currently, most UbiD family members that have been studied utilize Mn^{2+} and K^+ ions as counter-ions for the phosphate group of prFMN,[18] although a few enzymes have been found to use Fe^{2+} or Na^+.[20-22]

Recently, the α-helix that connects the prFMN-binding domain to the oligomerization domain (see Figure 1.3**Error! Reference source not found.**B) has been proposed to perform a hinge motion, allowing for significant domain motion to occur. FDC crystal structures show FDC in a "closed" conformation (in which the prFMN-binding domain and oligomerization domain are close together),[16] while other UbiD family members consistently adopt an "open" conformation (in which the prFMN-binding domain and oligomerization domain are further apart).[21-23] Transitioning between these two conformations has been observed in the three most recently characterized UbiD enzymes.[24-26] Furthermore, in vanillic acid decarboxylase (VdcC), the domain motion is suggested to be involved in catalysis.[25] Interestingly, native MS of FDC had previously suggested that the enzyme undergoes conformational changes upon cofactor binding,[27] providing additional evidence that the hinge motion is feasible for FDC.

1.5 Mechanism of prFMN-mediated Decarboxylation by FDC

Crystal structures of FDC complexed with variously substituted phenylacrylic acid substrates revealed that substrates were positioned similarly in the active site.[16] The substrate aryl groups were stacked directly above the isoalloxazine ring system with the substrate $C\alpha=C\beta$ double bond located directly above the prFMN C1' and C4a respectively. This positioning suggested the formation of a transient substrate-prFMN bond.

The crystal structure of FDC incubated with the reversible inhibitor phenylpyruvate allowed the first prFMN-inhibitor adduct to be characterized and hinted at how catalysis occurred. Phenylpyruvate can tautomerize into α-hydroxyphenylacrylic acid which is a substrate of FDC (Figure 1.4A). The resulting inhibitor-prFMN adduct was composed of a single covalent bond between the iminium prFMN C1' and the decarboxylated phenylacetaldehyde $C\alpha$ (Figure 1.4B). It is important to note that the iminium prFMN species possesses an azomethine ylide character, a known 1,3-dipole. Further, α,β-unsaturated carboxylic acids are well-known dipolarophiles. This suggested that 1,3-dipolar cycloaddition chemistry was feasible for FDC. Interestingly, while 1,3-dipolar cycloadditions are common in organic synthesis, this chemistry had never been documented in an enzyme before.[28]
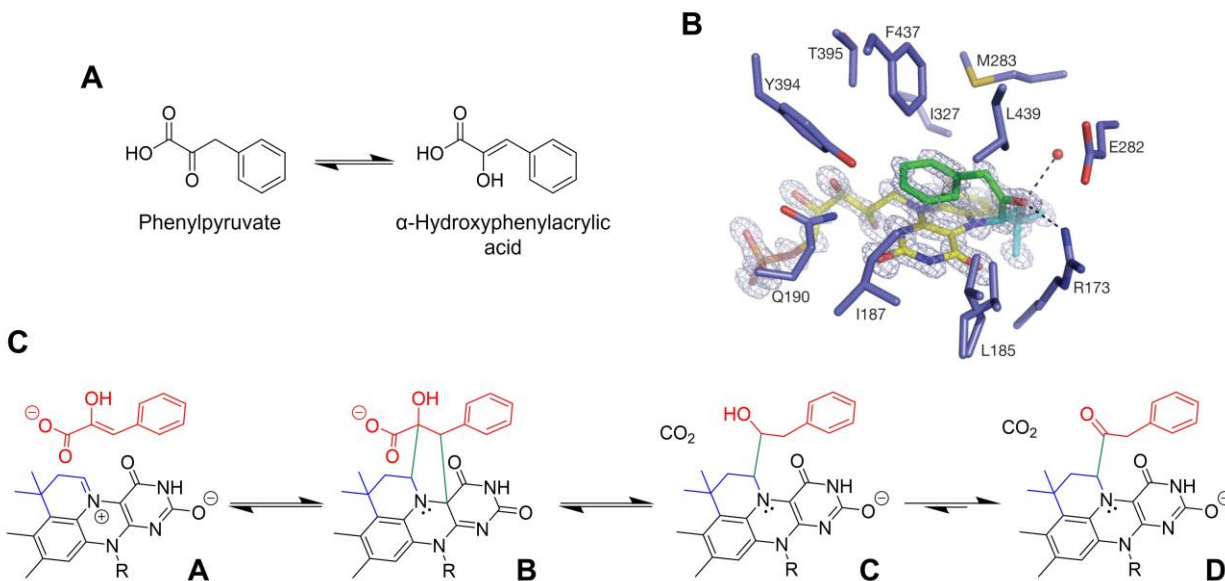
Figure 1.4: Phenylpyruvate-prFMN adduct in FDC. A) Phenylpyruvate tautomerizes into α-hydroxyphenylacrylic acid. **B)** Crystal structure of AnFDC incubated with phenylpyruvate. Electron density shows a single covalent bond between prFMN C1' and decarboxylated phenylacetaldehyde Cα. Figure from Payne *et al.*, *Nature*, 2015. **C)** Proposed mechanism for phenylpyruvate inhibition, in which species **D** is the observed inhibitor-prFMN adduct.

From these data, it was proposed that a 1,3-dipolar cycloaddition occurs between the iminium prFMN and the phenylacrylic acid substrate (Figure 1.5**B**), forming a pyrrolidine cycloadduct (Figure 1.5**C**). As suggested by the phenylpyruvate-prFMN adduct, decarboxylation through a Grob-type fragmentation occurs concomitant with ring opening through the cleavage of the C4a-Cβ bond. In this step, the prFMN acts as an electron sink, similar to other known decarboxylase cofactors such as pyridoxal phosphate (PLP) and thiamine pyrophosphate (TPP).[29] The resulting adduct possesses a single covalent bond between the C1' and Cα (Figure 1.5**D**), which is supported by the phenylpyruvate-FDC crystal structure and will here be referred to as the single-tethered adduct. Proton transfer from the conserved active site glutamic acid (E285 in *S. cerevisiae* FDC) is coupled to the formation of a second pyrrolidine cycloadduct (Figure 1.5**E**). Finally, the styrene product is formed through a cycloelimination step which also regenerates the iminium prFMN and completes the catalytic cycle (Figure 1.5**F**).
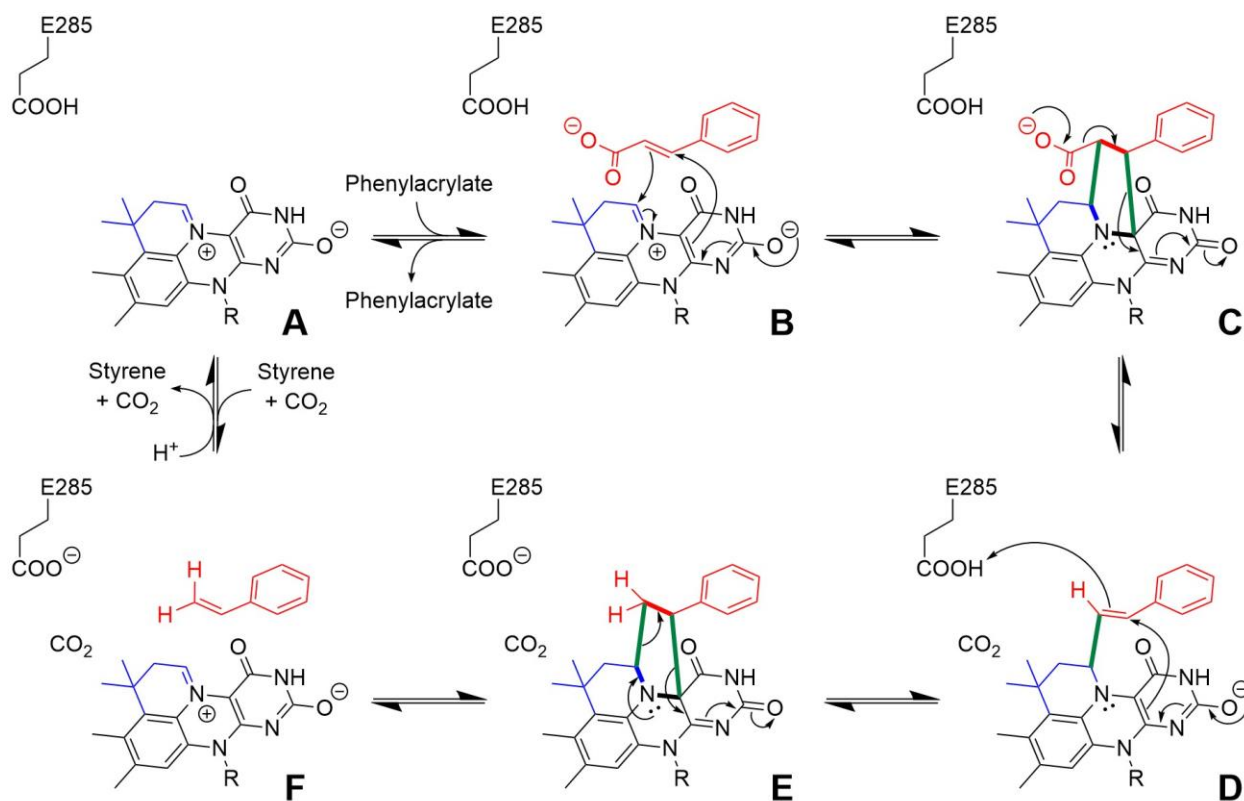
Figure 1.5: Proposed 1,3-dipolar cycloaddition mechanism for FDC. The iminium species of prFMN (species **A**) performs a 1,3-dipolar cycloaddition on the phenylacrylate substrate (intermediate **B**) resulting in a cycloadduct (intermediate **C**). Decarboxylation then occurs coupled to the cleavage of the C4a-Cβ bond, forming a single-tethered adduct (intermediate **D**). A proton is abstracted from a conserved active site glutamic acid as a second cycloadduct is formed (intermediate **E**). Finally, a cycloelimination reaction is performed, freeing the product styrene and re-generating the iminium species of prFMN (species **F**).

Subsequent studies into the mechanism of FDC provided further support for the unprecedented 1,3-dipolar cycloaddition mechanism. One study performed by Ferguson and coworkers investigated the rate-determining step of the FDC reaction.[30] Taking advantage of FDC's substrate promiscuity, a Hammett analysis was performed to probe the rate-limiting step. The catalytic efficiency of FDC did not correlate well to the Hammett parameter σ but had a strong linear correlation with the Hammett parameter σ⁻, which indicated that the rate-determining step was a chemical step instead of substrate binding or product release. Interestingly, the slope of the Hammett plot (ρ) was negative with substrates containing electron-donating groups reacting faster than substrates with electron-withdrawing groups. Typically,

decarboxylation is the rate-limiting step for decarboxylases due to the buildup of negative charge on the α carbon, resulting in a high-energy transition state. As a result, decarboxylases usually have a positive slope since electron-withdrawing groups can assist in stabilizing the negative charge built up. However, this data indicated that the rate-limiting step for the FDC reaction was not decarboxylation. Further, solvent isotope experiments revealed that protonation occurred before the rate-limiting step. Secondary deuterium kinetic isotope experiments found that both the α and β carbons experienced normal 2° KIEs (indicating a hybridization change from tetrahedral to planar) when both carbons were deuterated independent of the solvent being H_2O or D_2O. Additionally, it was determined that CO_2 did not dissociate until after protonation occurred. Taken all together, these data indicated the cycloelimination step was rate-limiting for the FDC reaction.

Computational analyses similarly found that 1,3-dipolar cycloaddition chemistry was feasible for FDC.[31] Moreover, a mechanism-based inhibitor, 2-fluoro-2-nitro-vinylbenzene (FNVB), allowed for the first prFMN cycloadduct to be characterized by native MS.[32] Since FNVB cannot undergo decarboxylation, FDC could only react with FNVB until this step, thus producing an adduct similar to the carboxylated substrate-prFMN cycloadduct (Figure 1.5**C**). The U.V.-visible spectrum of the FNVB-prFMN cycloadduct possessed a single peak at ~425 nm. This spectrum matches well with the spectra of known C4a,N5-dialkyl flavins which have an absorbance peak at ~400 nm,[33] providing additional support of the 1,3-dipolar cycloaddition mechanism. In contrast, N5-alkyl flavins have absorbance peaks at 350 nm and 550 nm.[34] Furthermore, native MS confirmed the identity of the FNVB-prFMN cycloadduct complexed with a K^+ ion, which had a mass of 730.167 amu.[32]

Most recently, in 2019, a series of high resolution crystal structures of AnFDC complexed with both inhibitors and substrates was published.[35] The authors were able to obtain structures of the single-tethered adduct (Figure 1.5**D**) and the styrene-prFMN cycloadduct (Figure 1.5**E**) produced from reaction with phenylacrylic acid. Specifically, the single-tethered adduct was obtained by substituting the catalytic glutamic acid with a glutamine, while the styrene-prFMN cycloadduct was observed in 30% of WT AnFDC crystals complexed with phenylacrylic acid. Using mostly alkyne-based substrate analogues, the structures of all three expected reaction intermediates (Figure 1.5**C-E**) were observed. Interestingly, comparison of the substrate-prFMN adducts with the respective inhibitor-prFMN adducts showed they were notably more strained. For example, the styrene-prFMN cycloadduct produced from phenylacrylic acid revealed the FDC active site provided little room for the rehybridization of Cα, Cβ, C1', and C4a from planar to tetrahedral, resulting in significant deviations from ideal bond angles. In contrast, the respective cycloadduct produced from the inhibitor 2-butenoic acid (which lacks an aryl ring) adopted a more ideal conformation for its pyrrolidine ring, resulting in less strain. However, this conformation is not feasible for the styrene-prFMN cycloadduct due to steric clashes between its aryl group and the active site.

From these crystal structures, the authors noted that the active site architecture appears to favor the substrate/product complexes rather than any reaction intermediate. Throughout the reaction, the enzyme did not allow the substrate aryl ring nor the carboxyl group to change positions much from their original positions in the enzyme-substrate complex. This resulted in considerable strain being placed on the reaction intermediates due to deviations from ideal bond angles and lengths. And this strain is proposed to facilitate the quick reaction progression observed in FDC.

1.6 Biosynthesis of the prFMN Cofactor

1.6.1 The Flavin Prenyltransferase UbiX

The UbiX family is responsible for producing the modified prFMN cofactor.[15-17] This is accomplished through the prenylation of $FMNH_2$ using either the common isoprenoid precursor DMAPP or the less common DMAP (Figure 1.6B).[17, 36-38] UbiX enzymes have specificity for either DMAP or DMAPP and are usually not able to use both. Moreover, reduced FMN as well as a dimethylallyl moiety in the prenyl donor are required for this reaction. This has been demonstrated by the lack of flavin prenylation observed in PaUbiX when oxidized FMN or DMAP analogues (including isopentenyl monophosphate, IMP) were used.[38] Further, geranyl monophosphate (GMP) was found to be a substrate for a PaUbiX variant in which the active site had been extended to accommodate larger substrates. The crystal structure of PaUbiX complexed with oxidized FMN and DMAP revealed that DMAP is located directly above the isoalloxazine ring system (Figure 1.6A).[17] A π-cage is formed by the flavin and aromatic active site residues (W84, Y169, and W200) around the dimethylallyl moiety, similar to other prenyltransferases and terpene synthases. The phosphate moiety of DMAP is positioned by several conserved cationic and polar residues.
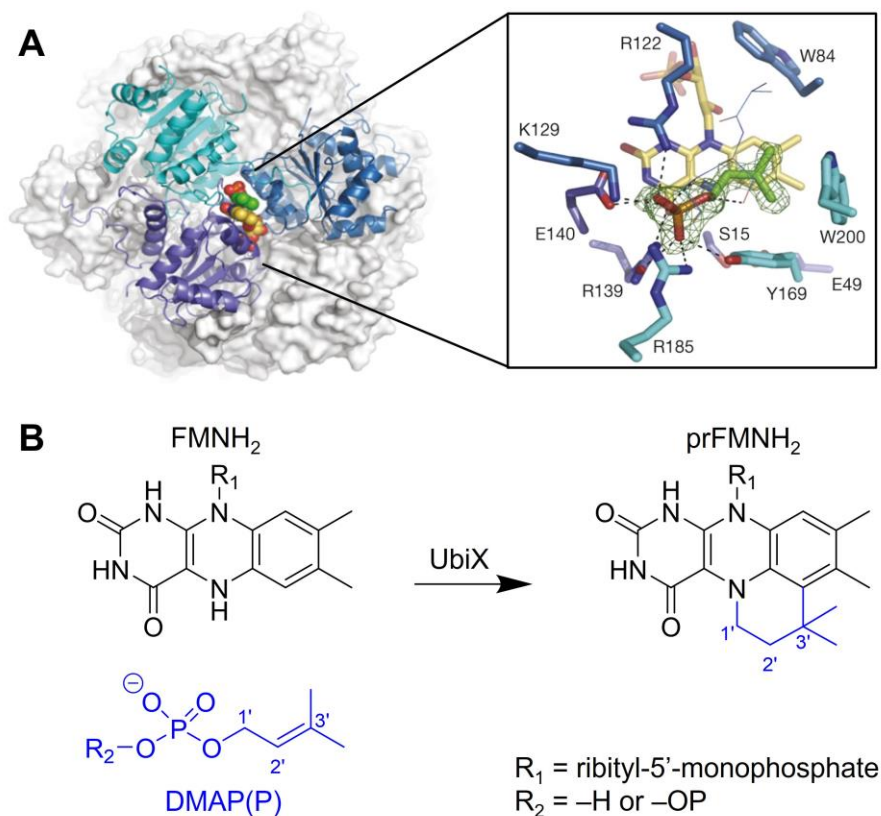
Figure 1.6: Structure and reaction of PaUbiX. A) Dodecameric structure of PaUbiX. The active site is located at the interface of the three monomers shown in cartoon (colored cyan, blue, and purple). FMN is displayed in yellow spheres and DMAP is shown in green spheres. A close-up of the active site is shown in the outlined box. Figure adapted from White *et al.*, *Nature*, 2015. **B)** Reaction catalyzed by UbiX. $FMNH_2$ is prenylated by UbiX using either DMAP or DMAPP depending on the species of UbiX.

Kinetic crystallographic studies on PaUbiX revealed that the formation of $prFMNH_2$ occurs in two steps: first the bond between the N5 of $FMNH_2$ and the C1' of DMAP forms and then the C6-C3' bond is formed (Figure 1.7).[17] The formation of the N5-C1' bond is thought to occur through an S_N1 mechanism in which a conserved active site glutamic acid (E140, PaUbiX numbering) protonates the α-phosphate of DMAP(P) to create the (pyro)phosphate leaving group.[38] The resulting allylic carbocation is likely stabilized by the π-cage in the active site. N5 prenylation then occurs along with N5 deprotonation by S15 and E49. Afterwards, formation of the C6-C3' bond occurs. Isomerization of the C2'-C3' bond is proposed to occur through acid/base catalysis by the retained (pyro)phosphate leaving group, generating a transient tertiary

carbocation. This allows for Friedel-Crafts alkylation of C6, forming the C6-C3' bond and thus the fourth ring of prFMN. Formation of the C6-C3' bond is proposed to occur with deprotonation of C6 by another conserved active site glutamic acid (E49). The role of the (pyro)phosphate leaving group was further supported by the observation that prFMNH$_2$ was produced upon addition of phosphate to DMAPP-specific UbiX enzymes that were stalled at the N5-prenylation adduct due to being given only DMAP. Thus, the retention of the (pyro)phosphate leaving group is essential for the second step of the UbiX reaction.
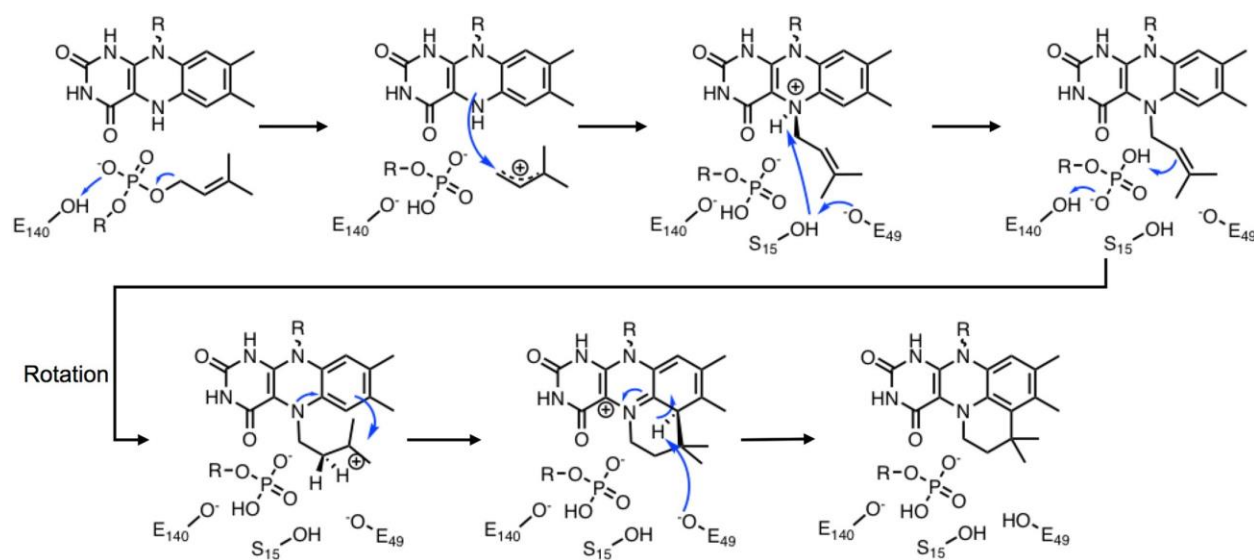
Figure 1.7: Proposed UbiX mechanism. E140 protonates the phosphate of DMAP(P), creating a (pyro)phosphate leaving group and an allyic carbocation. N5-C1' bond formation occurs via an S$_N$1 mechanism followed by deprotonation of N5 by S15 and E49. Retained (pyro)phosphate leaving group performs acid/base catalysis, allowing for rotation of the C2'-C3' bond and generation of a tertiary carbocation. C6-C3' bond formation occurs via Friedel-Crafts alkylation, followed by deprotonation of C6 by E49 yielding prFMNH$_2$. Figure from Bloor *et al.*, *Febs Journal*, 2022.

The preference of DMAP or DMAPP is dependent on the individual UbiX family member. For example, PaUbiX can only use DMAP as a substrate.[17, 38] Conversely, PAD1 (*S. cerevisiae* UbiX),[37] *A. niger* UbiX (AnUbiX),[38] and UbiX from *E. coli* K12 (EcUbiX)[38] all require DMAPP. Yet, UbiX from *E. coli* O157:H7 (O157UbiX) can utilize either form although its prFMN yield is slightly higher with DMAPP.[38] A study analyzing the architecture of UbiX enzyme active sites helped to elucidate these preferences.[38] The crystal structures of PaUbiX,

AnUbiX, and O157UbiX were compared and revealed that the overall active site is highly conserved. However, in PaUbiX, a phenylalanine residue (F181) is present where the β-phosphate of DMAPP would be positioned, suggesting that PaUbiX would be unable to bind DMAPP due to steric clashes. In contrast, AnUbiX possesses a glutamine residue at this position (Q203, AnUbiX numbering) and O157UbiX has a histidine (H164, O157UbiX numbering) both of which are proposed to form a hydrogen bond with the β-phosphate of DMAPP, thus allowing for DMAPP binding. Nevertheless, the residue at this position is not the sole determinant of DMAP(P) binding since both F181Q PaUbiX and F181H PaUbiX variants retained DMAP specificity. Another contributing factor appears to be how well the active site can retain the (pyro)phosphate leaving group during catalysis. As mentioned earlier, the (pyro)phosphate leaving group is required for the C6-C3' bond formation. Notably, when the DMAPP-specific EcUbiX was reacted with DMAP, the enzyme stalled after N5-prenylation. A similar stalling occurred with the F181Q PaUbiX variant (which mimics the active site of DMAPP-specific AnUbiX), although this variant was still DMAP-specific. In both cases, the addition of phosphate allowed for prFMNH$_2$ production. While this reveals that the pyrophosphate molecule itself is not necessary for catalysis, it does indicate that the active sites of DMAPP-specific UbiX enzymes are unable to retain the single phosphate from DMAP.

1.6.2 Oxidative Maturation of prFMN Cofactor

UbiX produces prFMNH$_2$; however, UbiD enzymes require the oxidized iminium prFMN species for decarboxylase activity. Oxidative maturation of the prFMN is proposed to occur within the UbiD enzyme and does not require UbiX.[15-17, 19, 37] The proposed process for oxidative maturation is the colorless prFMNH$_2$ is oxidized to the purple prFMN radical species and then further oxidation occurs to produce the active, pale yellow iminium species (Figure 1.8).

However, the exact steps for this process are still not fully understood. In FDC, prFMNH$_2$ can be oxidized to the iminium species using oxygen or potassium ferricyanide.[16, 37, 39] In a recent study, a highly stable prFMN-hydroperoxide species (prFMN C4a-OOH) was characterized in solution (Figure 1.8).[39] This species led the authors to propose that in FDC, prFMNH$_2$ undergoes oxidative maturation through a prFMN C4a-OO$^-$ intermediate (Figure 1.8). The intermediate is thought to be stabilized by a highly conserved active site arginine residue (R175 in *S. cerevisiae*), which has been previously shown to be important for proper oxidation of prFMN.[19] Afterwards, the prFMN C4a-OO$^-$ intermediate collapses through an intramolecular elimination reaction in which a proton from the C1' of prFMN is abstracted, producing the iminium prFMN species. Importantly, this proposed mechanism assumes oxygen is the oxidizing agent. However, as stated earlier, potassium ferricyanide can activate FDC complexed with prFMNH$_2$. Moreover, some studied UbiD enzymes were found to be sensitive to oxygen[22] while others are found in anaerobic microbes.[20] Taken together, this suggests that prFMN oxidative maturation may occur through different mechanisms, depending on the flavin's environment.
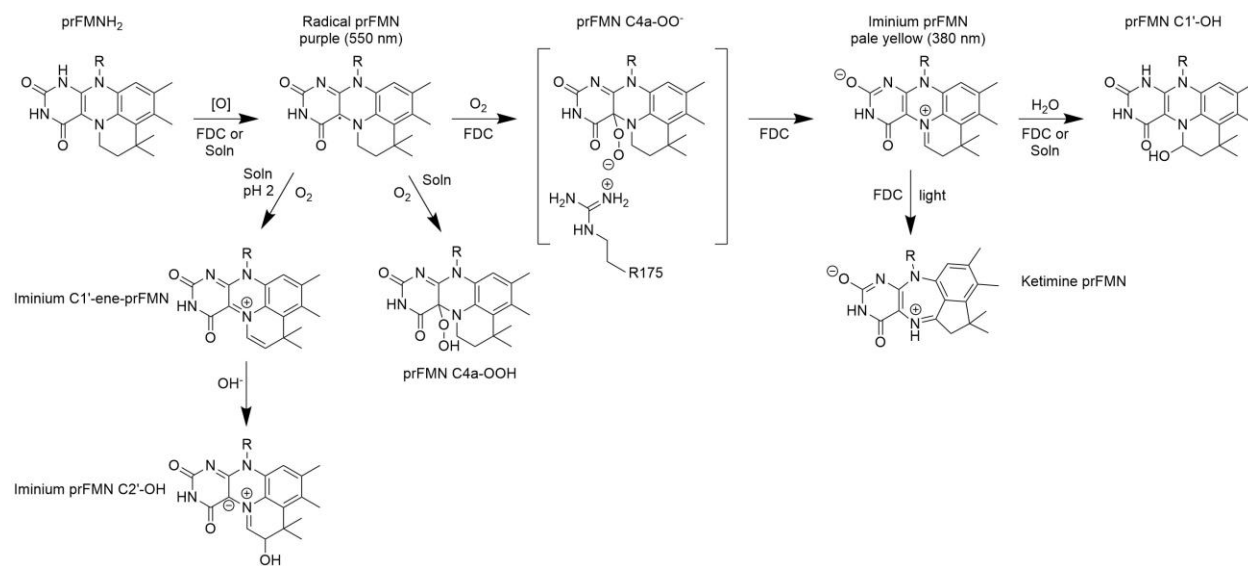
Figure 1.8: Proposed oxidative maturation of prFMN. Reduced prFMN (prFMNH$_2$) produced by UbiX is oxidized to the radical prFMN species using oxygen or potassium ferricyanide. This oxidation step does not require the FDC environment, but it is believed that FDC likely binds prFMNH$_2$ and oxidative maturation occurs within the

enzyme. The radical prFMN species is then oxidized into a prFMN C4a-OO⁻ intermediate and finally the catalytically relevant iminium prFMN species. The iminium species has been found to further oxidize to a prFMN C1'-OH species in enzyme or solution as well as isomerize into the ketimine species from prolonged light exposure. In solution, the radical prFMN species has also been observed to form a prFMN C4a-OOH species as well as two additional species proposed to be an iminium C1'-ene-prFMN species and an iminium prFMN C2'-OH species.

Additional prFMN species have been observed both in FDC and in solution. As stated in previous sections of this chapter, the iminium prFMN species can undergo hydrolysis in FDC, producing the inactive prFMN C1'-OH species.[16] The iminium species has also been found to irreversibly isomerize into the inactive ketimine species from prolonged light exposure.[19] Further, a study from 2018 by Wang and coworkers revealed that the prFMN can exist in a variety of forms in solution.[36] At low pH, the radical prFMN species initially becomes a protonated radical prFMN cation and then oxidizes overnight to a green species, proposed to be an iminium C1'-ene-prFMN cation based on LC-MS analysis. Storing the iminium C1'-ene-prFMN cation at pH 2 for 48 h resulted in the formation of a new species, proposed to be an iminium prFMN C2'-OH species. Interestingly, apo-AnFDC could be activated by the preparation of the proposed iminium prFMN C2'-OH species which would have azomethine ylide character. However, the exact structure of both prFMN species has not been confirmed yet.

1.7 Characterized Members of the UbiD Family

Genetic studies of the UbiD family have found more than 100 homologues, spanning all three microbial domains.[2, 40] Previously, many of these homologues were classified only as putative decarboxylases because the enzyme activities had not been unambiguously demonstrated. The discovery of prFMN in 2015 has finally allowed for in-depth investigations into many UbiD family members. While there are still challenges in obtaining active enzymes, the number of characterized UbiD homologues has grown significantly and has brought new insights into the properties of prFMN. Below, I will discuss the UbiD members that have been

characterized at the time of this dissertation (Figure 1.9). Table 1.1 provides a summary of the

characterized family members at the end of this section.
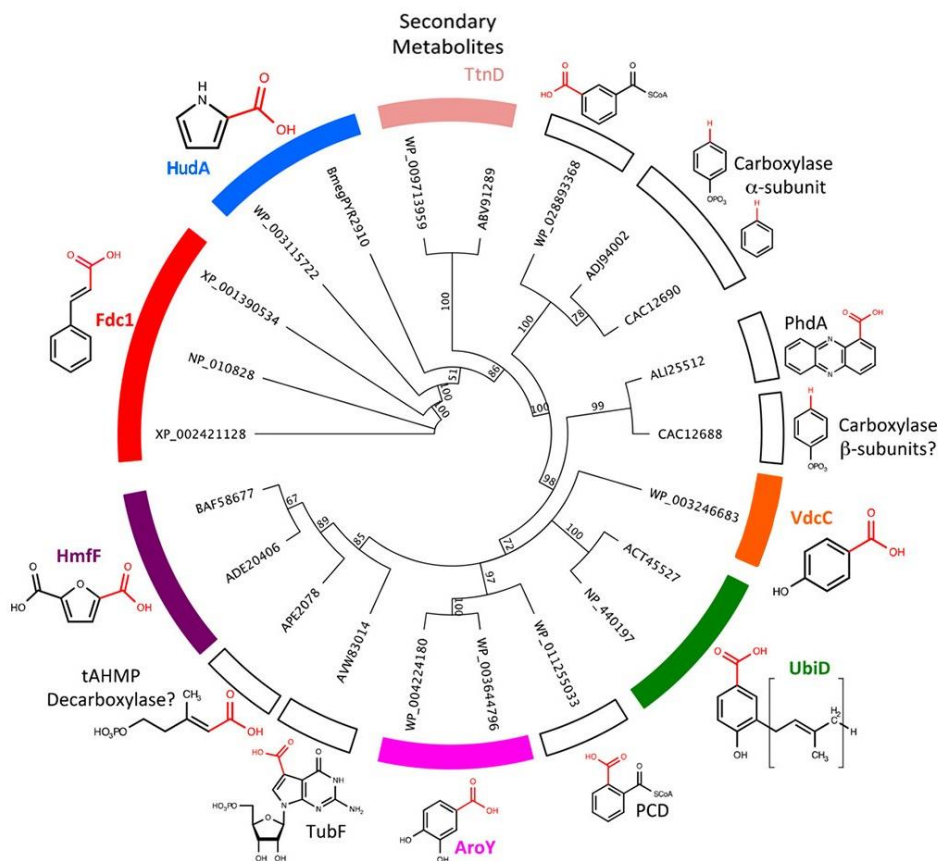
Figure 1.9: Phylogenetic tree of the known UbiD family. UbiD members can be organized into branches by substrate specificity. Structures of substrates are shown by their respective (de)carboxylase. Enzymes with crystal structures are indicated by colored segments. Figure adapted from Payne *et al.*, *ACS Catalysis*, 2021.

1.7.1 4-Hydroxy-3-polyprenylbenzoic Acid Decarboxylase (UbiD)

As stated previously, UbiD was the first member of the family to be discovered and

catalyzes the decarboxylation of 4-hydroxy-3-polyprenylbenzoic acid to 2-polyprenylphenol.[1, 3, 4]

Although a previous study[3] of EcUbiD reported decarboxylase activity against 4-hydroxy-3-

octaprenylbenzoic acid, a 2017 study[21] was unable to obtain active EcUbiD even with *in vitro*

reconstitution of the prFMN. EcUbiD is a hexameric protein with each monomer possessing the

same three sections as an FDC monomer. prFMN binding is dependent on Mn^{2+}.[3, 21] Crystal

structures of EcUbiD complexed with FMN and prFMN reveal a similar Mn^{2+} coordination with the prFMN phosphate group as well as a Na^+ ion in place of a K^+ ion.[21] EcUbiD appears to have a low affinity for prFMN as demonstrated by the observations that the enzyme could only be purified as the apoenzyme and that it would lose its cofactor during the desalting step of *in vitro* reconstitution. Further, EcUbiD was unable to properly oxidize $prFMNH_2$ into the iminium species, stalling at the radical species. All together, these issues highlight the challenges of studying members of the UbiD family even with the knowledge of the prFMN cofactor.

The presence of prFMN or FMN did not affect the structure of EcUbiD compared to apo-EcUbiD. However, when compared to FDC, the monomers of EcUbiD adopt a more "open" conformation in which the distance between the prFMN-binding domain and oligomerization domain is larger. This results in the EcUbiD active site being more solvent-exposed and could help explain the enzyme's lower affinity for prFMN and its inability to oxidize $prFMNH_2$ to the catalytic iminium species.

1.7.2 3,4-Dihydroxybenzoic Acid Decarboxylase (AroY)

AroY performs the decarboxylation of 3,4-hydroxybenzoic acid (protocatechuic acid) into 1,2-dihydoxybenzene (catechol) and is found in a variety of bacteria. Currently, two species of AroY have been studied: *Enterobacter cloacae* AroY (EcAroY) and *Klebsiella pneumoniae* AroY (KpAroY).[22] While holo-AroY can be purified after recombinant expression in *E. coli*, the decarboxylase activity of the enzyme is oxygen-sensitive suggesting that the enzyme cannot protect the iminium prFMN from further oxidation. AroY may be unable to perform complete cofactor maturation since *in vitro* reconstitution of AroY yielded an apparent mixture of iminium and radical prFMN. Similar to FDC, AroY has some substrate promiscuity. It can decarboxylate 3,4,5-trihydroxybenzoate to form 1,2,3-trihydroxybenzene (pyrogallol). Additionally, AroY can

carboxylate catechol and pyrogallol in the presence of bicarbonate or pressurized CO_2. The enzyme tolerates small electron-withdrawing and small electron-donating groups at the *meta*-position of the carboxylation site, but not modifications at the *ortho-* position. However, the studied carboxylation reactions never exceeded 20% after 24 h, likely reflecting the position of the chemical equilibrium for this reaction.

Crystal structures show AroY is hexameric (trimer of dimers) with each monomer possessing an "open" conformation similar to UbiD.[21] Interestingly, the prFMN cofactor is bound to the enzyme with only a Mn^{2+} ion complexing with the phosphate group. While attempts to crystallize AroY complexed with a substrate were unsuccessful, the presence of two adjacent water molecules in the active site allowed for the authors to speculate on how AroY binds its substrates. The authors modeled 3,4-dihydroxybenzoate into the active site by positioning the hydroxyl groups where the water molecules were located. This resulted in the $C\alpha$ of the substrate being directly above the N5 of prFMN, which differs from substrate positioning in FDC. Through DFT calculations, the authors determined that a 1,3-dipolar cycloaddition was not feasible due to the strain on the cycloadduct and the loss of aromaticity. Conversely, a quinoid-based mechanism was energetically feasible with the substrate performing a nucleophilic attack on the prFMN C1', creating a quinoid intermediate (Figure 1.10). Decarboxylation could then occur followed by the abstraction of a proton from the conserved active site glutamic acid (E289 in EcAroY). Lastly, cleavage of the $C\alpha$-C1' bond would free the decarboxylated product.
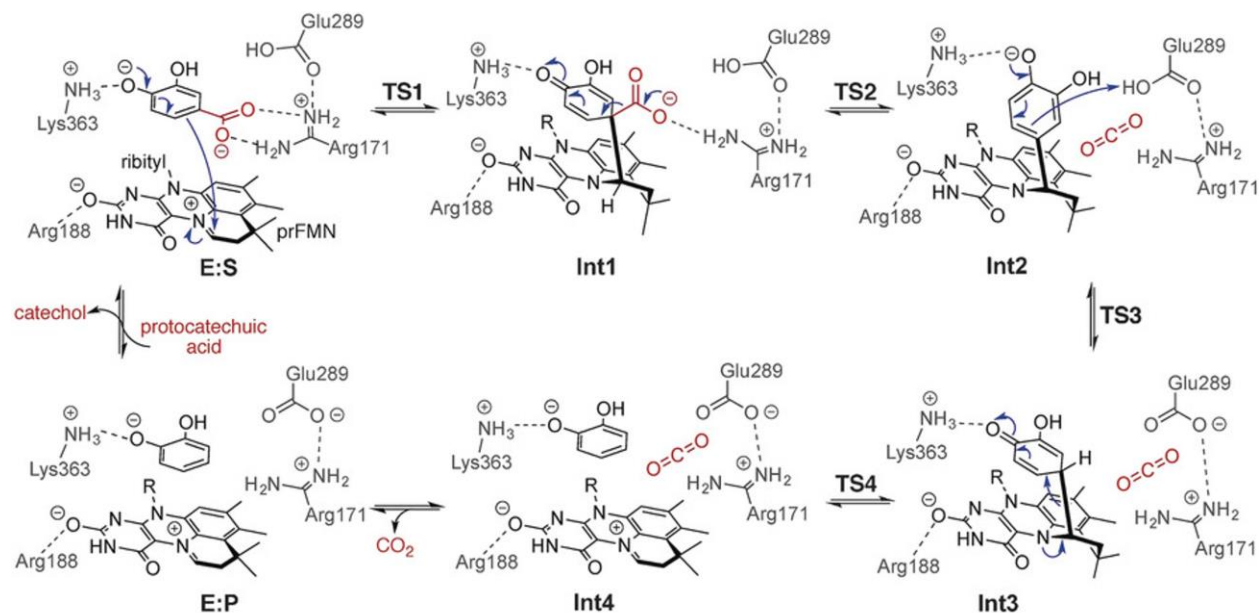
Figure 1.10: Proposed quinoid mechanism for AroY. 3,4-dihydroxybenzoate is proposed to perform a nucleophilic attack on the C1' of prFMN, resulting in a single-tethered quinoid intermediate. Decarboxylation then occurs with the quinoid ring stabilizing the transition state. Afterwards, the decarboxylated intermediate abstracts a proton from the catalytic glutamic acid residue. Finally, the C1'-Cα bond is cleaved, releasing the product. Figure from Payer *et al.*, *Angew. Chem. Int. Ed.*, 2017.

1.7.3 TTN D-1 Decarboxylase (TtnD)

TtnD is a decarboxylase found in *Streptomyces griseochromogenes* with its flavin prenyltransferase partner TtnC.[40] TtnD is part of a large gene cluster responsible for synthesizing the antifungal polyketide tautomycetin. In *S. griseochromogenes*, TtnD performs the penultimate step in the biosynthetic pathway: the decarboxylation of TTN D-1 (Figure 1.11) to TTN I-1.
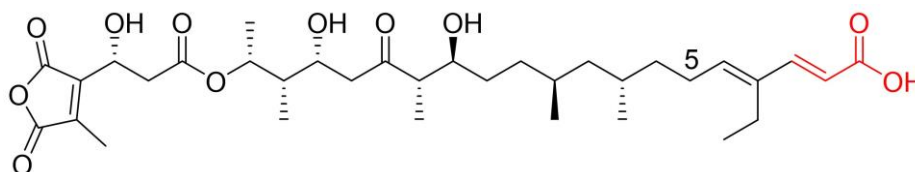
Figure 1.11: Structure of TTN D-1. The α,β-unsaturated carboxylic acid moiety is shown in red. C5 of TTN D-1 is also labeled.

Similar to UbiD, TtnD may have a lower affinity for prFMN since cofactor loss was noted in the purification of holo-TtnD. Additionally, purified holo-TtnD possessed a mixture of iminium prFMN, radical prFMN, and FMN, which may indicate that oxidative maturation does

not occur efficiently. Nevertheless, TtnD was able to decarboxylate TTN D-1 *in vitro* with a

k_{cat}^{app} of 0.65 min^{-1}. TtnD also possessed some promiscuity, decarboxylating TTN D-1 analogues

with an alcohol or ketone group at C5, although at even slower rates.

The crystal structure of holo-TtnD remains to be solved. However, apo-TtnD and TtnD

complexed with FMN have both been crystallized. These structures reveal TtnD is a tetramer and

as seen with UbiD, the enzyme structure is not affected by the presence of flavin. TtnD binds

FMN using Mn^{2+} as a counter-ion to the phosphate group and appears to be in the "closed"

conformation adopted by FDC. The authors were unable to crystallize TtnD complexed with a

substrate but hypothesized that TtnD could perform a 1,3-dipolar cycloaddition.

1.7.4 Phthaloyl-CoA Decarboxylase (PCD)

PCD is found in denitrifying bacteria that are capable of the anaerobic degradation of

toxic phthalic acid esters (PAEs).[20, 41, 42] PCD catalyzes the decarboxylation of phthaloyl-CoA to

benzoyl-CoA and this step is thought to be rate-limiting in the degradation pathway of PAEs.

The gene for PCD is in a phthalate-induced gene cluster along with its UbiX-like partner.[41, 42]

In 2017, PCD from *Thauera chlorobenzoica* (TaPCD) was purified from its native host

(grown with phthalate and nitrate) under anaerobic conditions.[20] TaPCD appears to be more

similar to FDC in terms of prFMN affinity and maturation. Purified TaPCD was faintly yellow in

color and possessed an absorbance spectrum with a small peak around 400 nm, aligning well

with the iminium prFMN species. The identity of the cofactor was confirmed through

UPLC/ESI-Q-TOF-MS. TaPCD possessed decarboxylase activity but was unable to perform

carboxylation even with bicarbonate present. Surprisingly, TaPCD requires Fe^{2+} (instead of

Mn^{2+}) as well as K^+ to bind the prFMN cofactor, likely using these ions as counter-ions for the

prFMN phosphate group. The enzyme is also sensitive to oxygen but this appears to be due to

loss of bound prFMN rather than inactivation of the cofactor. TaPCD is proposed to be a hexamer based on gel-filtration studies but no other structural or mechanistic studies have been performed yet. Sequence alignment of UbiD and FDC with PCDs from various bacteria reveal PCDs possess the conserved catalytic glutamic acid residue (E284 in TaPCD), which is likely located in the active site.

1.7.5 2,5-Furandicarboxylic Acid Decarboxylase (HmfF)

HmfF is a bacterial enzyme named from its involvement in the bacterial degradation and utilization of hydroxymethylfurfural (HMF) and furfural as the organisms' only carbon sources. Further investigations into this pathway determined HmfF performed the *in vivo* decarboxylation of 2,5-furandicarboxylic acid (FDCA) to furoic acid.[43] Currently, HmfF from *Pelotomaculum thermopropionicum* (PtHmfF) and from *Geobacillus kaustophilus* (GkHmfF) have been studied.[23]

Similar to other characterized UbiD enzymes, purified PtHmfF possessed a mixture of FMN, radical prFMN, and iminium prFMN. Further, PtHmfF was unable to efficiently oxidize prFMNH$_2$ to the iminium species even with *in vitro* reconstitution, resulting in a similar mixture of FMN and prFMN species. The enzyme was also found to be light- and oxygen-sensitive. Nevertheless, PtHmfF can decarboxylate FDCA and since it is from a thermophile, is most active at 50 °C with a k_{cat}^{app} of 2.39 s^{-1}. PtHmfF can also decarboxylate 2,5-pyrroledicarboxylic acid, albeit very slowly. However, it is unable to decarboxylate many FDCA-like compounds nor furoic acid, indicating an important substrate specificity. Lastly, both species of HmfF will carboxylate furoic acid to a limited extent in the presence of 1 M potassium bicarbonate, pressurized CO_2, or both.

28

Crystal structures of apo-PtHmfF and FMN-PtHmfF reveal the enzyme oligomerizes into a hexamer and the phosphate group of FMN is complexed with a Mn^{2+} and K^+ ion. Additionally, the enzyme adopts the "open" conformation, leaving the predicted active site partially solvent-exposed. Although attempts to obtain HmfF complexed with a substrate have been unsuccessful, the authors hypothesize that either a 1,3-dipolar cycloaddition mechanism or an electrophilic aromatic substitution mechanism are feasible.

1.7.6 Phenazine-1-carboxylic Acid Decarboxylase (PhdA)

PhdA from *Mycobacterium fortuitum* (MfPhdA) is an enzyme involved in the degradation of phenazine-1-carboxylic acid (PCA).[44] PCA is secreted by other bacterial species such as *Pseudomonas* and provides the organism with an advantage over other microbes. In response, *M. fortuitum* evolved the PhdA enzyme (and its UbiX-like partner PhdB) to decarboxylate PCA so that it can be metabolized.

As is common in the UbiD family, MfPhdA is oxygen-sensitive, was unable to retain its cofactor during purification, and possessed a mixture of prFMN species including the iminium and radical species after *in vitro* reconstitution. Mn^{2+} was proposed to be the counter-ion for the prFMN phosphate group and was included in the *in vitro* reconstitution protocol. While PCA can exist in several redox states, only oxidized PCA is a substrate of MfPhdA.[45] Furthermore, MfPhdA can decarboxylate 2,3-dimethyl-quinoxaline-5-carboxylic acid and is able to slowly decarboxylate 2-methyl-quinoxaline-5-carboxylic acid, 3-methyl-quinoxaline-5-carboxylic acid, and even anthracene-1-carboxylic acid. However, MfPhdA is regioselective for the C-1 position of acridine/anthracene and cannot decarboxylate substrate analogues with a C-2 carboxylic acid. Interestingly, acridine and anthracene can form 1,3-dipolar cycloadducts with strong 1,3-dipoles

29

with the same regioselectivity observed in MfPhdA. Thus, a 1,3-dipolar cycloaddition mechanism is the most likely mechanism for MfPhdA.

1.7.7 Pyrrole-2-carboxylate Decarboxylase (PA0254/HudA)

HudA is identified as a virulence attenuation factor in *P. aeruginosa* and was the first UbiD family member to be successfully analyzed through X-ray crystallography in 2013.[14] Since the discovery of the prFMN cofactor, HudA has now been biochemically characterized as a pyrrole-2-carboxylic acid decarboxylase.[24] HudA has also some decarboxylase activity against indole-3-carboxylate, furan-2-carboxylate, and imidazole-4-carboxylate. Moreover, HudA can carboxylate pyrrole to pyrrole-2-carboxylate in the presence of potassium bicarbonate and pressurized CO_2. Nevertheless, purified HudA also contains a mixture of iminium and radical prFMN species, indicating that it cannot perform oxidative maturation efficiently.

HudA is a dimer and utilizes a Mn^{2+} and K^+ ion as counter-ions to the prFMN phosphate group.[24] Unexpectedly, apo-HudA adopts the "open" conformation, whereas holo-HudA adopts the "closed" conformation. Up until this point, individual UbiD family members had only been observed crystallographically in either the "closed" conformation or the "open" conformation, never both. HudA, on the other hand, appears to transition between these two conformations through cofactor binding. In addition, a complex of holo-HudA with the reversible inhibitor imidazole has provided some insight into the enzyme's mechanism. The resulting inhibitor-prFMN adduct is composed of a single covalent bond between the prFMN C1' and the C2 of imidazole. Using this adduct and DFT calculations in which the prFMN adducts were modeled in water, the authors proposed that HudA performs an electrophilic aromatic substitution mechanism (Figure 1.12). In this mechanism, the lone pair of electrons on N1 of the substrate is used to create a bond between the C1' of prFMN and the C2 of pyrrole, generating the Wheland-

type intermediate Int 1[open]. Afterwards, decarboxylation occurs followed by protonation of the pyrrole C2 by the conserved glutamic acid E278, which generates the Wheland-type intermediate Int 3[open]. Finally, the C1'-C2 bond is cleaved, releasing the product pyrrole.
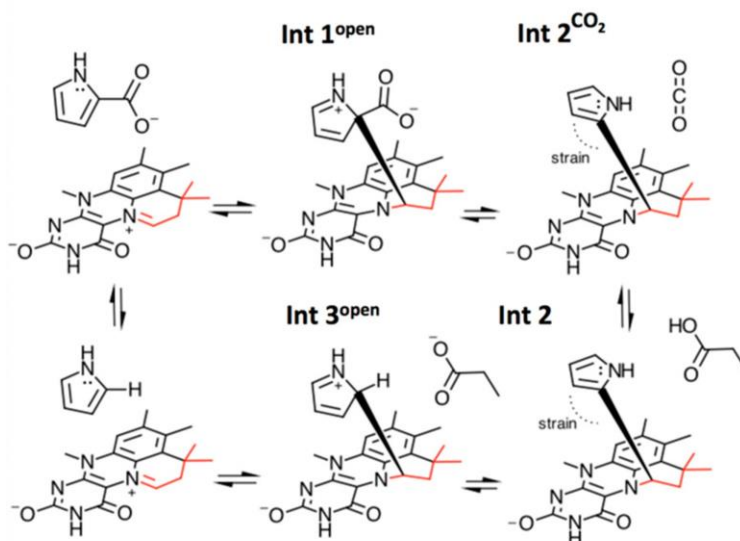
Figure 1.12: Proposed electrophilic aromatic substitution mechanism for HudA. Through electrophilic aromatic substitution, a covalent bond is formed between pyrrole-2-carboxylic acid's C2 and the prFMN C1' (Int 1[open]). Decarboxylation then occurs, producing Int 2[CO2]. Carbon dioxide is then released and the catalytic glutamic acid residue takes its place (Int 2). Int 2 abstracts a proton from the glutamic acid, producing Int 3[open]. Lastly, cleavage of the C1'-C2 bond occurs, releasing the product pyrrole and regenerating the iminium prFMN. Figure adapted from Payne *et al.*, *ACS Catalysis*, 2021.

1.7.8 Vanillic Acid Decarboxylase (VdcC)

Interestingly, the operon of vanillic acid decarboxylase is composed of three genes: the *ubiX*-like gene *vdcB*, the *ubiD*-like gene *vdcC*, and an additional gene referred to as *vdcD*.[2, 46] While VdcC performs the decarboxylation of vanillic acid and 4-hydroxybenzoic acid, the smaller VdcD protein is required for this decarboxylase activity.[25] VdcD is a zinc ribbon protein that forms a tight complex with VdcC and specifically interacts with the loops containing the catalytic RX_nEX_2E motif of VdcC, likely assisting in the positioning of these active site residues. VdcC could only be purified in the apoenzyme form, potentially suggesting a lower affinity for

prFMN. Although no discussion about cofactor maturation was given, Mn^{2+} is proposed to be the counter-ion for the phosphate group of prFMN.

VdcC forms a hexamer in which each of its monomers is complexed with a VdcD protein. Importantly, crystal structures of the VdcCD complex reveal that the VdcC monomers can adopt either the "open" or "closed" conformation. This transition occurs through a hinge motion in the α-helix connecting the prFMN-binding domain to the oligomerization domain. Docking studies to create a holo-VdcCD model coupled with DFT calculations found that domain motions were likely important throughout catalysis to facilitate the initial reaction between prFMN and its aromatic substrates as well as to accommodate the significant changes in shape of the various substrate-prFMN adducts and to prevent the buildup of dead-end adducts through exerting strain on the reaction intermediates. Currently, VdcCD is proposed to utilize the quinoid-based mechanism due to its aromatic substrates.
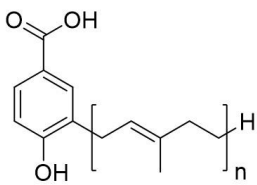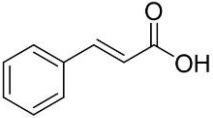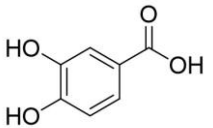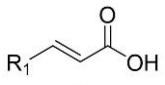
1.7.9 Indole-3-carboxylate Decarboxylase (IndD)
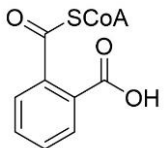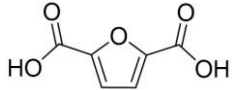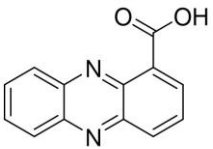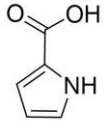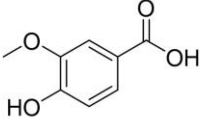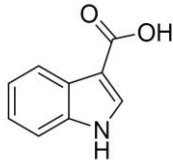
The most recent UbiD member to be characterized is IndD from *Arthrobacter nicotianae*.[26] Crystal structures and EPR spectroscopy revealed IndD utilizes a Mn^{2+} and Na^+ ion to act as counter-ions to the phosphate group of prFMN in its active site. IndD is unable to efficiently oxidize $prFMNH_2$ resulting in a mixture of iminium and radical prFMN species and is both light- and oxygen-sensitive. Interestingly, in contrast to many other UbiD family members, IndD is specific for indole-3-carboxylic acid with a k_{cat}^{app} of 4.4 s^{-1}.

In crystal structures, IndD is a hexamer and adopts the "open" conformation. Similar to VdcCD, IndD appears to have a hinge region located in the α-helix connecting its two main domains and small-angle X-ray scattering (SAXS) data indicates that IndD adopts a variety of different conformations in solution. Taken together, the domain motions of HudA, VdcCD, and

IndD suggest that this is a conserved trait of the UbiD family. Using the closed structure of

VdcCD, a model of the closed conformation of IndD was made and used for docking studies

with indole-3-carboxylate. IndD was found to bind its substrate in a similar position regardless of

open or closed conformation. The carboxylic acid moiety of the substrate was found to interact

with two highly conserved active site residues (R155 and the backbone of the catalytic E266),

while the substrate's nitrogen hydrogen bonds with D169. The authors propose that the iminium

prFMN species reacts with indole-3-carboxylate through either a 1,3-dipolar cycloaddition

mechanism or an electrophilic aromatic substitution mechanism.

Table 1.1: Characterized UbiD family members.

Name	Substrate	Proposed Mechanism	Oligomerization	Ref
UbiD	 4-Hydroxy-3-polyprenylbenzoic acid	1,3-Dipolar cycloaddition Or Quinoid-based mechanism	Hexamer	3, 12, 21
FDC	 Phenylacrylic acid	1,3-Dipolar cycloaddition	Dimer	16, 30, 32, 35
AroY	 3,4-Dihydroxybenzoic acid	Quinoid-based mechanism	Hexamer	22
TtnD	 TTN D-1	1,3-Dipolar cycloaddition	Tetrameric	40

PCD	Phthaloyl-CoA	1,3-Dipolar cycloaddition	Hexamer	20
HmfF	2,5-Furandicarboxylic acid	1,3-Dipolar cycloaddition Or Electrophilic aromatic substitution	Hexamer	23
PhdA	Phenazine-1-carboxylic acid	1,3-Dipolar cycloaddition	Not known	44, 45
HudA	Pyrrole-2-carboxylic acid	Electrophilic aromatic substitution	Dimer	14, 24
VdcC	4-Hydroxy-3-methoxybenzoic acid	Quinoid-based mechanism	Hexamer	25
IndD	Indole-3-carboxylic acid	1,3-Dipolar cycloaddition Or Electrophilic aromatic substitution	Hexamer	26

1.8 My Research Goals

At the start of my work in 2017, the mechanism of FDC was still uncertain. While the 1,3-dipolar cycloaddition mechanism was feasible due to the nature of the iminium prFMN and FDC's substrates, the strongest evidence for the mechanism were inhibitor-prFMN adducts (the phenylpyruvate-prFMN adduct[16] and the FNVB-prFMN cycloadduct[32]) and linear free energy

34

analysis coupled with isotope effect experiments that disagreed with an alternative Michael addition-like mechanism. Therefore, the first goal of my research was to characterize the reaction intermediates of the FDC (de)carboxylation reaction to further elucidate its mechanism. Using native MS, I was able to characterize the prFMN intermediate that builds up at chemical equilibrium. The second goal of my research was to investigate the pre-steady state kinetics of the FDC reaction as this area had not been explored at all. Understanding the kinetics of intermediate formation and breakdown provides valuable information on how an enzyme catalyzes its reaction. Using stopped-flow absorption spectroscopy, I investigated the decarboxylation reaction of FDC with phenylacrylic acid as well as the enzyme's reaction with styrene (which could not progress past the styrene-prFMN cycloadduct under the experimental conditions). While the kinetic behavior of FDC is far more complex than I initially expected and will require additional experiments before a full model can be proposed, my experiments indicate that FDC possesses half-of-sites reactivity. Specifically, FDC possesses a "fast, tight" monomer that can react with phenylacrylic acid until the rate-limiting cycloelimination step. At this point, a conformational change occurs in FDC, allowing cycloelimination to occur as well as the conversion of the "slow, loose" monomer into a "fast, tight" monomer. As proposed for other UbiD family members, this conformational change may be due to hinge motion of the α-helix linker and may provide the energy needed to overcome the activation energy barrier for cycloelimination.[25, 26]

Chapter 2 Kinetic Analysis of Transient Intermediates in the Mechanism of Ferulic Acid Decarboxylase[1]

2.1 Introduction

Enzyme-catalyzed decarboxylations are an important class of biological reactions that are ubiquitous in both primary and secondary metabolism. However, decarboxylation reactions are challenging to catalyze, as they generally possess high-energy barriers associated with the buildup of negative charge on the α-carbon in the transition state. Indeed, decarboxylases catalyze some of the largest rate enhancements (~10^{17}-fold) so far measured for enzymes.[47, 48] Therefore, Nature has evolved a remarkably wide variety of catalytic strategies to facilitate decarboxylation reactions, using cofactors such as pyridoxal phosphate and thiamine pyrophosphate that serve as electron sinks, and Lewis acidic metal ions.[49-51]

Decarboxylases have also attracted increasing interest for their potential to function as "green" catalysts capable of catalyzing regio- and stereo-specific reactions under mild conditions.[52, 53] Decarboxylases have been employed in engineered biosynthetic pathways designed to produce commodity chemicals such as styrene[54] and acrylamide; bi-functional alcohols, e.g., 1,3-propanediol and 1,4-butanediol; isobutanol, which are a promising new

biofuel;[55] and high value fine chemicals and pharmaceuticals.[52, 53] Importantly, under favorable conditions decarboxylases can function as carboxylases and hydratases, leading to interest in using them for CO_2 capture and the hydration of double bonds to produce chiral alcohols.[53]

The newest family of decarboxylases to be discovered employ a novel modified flavin, termed prenylated FMN (prFMN), as a cofactor to effect decarboxylation reactions on otherwise unreactive aromatic substrates.[15, 16, 36, 56-58] prFMN contains an additional 6-membered ring, appended between the C6 and N5 positions of the isoalloxazine flavin moiety, that is derived from dimethylallyl phosphate in bacteria[17] or dimethylallyl pyrophosphate in yeast.[37] This additional ring is installed by a specialized prenyltransferase enzyme.[38] Collectively, the two components of this class of decarboxylases are known as UbiD/UbiX-like decarboxylases. The canonical member, UbiD, catalyzes the decarboxylation of 4-hydroxy-3-octaprenylbenzoic acid to 2-octaprenylphenol as part of ubiquinone biosynthesis in many bacteria, whereas UbiX is the corresponding bacterial prenyltransferase.[5, 7, 59]

Since their discovery, it has become apparent that the UbiD/UbiX-like system is widely distributed in microbes where it is involved in the metabolism of a range of aromatic poly-unsaturated molecules. A recent phylogenetic analysis[40] identified over 200 UbiD-like decarboxylases that fall into 3 subgroups: a) phenylacrylic acid decarboxylases, of which ferulic acid decarboxylase (FDC)[16, 32, 58] is the best characterized; b) aromatic (de)carboxylases, of which 3,4-dihydroxybenzoic acid decarboxylase (AroY)[22] is best understood; c) α,β-unsaturated aliphatic decarboxylases, exemplified by TTN D-1 decarboxylase (TtnD)[40] – these latter enzymes are involved in secondary metabolism and are the most recently identified subgroup.

The mechanism by which prFMN-dependent enzymes catalyze decarboxylations remains to be fully elucidated and is especially interesting because the cofactor may function by more

than one mechanism. For the phenylacrylic acid and α,β-unsaturated aliphatic decarboxylases, a mechanism involving a novel 1,3-dipolar cycloaddition between the substrate and prFMN has been proposed.[16, 32] This proposal has attracted considerable interest because genuine thermal pericyclic reactions are very rare in enzymes and 1,3-dipolar cycloadditions have no precedent in other enzymatic reactions.[28, 60] However, it seems implausible that a cycloaddition mechanism could operate for aromatic decarboxylases, because this would require breaking the aromaticity of the ring. Instead, as in the case of AroY, it appears more likely that prFMN may act as an electrophilic catalyst in these decarboxylations.[22]

FDC catalyzes the decarboxylation of a range of ring-substituted phenylacrylic acid derivatives to produce the corresponding substituted styrene derivatives.[15, 16] The proposed mechanism is shown in Figure 1.5. The formation of cycloaddition adducts in the mechanism is supported by crystallographic studies[35] of the enzyme complexes that provide evidence for the formation of various covalent adducts between prFMN and substrates or substrate analogs. Structures have been solved that are similar to several of the proposed intermediates depicted in Figure 1.5. Another line of evidence supporting this mechanism derives from the reaction of FDC with a mechanism-based inhibitor that allowed the prFMN-inhibitor cycloadduct to be characterized by high resolution native tandem mass spectrometry.[32] Linear free energy analyses using a series of substituted phenylacrylic acid derivatives, combined with primary and secondary deuterium kinetic isotope effect measurements, point to cycloelimination of the styrene product (intermediate **E** in Figure 1.5) as the rate-determining step in the reaction.[30] Computational studies have provided further support of the energetic feasibility of forming cycloadducts between prFMN and phenylacrylic acid.[31]

Although there is now experimental evidence supporting the existence of some of the intermediates proposed in the mechanism of FDC, the kinetics of the reaction remain to be fully developed. In this chapter, I describe pre-steady state kinetic analyses of FDC reacting with phenylacrylic acid, together with native tandem MS analyses of prFMN-substrate adducts. These data provide evidence for the formation and decay of the first cycloadduct in the reaction cycle and identify the kinetics of formation for the second cycloadduct that forms between styrene and prFMN, which is the intermediate that accumulates on the enzyme.

2.2 Materials and Methods

2.2.1 Reagents

trans-Phenylacrylic acid, d_7-trans-phenylacrylic acid, styrene, and d_8-styrene were all purchased from Sigma-Aldrich Co. All other materials were purchased from Sigma-Aldrich Co. or Thermo Fisher Scientific Co.

2.2.2 Expression and Purification of FDC

Expression and purification of recombinant holo-FDC from *E. coli* were performed as described previously.[15] In short, a pET28b plasmid containing in tandem *tPAD* (not tagged) and *FDC* with a C-terminal 6x-His tag was transformed into *E. coli* BL21 DE3 star (Invitrogen). *E. coli* cultures were grown at 37 °C in LB supplemented with 50 µg/mL kanamycin. Once an OD_{600} of 0.6 – 0.8 was reached, cultures were induced with 0.2 mM IPTG and incubated at 18 °C overnight (~18 h). Cells were harvested by centrifugation and either immediately purified or stored at -20 °C.

Cell pellets were resuspended in Buffer A (50 mM potassium phosphate, 500 mM potassium chloride, 5 mM imidazole pH 7.5; 4 mL of Buffer A/1 g of cell pellet), EDTA-free

protease inhibitor tablets (Roche), lysozyme (4 mg lysozyme/1 g of cell pellet), and Benzonase nuclease (Sigma-Aldrich). Cells were lysed via sonication (10 s pulses with 30 s pauses for a total of 15 min of sonication) and the resulting lysate clarified by centrifugation at 18,500 rpm at 4 °C for 45 min. The supernatant was loaded onto a HisTrap column (GE Healthcare) equilibrated with Buffer A. Due to a previous report[19] that found prolonged light exposure could inactive FDC, the HisTrap column was wrapped in foil to reduce light exposure. (However, we would like to note that this inactivation had not been observed with any of our FDC preps.) Protein purification was performed using a Bio-Rad NGC chromatography system. The protein loaded on the HisTrap column was first washed with Buffer A and then increasing percentages of Buffer B (50 mM potassium phosphate, 500 mM potassium chloride, 500 mM imidazole pH 7.5). First, a 10% Buffer B wash (55 mM imidazole) and then a 20% Buffer B wash (104 mM imidazole) were performed to remove undesired proteins. To obtain concentrated FDC, FDC was eluted with a 100% Buffer B wash (500 mM imidazole). The FDC fractions were immediately placed in a covered ice bucket to minimize light exposure. Fractions were analyzed by SDS-PAGE on a 10% gel (BioRad) and then desalted into Buffer C (50 mM potassium phosphate, 20% (v/v) glycerol pH 7.5) using PD-10 desalting columns (GE Healthcare). All purified FDC were flash-frozen and stored at -80 °C.

2.2.3 Native Mass Spectrometry Assay

Purified FDC was buffer exchanged into 200 mM ammonium acetate using Micro Bio-Spin 30 columns (Bio-Rad, Hercules, CA). Substrates were first dissolved in DMSO to improve solubility. All reactions were performed in 200 mM ammonium acetate with a substrate to enzyme ratio of 5:1 and incubated on ice for 10 min before analysis. A pH of 6.6 was used for

the reaction of FDC with styrene substrates and a pH of 8 was used for phenylacrylic acid substrates.

Sample aliquots (5 µL) were analyzed under native MS conditions[61] by ion mobility-mass spectrometry (IM-MS) on a quadrupole-ion mobility-time-of-flight mass spectrometer (Q-IM-ToF MS) instrument (Synapt G2 HDMS, Waters, Milford, MA). The complex of FDC with substrate-prFMN adduct ions were generated using nano-electrospray ionization (nESI). The initial instrument settings were set to minimize ion activation, thereby maintaining non-covalent interactions such that no significant signals were observed for free FMN-related peaks. The capillary voltage was set to 1.5 kV, and the sampling and extraction cones were set to 30 V and 0 V with the trap collision energy at 20 V. For CID experiments, the trap collision energy was raised to 100 V to dissociate the noncovalently-bound substrate-prFMN adducts, giving rise to a series of substrate-prFMN derived peaks at low *m/z*. Data was processed in Masslynx (Waters Inc, Milford, MA).

2.2.4 Stopped-flow Absorption Spectroscopy

Purified concentrated FDC was stored in 50 mM potassium phosphate, 10% (v/v) glycerol pH 7.5. A stock solution of 10 mM phenylacrylic acid was prepared in the same buffer as the enzyme and was used to make more dilute phenylacrylic acid solutions for experiments. FDC was transferred into a glass tonometer and made anaerobic by cycling between evacuation and flushing with argon gas. The tonometer had a glass ice bath feature that kept the enzyme cool and stable. Buffer and phenylacrylic acid solutions were transferred to glass syringes and made anaerobic by bubbling argon gas through for 10 min before use.

A Hi-Tech Scientific SF-61 DX2 double-mixing instrument (TGK Scientific) controlled by Kinetic Studios software package (TGK Scientific) was used for pre-steady state experiments.

Single-wavelength absorbance traces were collected using a monochromator, whereas a charge coupled device was used to collect absorbance spectra from 300 to 800 nm. The stopped-flow apparatus was made anaerobic by soaking the system overnight with an oxygen-scrubbing solution of containing ~0.1 unit mL^{-1} protocatechuate dioxygenase and 1 mM protocatechuate (3,4-dihydroxybenzoate) in 0.1 M potassium phosphate buffer (pH 7.0). The apparatus was rinsed thoroughly with anaerobic buffer before use. Reactions were performed at 4 °C. Time-dependent spectra were analyzed by singular-value decomposition[62] and modeled to calculate the spectra of reaction intermediates using KinTek Explorer (KinTek Corp.).

2.2.5 Data Averaging

For some stopped flow data recorded at single wavelengths, the data were recorded under identical experimental conditions at different timescales to obtain data with high temporal resolution on the millisecond to second timescale. These data were then averaged to maximize the signal-to-noise ratio before fitting. Generally, 3-5 stopped-flow shots were recorded using the same conditions and time range and the traces averaged. This process was repeated for a variety of time ranges to improve the quality of data at all times of interest. The exact time points at which the spectrometer recorded the individual data points were unique to each time scale. Therefore, the time dimension was first binned using Microsoft Excel. 100 bins were used for each order of magnitude within the range of 10^{-3} to 5 seconds. The absorbance values corresponding to each time were then averaged. Figure 2.5 shows an example of this procedure.

2.2.6 Steady State Analysis

The decarboxylase activity of FDC was measured spectrophotometrically at 304 nm to monitor the consumption of phenylacrylic acid.[15] Reactions were performed in 50 mM potassium

phosphate, 10% (v/v) glycerol pH 7.5 at 4-7 °C. Stock solutions of FDC and phenylacrylic acid

were also prepared in this buffer and kept on ice to keep solution temperatures close to 4 °C.

Reactions of 100 nM FDC with concentrations of phenylacrylic acid ranging from 20 to 800 μM

were carried out in triplicate. The initial velocities were fit to the Michaelis-Menten equation

using KaleidaGraph 4.0 (Synergy Software).

2.2.7 Spectrum of FDC Reacted with Styrene

A 253 μM solution of FDC was prepared in 50 mM potassium phosphate, 10% (v/v)

glycerol pH 7.5 buffer. The buffer was bubbled with argon gas that had been passed through a 5

M potassium hydroxide trap for ~24 h to remove dissolved CO_2. A stock solution (87 mM) of

styrene was prepared in DMSO. The enzyme was introduced into an aerobic cuvette, final

concentration 76 μM, and the reaction was initiated by addition of styrene, final concentration

870 μM. The U.V.-visible spectrum was recorded for a duration of 1 min using a Hewlett-

Packard 8452a diode array spectrophotometer. Each reaction condition was performed in

triplicate.

2.3 Results and Discussion

2.3.1 Reaction of FDC with Styrene

Previous studies from the Marsh laboratory on the FDC reaction, employing linear free

energy analysis and primary and secondary deuterium kinetic isotope effects, suggested that the

rate-limiting step is likely to be the cycloelimination of the styrene-prFMN adduct, which would

be expected to accumulate on the enzyme during catalysis.[30] To obtain more direct evidence that

styrene accumulates on the enzyme, we studied the reaction of FDC with styrene in buffer that

had been purged of CO_2 by sparging with argon. Under these conditions, carboxylation of

styrene (the reverse reaction) is unable to proceed and therefore, if stable, the prFMN-styrene adduct (intermediate **E** in Figure 1.5) should accumulate on the enzyme. As shown in Figure 2.1, the spectrum of holo-FDC (76 μM final concentration) in degassed buffer has a clear peak at 380 nm characteristic for prFMN. Upon addition of styrene (870 μM final concentration) the peak at 380 nm is decreased in intensity along with the formation of a new, broad peak at 460 nm (Figure 2.1), indicating that a reaction between the prFMN and styrene has occurred. The resulting species was stable at room temperature for several minutes. The previous studies of FDC reacting with the mechanism-based inhibitor 2-fluoro-2-nitrovinylbenzene,[32] together with spectroscopic characterization of model C4a,N5-alkylated flavins,[33, 63, 64] which are also characterized by an absorbance band with a maximum between 425 nm and 460 nm, support the idea that the spectrum of FDC that had reacted with styrene represents the cycloadduct with prFMN.
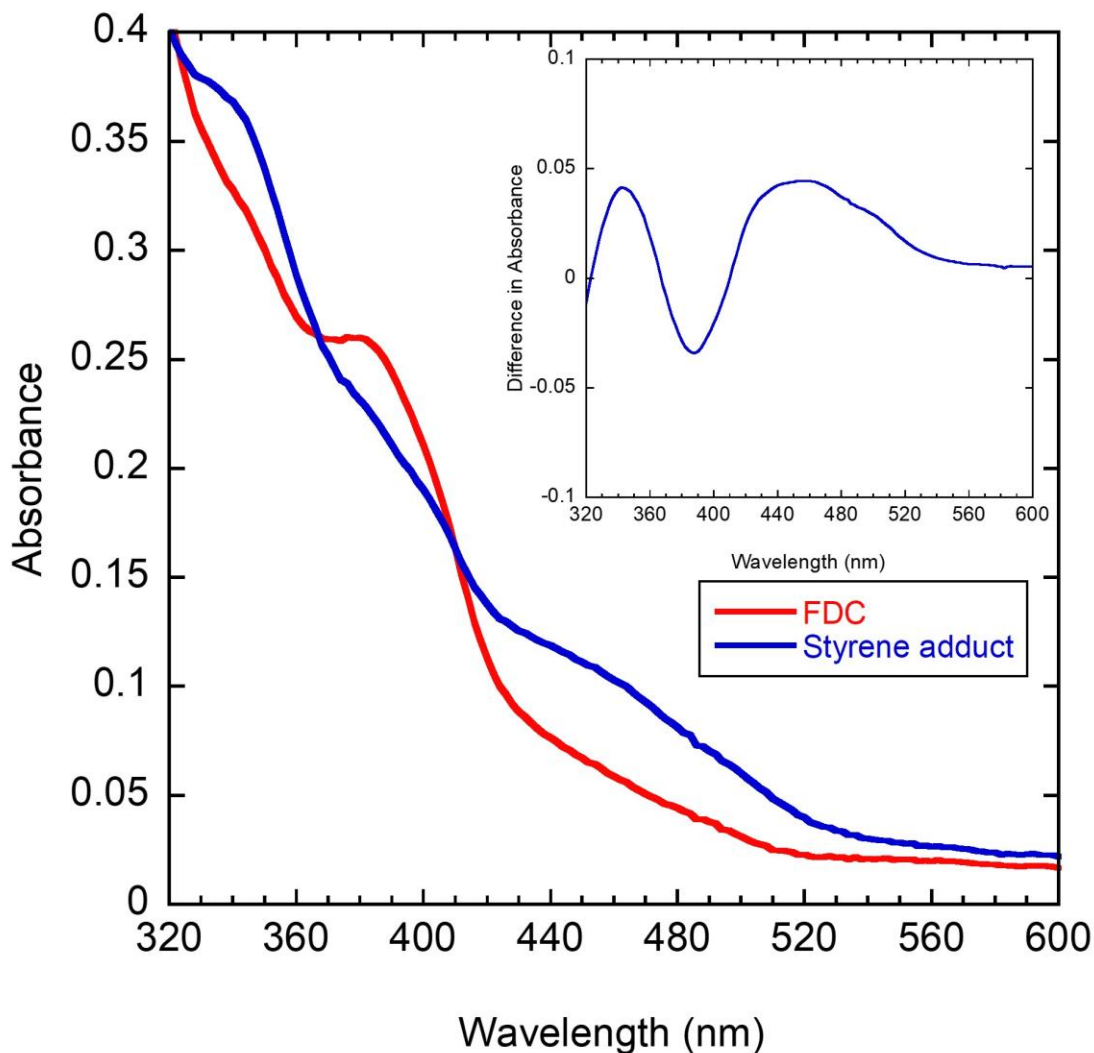
Figure 2.1: Spectral changes accompanying the reaction of prFMN with styrene. Spectrum of unreacted FDC is shown in red; the spectrum of the proposed styrene adduct is shown in blue. Inset: Difference spectrum calculated by subtracting the spectrum of FDC.

2.3.2 Identification of prFMN Adducts by Native MS

To obtain more information on the identity of the spectroscopically observed prFMN adduct, we used native MS to characterize prFMN adducts formed by reaction with substrate or products. Holo-FDC, 20 μM, in 200 mM ammonium acetate was incubated with either 100 μM styrene or 20 μM phenylacrylic acid for 10 min on ice. The protein solution was then directly introduced into the mass spectrometer. The prFMN-substrate adduct was then dissociated from the protein *in situ*, allowing the mass of the adduct to be determined before it could decompose.
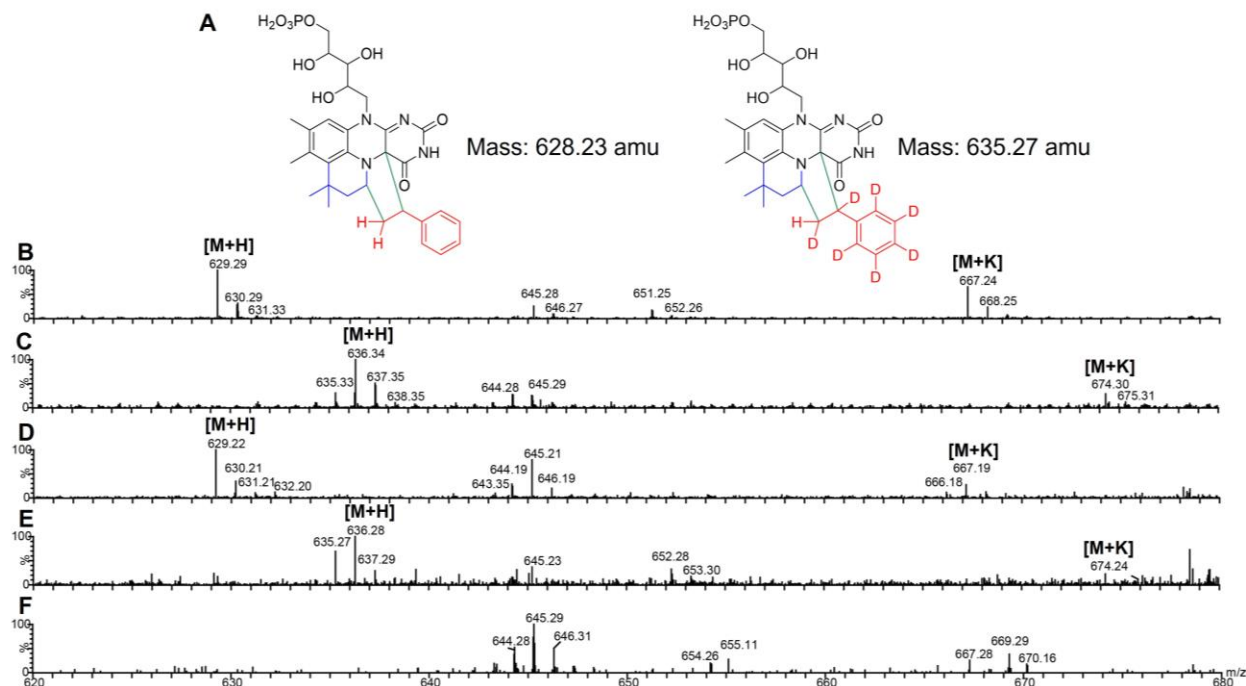
Figure 2.2: Identification of the prFMN-styrene cycloadduct reaction intermediate by native MS. A) Structures of the proposed unlabeled and deuterated prFMN-styrene cycloadducts. **B)** FDC reacted with phenylacrylic acid; the peaks at 629.29 and 667.24 correspond to the styrene cycloadduct complexed with a proton and a potassium ion, respectively. **C)** FDC reacted with d_7-phenylacrylic acid; the peaks at 636.34 and 674.30 correspond to the deuterated styrene cycloadduct complexed with a proton and a potassium ion, respectively. **D)** FDC reacted with styrene; the peaks at 629.22 and 667.19 similarly correspond to the styrene cycloadduct complexed with a proton and a potassium ion, respectively. **E)** FDC reacted with d_8-styrene; the peaks at 636.28 and 674.24 correspond to the deuterated styrene cycloadduct complexed with a proton or a potassium ion, respectively. **F)** Unreacted FDC. The peak at 645.29, which is present in all spectra, is likely due to small amounts of a prFMN-phenylpyruvate adduct, as noted previously.[16]

The mass spectrum of the prFMN-substrate adduct (Figure 2.2B, D) showed two peaks at

$m/z = 629.29$ and 667.24 that matched exactly the expected values for the cycloaddition adduct

of prFMN with styrene complexed with either a proton or a K^+ ion, respectively. These peaks

were absent in control samples (Figure 2.2F). The same adducts were observed whether the

enzyme was reacted with phenylacrylic acid or with styrene, indicating that the styrene-prFMN

cycloadduct is the species that accumulates on the enzyme at equilibrium. The identity of the

adduct was further confirmed when FDC was reacted with either d_8-styrene or d_7-phenylacrylic

acid. In this case, the masses of the peaks due to the adduct were shifted higher by 7 a.m.u. to

$m/z = 636.34$ and 674.30 due to the presence of the deuterium label (Figure 2.2C, E). The loss of

one deuterium atom from the adduct with d_8-styrene is explained by the enzyme-catalyzed exchange of the proton at the site of (de)carboxylation[30] through the transient formation of the deprotonated intermediate **D**, shown in Figure 1.5.

2.3.3 Pre-steady State Kinetic Analysis

Having established that the intermediate that accumulates on the enzyme is the cyclo-addition adduct of prFMN with styrene, we proceeded to investigate the kinetics of its formation from phenylacrylic acid in more detail using stopped-flow U.V.-visible spectroscopy. Holo-FDC, 165 µM, was reacted with 1 mM phenylacrylic acid (final concentrations after mixing) at 4 ℃ in the stopped-flow spectrometer and U.V.-visible spectra were recorded between 300 and 800 nm at various times over a period of 12.5 s. The spectra were characterized by an increase in absorbance at 460 nm and a decrease at 380 nm, indicating the accumulation of a prFMN-substrate adduct (Figure 2.3). After 1 s, the spectrum closely matched that of the enzyme reacted with styrene, which is consistent with the styrene-prFMN cycloadduct being the intermediate that accumulates at equilibrium. Signs of photodegradation were observed after 3 seconds, so in subsequent stopped-flow experiments data collection was limited to the first second of reaction.
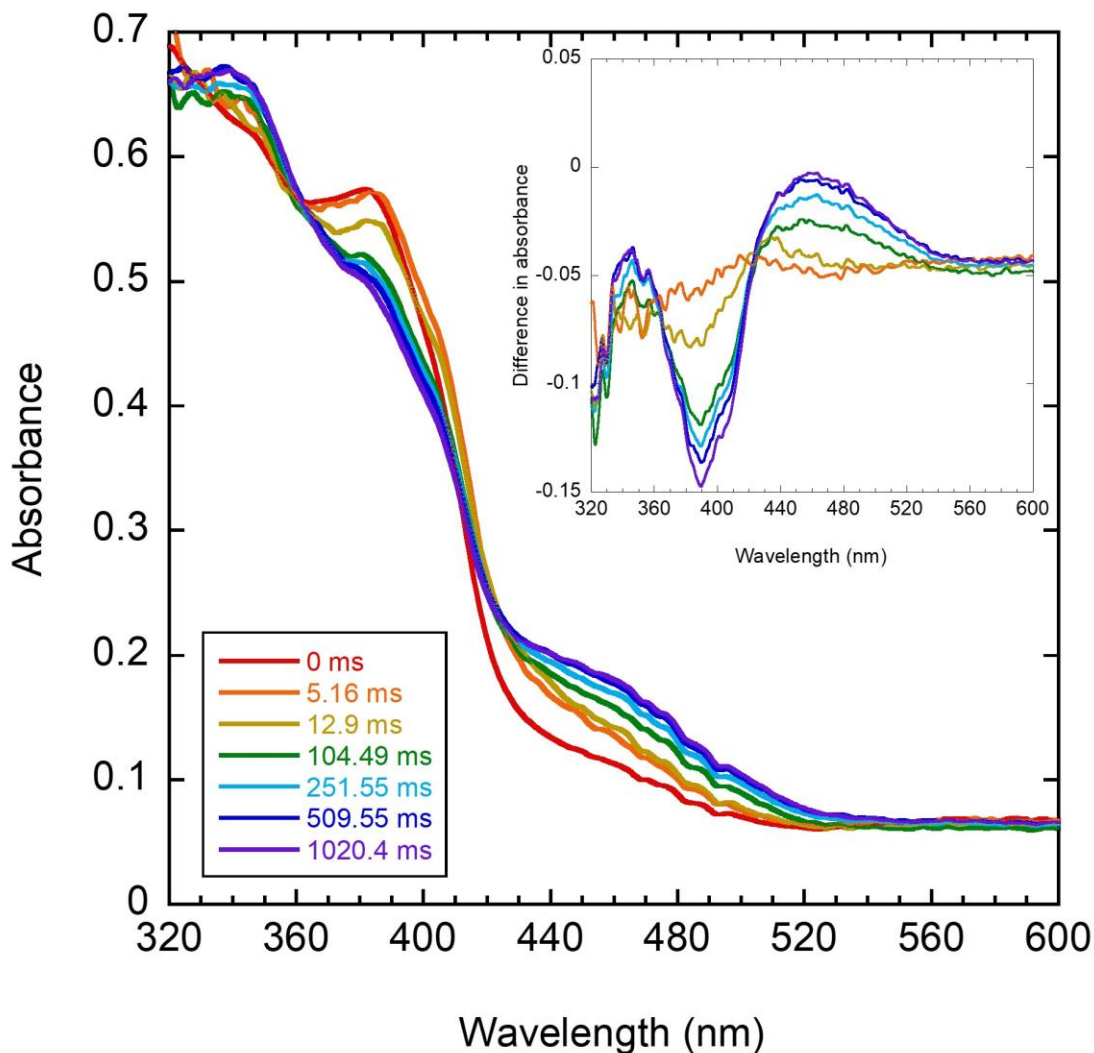
Figure 2.3: Pre-steady state spectral changes observed in reaction of FDC with phenylacrylic acid. Representative spectra are shown recorded at times ranging from 5 ms to 1 s after mixing. The final enzyme and substrate concentrations were 165 μM and 1 mM, respectively. The zero-time point spectrum was recorded by mixing FDC with buffer in the stopped-flow instrument. Inset: Difference spectra calculated by subtracting the zero-time point spectrum of FDC.

The steady-state kinetic parameters for FDC were determined under the conditions used for the stopped-flow experiments: 4 ℃ in 50 mM potassium phosphate, 10% glycerol pH 7.5. Under these conditions, k_{cat} for the decarboxylation of phenylacrylic acid was 11.3 ± 0.6 s^{-1} and K_M was 60 ± 9 μM (Figure 2.4). Therefore, in the stopped-flow experiments with substrate only in a small molar excess over enzyme (~6-fold), the reaction would have reached chemical equilibrium within a few turnovers and well within the initial 1 s of the experiment. This

information coupled with our above characterization of the styrene-prFMN cycloadduct indicates

that this stable substrate-prFMN adduct is the styrene-prFMN cycloadduct.
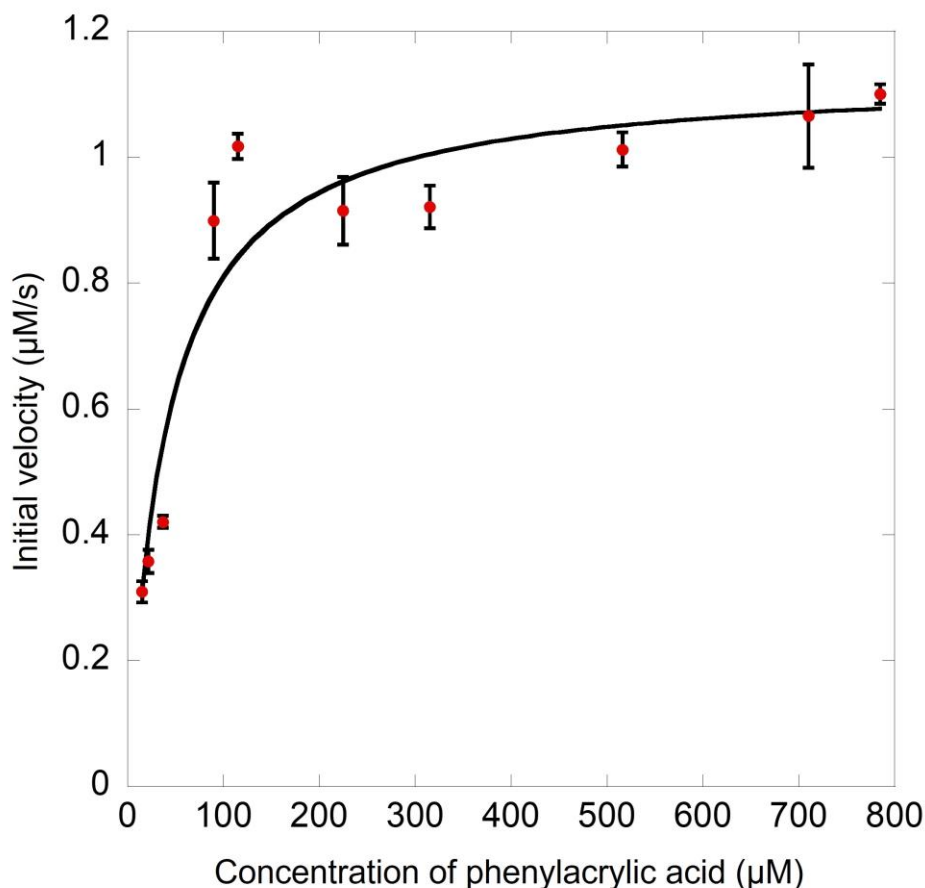
Figure 2.4: Steady-state kinetic analysis of FDC with phenylacrylic acid as substrate as determined at 4 °C.
$k_{cat} = 11.3 \pm 0.6$ s^{-1} and K$_M$ = 60 ± 9 μM.

Based on the spectral changes we observed in the initial experiments, we chose 4

wavelengths to monitor the kinetics of the reaction using monochromatic light so that

photochemistry was minimized: 380 and 460 nm were selected because these wavelengths

exhibited the largest absorbance changes, whereas 344 nm exhibited smaller absorbance

changes. Lastly, we selected 425 nm, which from initial experiments appeared to be an isosbestic

point, however, as discussed below, this is not in fact the case. As noted in the Materials and

Methods section, individual traces at each wavelength were binned and averaged to improve

signal to noise and to allow for more traces to be used in the full-length time analysis. An example of the binning and averaging protocol is shown below in Figure 2.5.
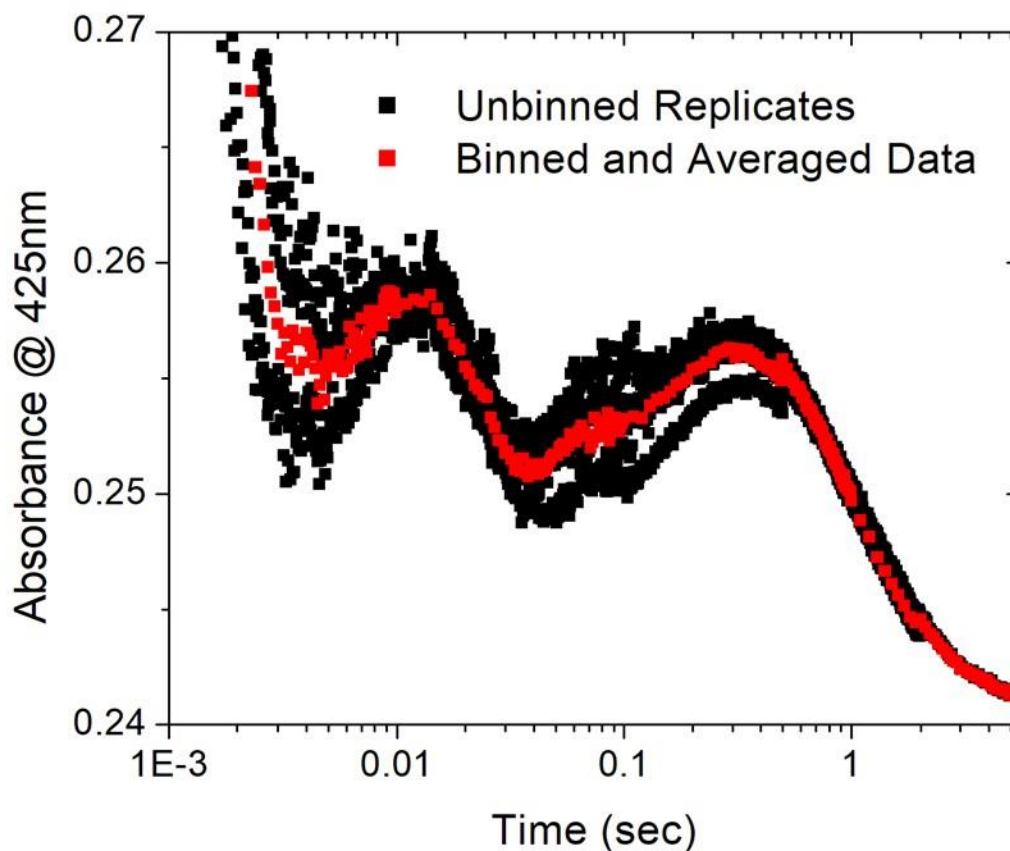
Figure 2.5: Improvement of signal-to-noise obtained by averaging of stopped-flow kinetic data. Black traces represent replicates before averaging. Red traces represent the averaged data after applying the binning procedure described in the Materials and Methods section.

Representative traces from single-wavelength stopped-flow kinetic experiments are shown in Figure 2.6. At each of the wavelengths investigated, multiple kinetic phases were observed within the first second. These spectral changes are sufficiently rapid to represent the kinetics of reactions occurring on the enzyme that are likely to have mechanistic significance. Traces were fitted to a series of exponential functions using the program KaleidaGraph to obtain values for the amplitudes and observed rate constants associated with each phase:

$$A_{(t)} = A_0 + A_1 e^{(-k_{obs1}*t)} + A_2 e^{(-k_{obs2}*t)} \ldots \qquad (2.1)$$

Where A_0 is the initial absorbance, and $A_{(n)}$ and $k_{obs(n)}$ for n = 1, 2, 3, 4 are the amplitude and

observed rate constant, respectively, associated with phase n. In each trace, there is an initial

very rapid decrease in absorbance that occurs largely within the mixing time of the spectrometer

with k_{obs} >1000 s^{-1}. This may represent changes to the absorption characteristics of the cofactor

in response substrate binding. At slower timescales, the spectral changes depend upon the

wavelength as described below.
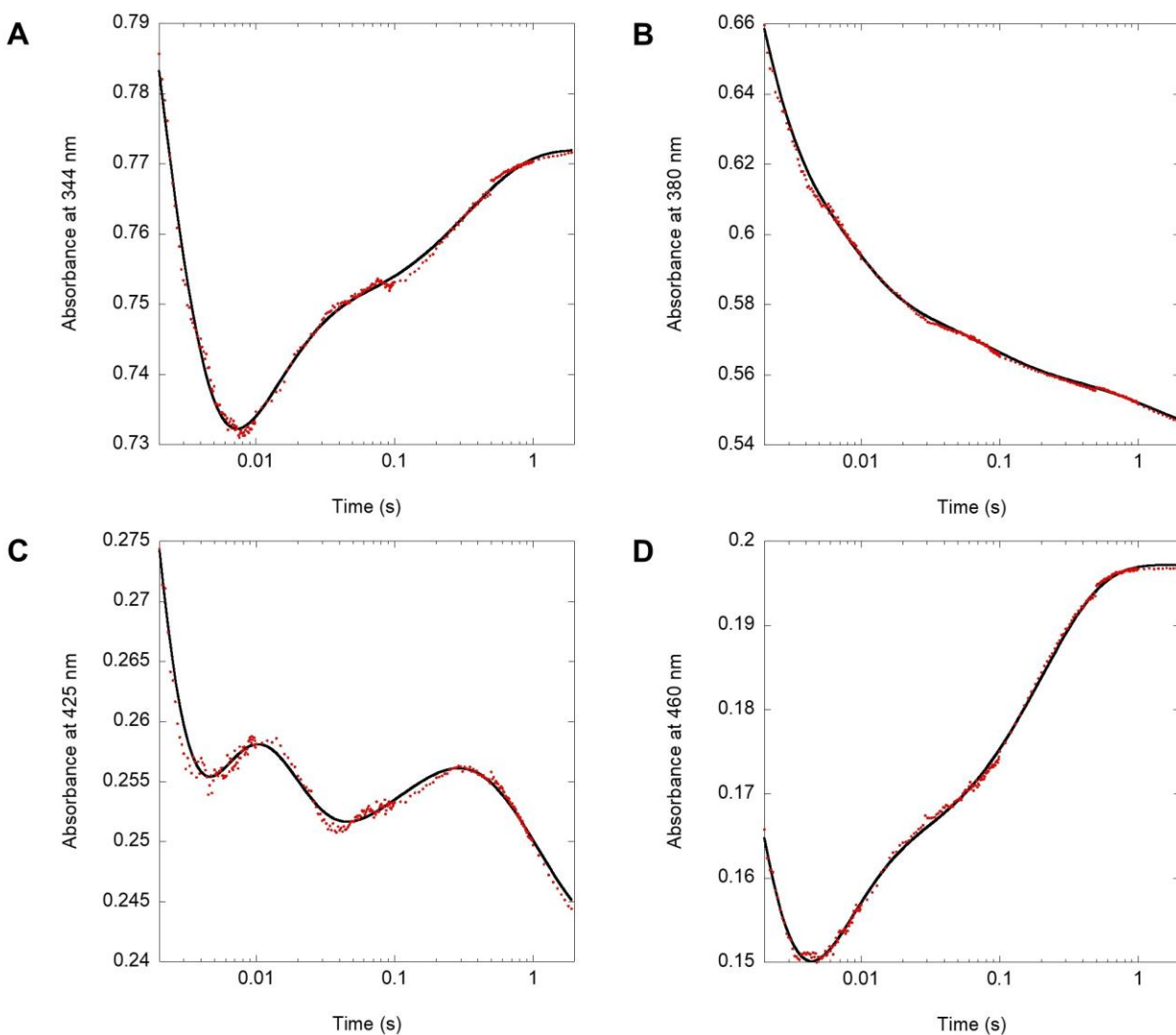
Figure 2.6: Pre-steady state kinetics for FDC reacting with phenylacrylic acid. The reaction of FDC (165 µM) with phenylacrylic acid (1 mM) was monitored at 4 representative wavelengths and the absorbance changes were fitted to exponential functions. **A)** 344 nm, fitted to a three-exponential function. **B)** 380 nm, fitted to a four-exponential function. **C)** 425 nm, fitted to a five-exponential function. **D)** 460 nm, fitted to a three-exponential function. The traces shown are averaged using the procedure described in the Materials and Methods section. Similar fits were obtained from non-averaged data (Figure 2.7).

At 380 nm, two main phases are observed that occur with k_{obs} ~130 s^{-1} and k_{obs} ~7 s^{-1} (Figure 2.6B). We note that a further, very slow decrease in absorbance was also observed at this wavelength that required an additional exponential function to adequately fit the data. It is unclear why this occurs, but it appears too slow to represent catalysis. Comparably, there are two phases observed at 460 nm characterized by similar but opposite amplitudes with k_{obs} ~114 s^{-1}

and k_{obs} ~5 s^{-1} (Figure 2.6D). We consider that the biphasic increase in absorbance at 460 nm over time most likely represents the accumulation of the prFMN-styrene cycloadduct on the enzyme, which our mass spectrometry measurements and recent crystallographic studies[35] indicate is the enzyme species that accumulates at chemical equilibrium.

When the reaction was monitored at 344 nm, we observed kinetic behavior similar to that observed at 460 nm (Figure 2.6A). More complex kinetic behavior was observed when the reaction was monitored at 425 nm. In this case, there is an initial increase in absorbance followed by a partial decrease before a second slight rise and final slower decrease (Figure 2.6C). Although the absorbance changes at these wavelengths are quite small and the data are therefore somewhat noisy, this kinetic behavior was observed over multiple shots. The apparent rate constants and amplitudes calculated from fitting these traces are reported in Table 2.1.
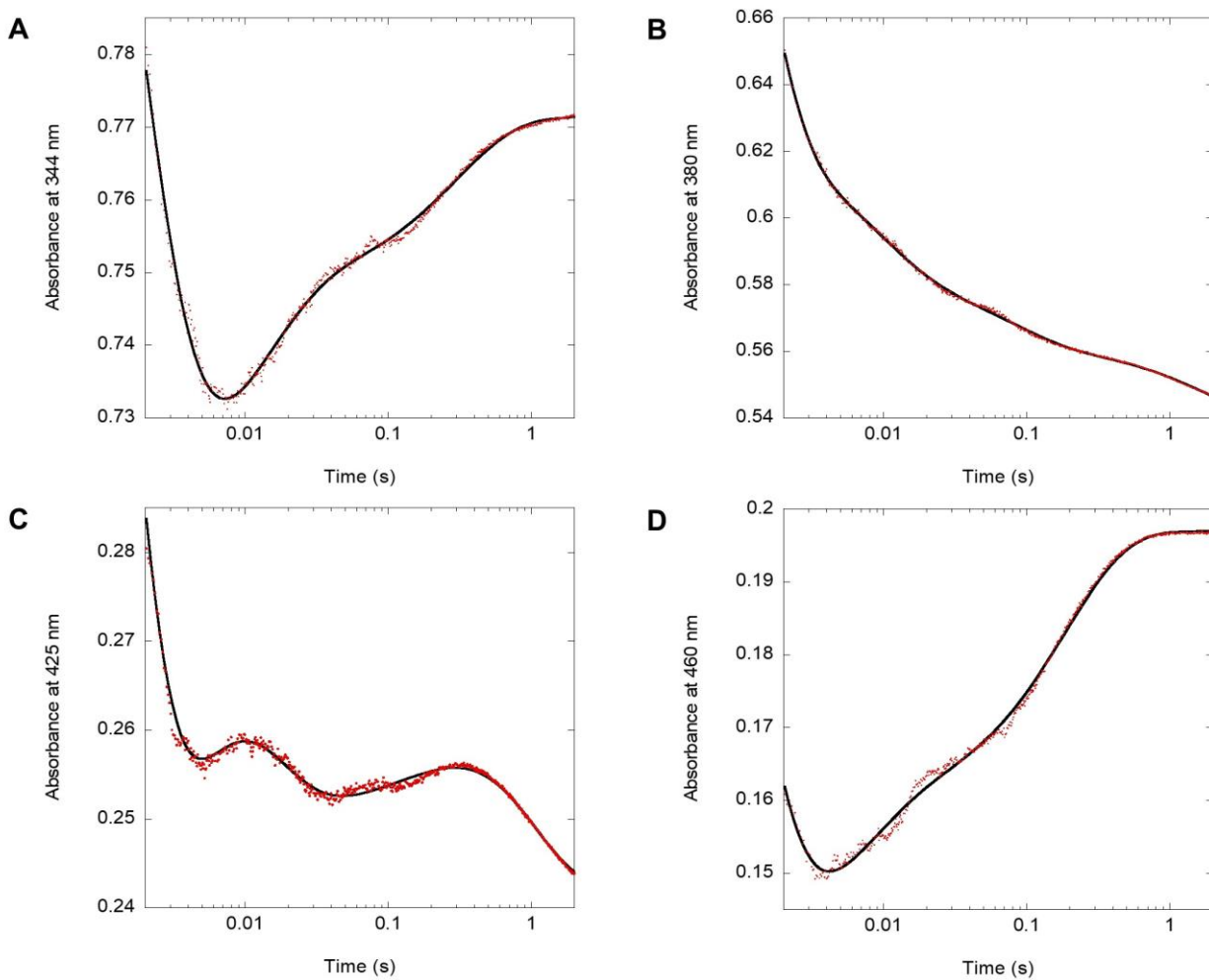
Figure 2.7: Pre-steady state kinetics for FDC reacting with phenylacrylic acid – fits to non-averaged traces.
The reaction of FDC (165 µM) with phenylacrylic acid (1 mM) was monitored at 4 representative wavelengths and the absorbance changes were fit to exponential functions. **A)** 344 nm, fitted to a three-exponential function. **B)** 380 nm, fitted to a four-exponential function. **C)** 425 nm, fitted to a five-exponential function. **D)** 460 nm, fitted to a three-exponential function. In this case, the fits are to representative traces rather than averaged data (shown in Figure 2.6). The fits are similar.

Table 2.1: Amplitudes and apparent rate constants for single wavelength traces.

Wavelength (nm)	Substrate concentration (μM)	A_1	$k_{obs,1}$ (s^{-1})	A_2	$k_{obs,2}$ (s^{-1})	A_3	$k_{obs,3}$ (s^{-1})	A_4	$k_{obs,4}$ (s^{-1})	R^2
344	1000			-0.0324 ± 0.0007	82 ± 3	-0.0241 ± 0.0002	2.92 ± 0.08			0.99699
344	700			-0.0251 ± 0.0004	71 ± 2	-0.0225 ± 0.0002	2.98 ± 0.08			0.99742
344	500			-0.0292 ± 0.0006	75 ± 3	-0.0207 ± 0.0003	3.9 ± 0.2			0.99529
344	150			-0.0274 ± 0.0004	58 ± 2	-0.0122 ± 0.0004	2.3 ± 0.3			0.99255
380	1000			0.0621 ± 0.0006	130 ± 2	0.0243 ± 0.0003	7.2 ± 0.2			0.99855
380	700			0.0466 ± 0.0005	123 ± 3	0.0198 ± 0.0004	12.1 ± 0.4			0.99873
380	500			0.0532 ± 0.0009	137 ± 5	0.0193 ± 0.0007	14.1 ± 0.9			0.99652
380	150			0.0634 ± 0.0007	116 ± 2					0.99598
425	1000	-0.06 ± 0.03	182 ± 35	0.05 ± 0.03	95 ± 16	-0.0181 ± 0.0009	5.6 ± 0.4	0.0246 ± 0.0010	1.07 ± 0.05	0.98978
425	700	-0.054 ± 0.007	203 ± 23	0.042 ± 0.008	74 ± 9	-0.0145 ± 0.0007	8 ± 1	0.0189 ± 0.0009	1.32 ± 0.08	0.98785
425	500	-0.06 ± 0.02	200 ± 37	0.05 ± 0.02	80 ± 20	-0.011 ± 0.003	15 ± 3	0.0221 ± 0.0003	0.75 ± 0.04	0.98714
425	150	-0.05 ± 0.05	142 ± 52	0.03 ± 0.05	72 ± 55	0.011 ± 0.003	12 ± 4	0.0170 ± 0.0005	0.86 ± 0.07	0.98906
460	1000			-0.0204 ± 0.0005	114 ± 5	-0.0356 ± 0.0002	4.87 ± 0.08			0.99833
460	700			-0.0231 ± 0.0005	115 ± 5	-0.0305 ± 0.0003	6.7 ± 0.1			0.99798
460	500			-0.0303 ± 0.0006	114 ± 4	-0.0249 ± 0.0002	6.6 ± 0.1			0.99865
460	150			-0.0319 ± 0.0003	93 ± 2	-0.0162 ± 0.0002	4.2 ± 0.2			0.99764

To obtain further information on this complex pre-steady state kinetic behavior, we investigated the effect of lowering the substrate concentration on the reaction kinetics. The enzyme was reacted with 700 μM, 500 μM or 150 μM phenylacrylate (final concentrations after mixing), with the lowest concentration representing an approximately stoichiometric ratio of enzyme to substrate, and the reaction was monitored at the same wavelengths described above. The concentration-dependent kinetics for the reaction are shown in Figure 2.8 and the apparent rate constants and amplitudes calculated from fitting the kinetic traces obtained at the various wavelengths and substrate concentrations are reported in Table 2.1.
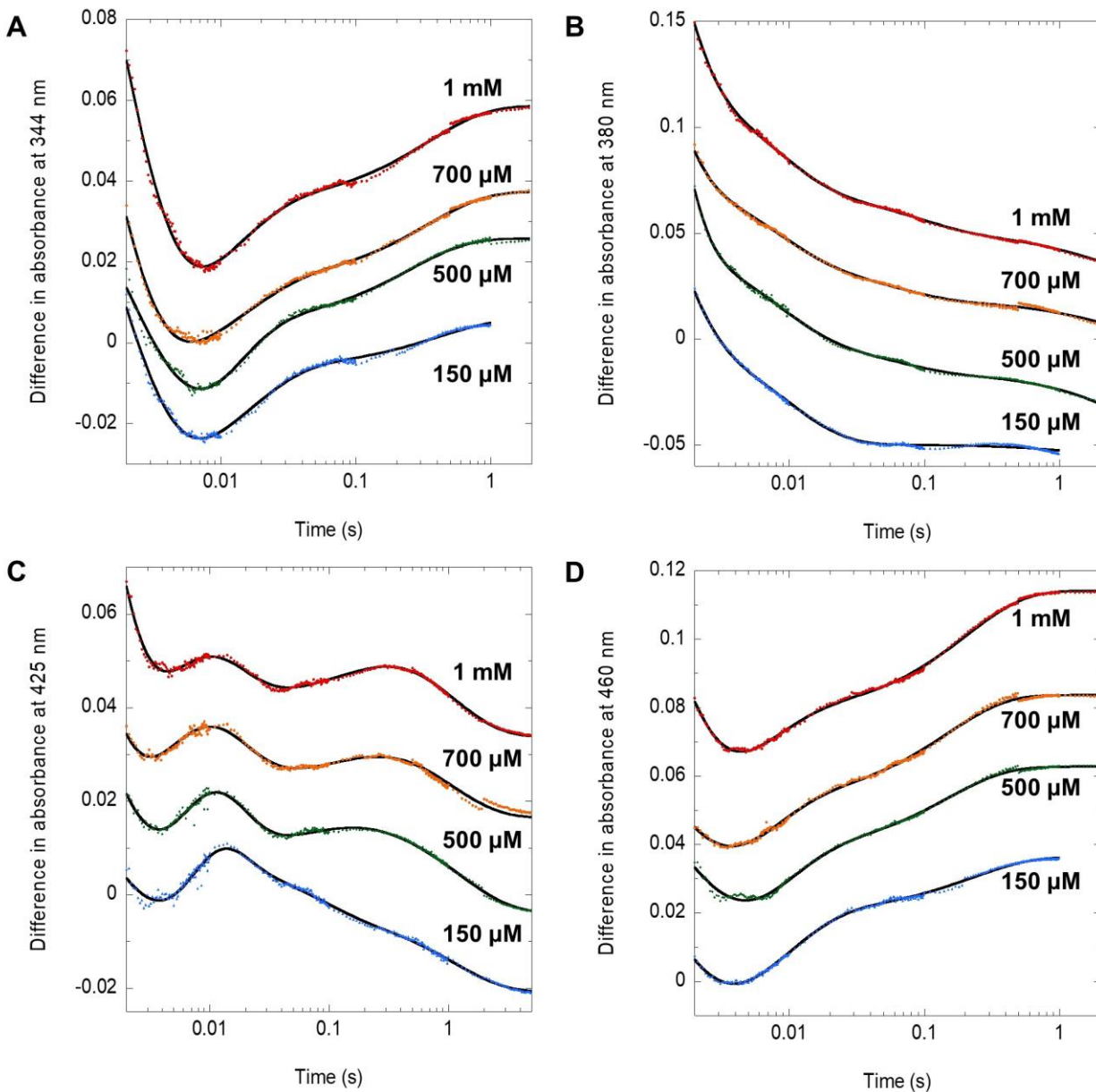
Figure 2.8: Concentration dependence of spectral changes observed for reaction of FDC with phenylacrylic acid. The reaction of FDC (165 µM) with phenylacrylic acid (1 mM) was monitored at 4 representative wavelengths: **A)** 344 nm; **B)** 380 nm; **C)** 425 nm; **D)** 460 nm. The traces have been offset for clarity and the absorbance changes were fitted to exponential functions as described in Figure 2.6.

Although the apparent rate constants associated with the various reaction phases change little, there are marked changes in the amplitudes associated with these phases. Notably, the slower two phases are reduced in amplitude, whereas the faster two phases increase slightly in amplitude as the substrate concentration is lowered. This effect becomes most pronounced when

the substrate and enzyme are in stoichiometric concentrations and is especially evident at 425 nm

(Figure 2.8). The concentration-dependence of the reaction suggested that FDC may exhibit half-

of-sites reactivity arising from negative cooperativity between the two subunits of the dimeric

enzyme. Such behavior is not uncommon in oligomeric enzymes and has been well-studied in

other enzymes, an example being the homodimeric enzyme thymidylate synthase.[65, 66] In the

present case, the data suggest a tighter-binding 'fast' subunit and a weaker-binding 'slow'

subunit.

2.3.4 Global Analysis

The data obtained at the various wavelengths shown in Figure 2.6 illustrate the

complicated nature of the kinetic behavior observed. Therefore, rather than attempt to fit the data

from each specific wavelength to a kinetic model, we recorded a complete set of time-dependent

spectra for the reaction of 165 μM FDC with 1 mM phenylacrylic acid. This data set was

obtained using a charge coupled device stopped-flow spectrophotometer and the data subjected

to global analysis using the program Kintek Explorer. Experiments were analyzed as difference

spectra by subtracting the initial spectrum at ~2.0 ms from each subsequent spectrum. Spectra

were first filtered by singular value decomposition (SVD)[62] to decrease noise and the four most

significant components (Figure 2.9) were used for further analysis using Kintek Explorer using

the apparent rate constants estimated from fitting the single-wavelength data at 425 nm as initial

values for the model.
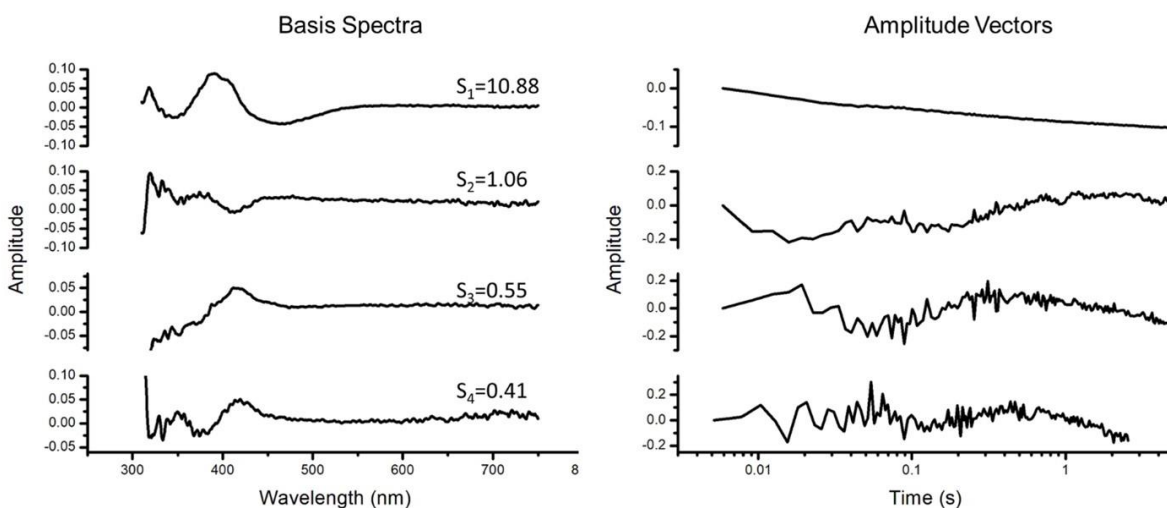
Figure 2.9: Singular value decomposition of a representative stopped-flow experiment of 165 μM FDC reacting with 1 mM phenylacrylic acid.

The data were reasonably fitted by the scheme below (Figure 2.10) that assumes rapid substrate binding and that the two active sites on the enzyme, a and b, react with different kinetics, i.e., half-of-sites reactivity. An initial, fast substrate-binding step to form the Michaelis complex on either subunit a or b of the FDC dimer is followed by 2 kinetically distinct steps (I_{1a}, I_{1b}, I_{2a}, and I_{2b} in the reaction scheme, Figure 2.10) through which the Michaelis complex is converted first to the phenylacrylate-prFMN cycloadduct and then to the final styrene-prFMN cycloadduct that accumulates on the enzyme. The choice of a mechanism with 4 measurable kinetic steps was dictated as the minimum needed to model the changes in the absorbance observed at 425 nm. Attempts to fit the data with fewer kinetic intermediates yielded significantly worse fits.
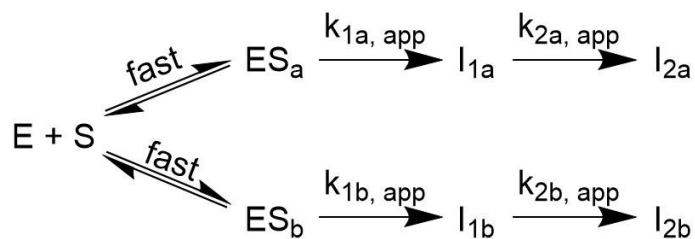
Figure 2.10: Scheme 1.

The apparent rate constants calculated from fitting the data to the half-of-sites model are given in Table 2.2. The experimental data fit well to this kinetic model; representative fits of the model to the data at 344, 380, 425 and 460 nm are shown in Figure 2.11. We assumed that although the half-of-sites reactivity allowed for differing kinetic profiles between the two active sites of the FDC dimer, the spectra of the intermediates would be the same for each active site. Using this model, we ascribe the fastest phase, described by $k_{1a,app}$, to the formation of the cycloadduct between phenylacrylate and prFMN (intermediate **C** in Figure 1.5) at the fast site. The slower phase described by $k_{2a,app}$, is ascribed to the conversion of **C** to **E**, the prFMN-styrene cycloadduct, at the fast site. Similarly, $k_{1b,app}$ and $k_{2b,app}$ are ascribed to the formation of intermediate **C,** and its subsequent conversion to **E**, at the slow site.

Table 2.2: Apparent rate constants calculated from global fitting of pre-steady state kinetic data.

Parameter	Value (s^{-1})	Standard error (s^{-1})
$k_{1a,app}$	131	7
$k_{2a,app}$	75	4
$k_{1b,app}$	4.5	0.1
$k_{2b,app}$	0.55	0.02
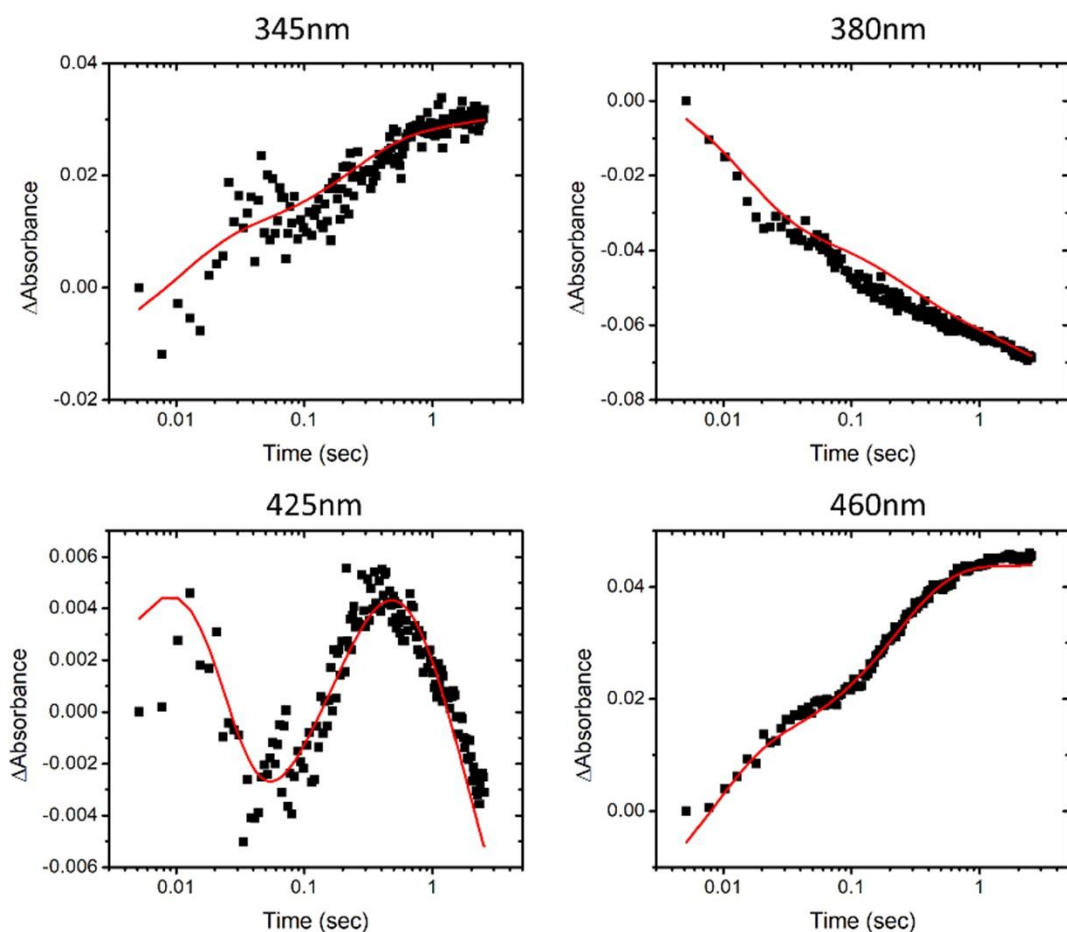
Figure 2.11: Comparison of model (red line) and data (black squares) at different wavelengths from global analysis of a representative experiment of 165 µM FDC reacting with 1 mM phenylacrylic acid. Data modeled assuming half-of-sites reactivity (Figure 2.10) and that each subunit had identical spectroscopic parameters.

The component spectra of the intermediates calculated from global fitting are shown as difference spectra in Figure 2.12, left. The difference spectrum of the initially formed intermediate, I_1 (intermediate **C** in Figure 1.5), is distinguished by a positive absorption peak at 425 nm with shoulder extending to ~520 nm, and a negative absorbance at 390 nm. In comparison, the later intermediate I_2 (intermediate **E** in Figure 1.5) is characterized by difference spectra with a large negative peak at 390 nm and a broad positive peak at ~460 nm. This latter

61

spectrum matches well to the spectrum of the stable styrene-prFMN cycloadduct obtained by

reaction of styrene to FDC.
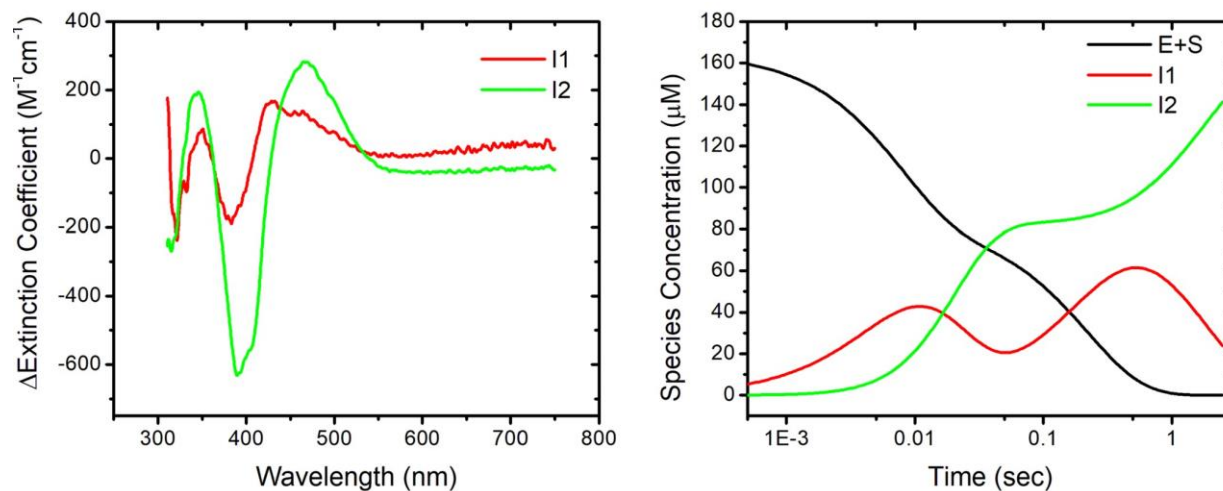
Figure 2.12: Global fitting of pre-steady state kinetic data for FDC reacting with phenylacrylic acid. *Left*: Difference spectra calculated for the intermediates I_1 and I_2, in Figure 2.10 (a and b active sites assumed to have the same spectra). *Right*: Calculated time course for the accumulation and decay of reaction intermediates in Figure 2.10. Data fitting performed using the program KinTek Explorer.

The spectrum of the first intermediate to form is very similar to that of the adduct formed

by reacting FDC with 2-fluoro-2-nitro-vinylbenzene, which is a mechanism-based inhibitor that

mimics the structure of phenylacrylate. This adduct was previously characterized, demonstrating

by native tandem MS analysis that it reacts to form a cycloadduct with prFMN.[32] These

observations support the idea that the transiently formed intermediate is the phenylacrylate-

prFMN cycloadduct (intermediate **C** in Figure 1.5). The spectrum is unlikely to represent the

other proposed prFMN adduct – the phenylethylene adduct formed after decarboxylation

(intermediate **D** in Figure 1.5) – because, by analogy with the spectra of model flavin

compounds, this species is expected to have absorption maxima at ~350 nm with a lower

intensity band that extends out to ~800 nm.[16]

That the complicated spectral signature of this reaction can be modeled using 3 spectral

components (ES, I_1, and I_2) is consistent with our proposal for half-of-sites reactivity. The

structural details of how substrate binding at one active site may introduce asymmetry into the FDC homodimer that could result in differing reaction kinetics will require further study. It is worth noting that the apparent rate constant for the formation of the final intermediate, $k_{2b,app}$ = 0.55 s^{-1}, is an order of magnitude slower than k_{cat} = 11.3 s^{-1} measured under the same conditions. This observation suggests that the enzyme-prFMN-styrene cycloadduct that ultimately accumulates on the enzyme may not represent a true, kinetically competent intermediate, but rather may be a product-inhibited form of the enzyme.

2.4 Conclusions

This chapter presents the first detailed kinetic analysis of a member of the recently identified and rapidly expanding family of prFMN-dependent decarboxylases. We demonstrate that the species that accumulates on the enzyme is the cycloadduct of styrene with prFMN. This implies that cycloelimination of this adduct to release the product is most likely the rate-determining step in catalysis, consistent with the Marsh laboratory's earlier Hammett analysis of FDC.[30] FDC exhibits complicated pre-steady state kinetic behavior that can be ascribed to half-of-sites reactivity, with one subunit of the FDC dimer reacting an order of magnitude faster than the other. These studies have allowed the apparent rate constants for the reaction of prFMN with phenylacrylate to be determined. For the fast site, formation of the initial cycloadduct of phenylacrylate with prFMN occurs with k_{app} ~130 s^{-1}; the conversion of this intermediate to the decarboxylated cycloadduct of prFMN with styrene occurs with k_{app} ~75 s^{-1}; finally, cycloelimination of the product and diffusion from the active site is likely the rate-determining step represented by k_{cat} = 11.3 s^{-1}. The spectral changes described by k_{app} of 4.5 s^{-1} and 0.55 s^{-1} are thought to be due to reaction at the slower second subunit and appear to be too slow to be kinetically competent.

Chapter 3 Negative Cooperativity in the Mechanism of Ferulic Acid Decarboxylase: A Proposal for a "Two-Stroke" Decarboxylation Cycle[2]

3.1 Introduction

Enzyme-catalyzed decarboxylation reactions are ubiquitous in both primary and secondary metabolism; however, decarboxylation reactions often proceed through highly unfavorable transition states associated with the accumulation of negative charge on the α-carbon.[47, 48] Therefore, Nature has evolved a remarkably diverse range of cofactors that can function as electron sinks in decarboxylation reactions; well-studied examples include pyridoxal phosphate and thiamine pyrophosphate, and Lewis acidic metal ions.[49-51] Decarboxylases have also attracted considerable interest for their ability to function as "green" catalysts capable of catalyzing both decarboxylation and C-C bond forming reactions under mild conditions.[52, 53]

The most recently discovered decarboxylation cofactor is prenylated FMN (prFMN). This cofactor appears to be widespread in microbes and is used to facilitate decarboxylation reactions at sp[2]-hybridized carbon atoms in double bonds and aromatic rings that otherwise would be unreactive.[15, 16, 36, 56-58, 67] In prFMN, the isoalloxazine ring system of the flavin is modified by the addition of a 4th ring that bridges the flavin C6 and N5 positions and is derived from an isoprene unit. This modification is performed by a specialized prenyltransferase that

uses reduced FMN and either dimethylallyl phosphate (in bacteria)[17] or dimethylallyl pyrophosphate (in yeast)[37] as substrates.[38] prFMN-dependent decarboxylases are often referred to as UbiD-like decarboxylases after UbiD, the enzyme that catalyzes the decarboxylation of 4-hydroxy-3-octaprenylbenzoic acid to 2-octaprenylphenol as part of ubiquinone biosynthesis in many bacteria.[5, 7, 59]

Ferulic acid decarboxylase (FDC)[16, 32, 58] was the first UbiD-like enzyme to be structurally characterized in its holo-form, leading to the identification of prFMN. Today, FDC remains the best understood member of the UbiD family. The decarboxylation mechanism involves an unusual 1,3-dipolar cycloaddition between the substrate and prFMN, as shown in Figure 1.5 for the decarboxylation of phenylacrylic acid.[16, 32] The crystal structures[35] of the enzyme reacted with either substrates or substrate analogs that form covalent adducts with prFMN support the formation of several of the intermediates shown in Figure 1.5. Complementary evidence comes from high resolution native mass spectrometry experiments that allowed the cycloadducts of prFMN with the product, styrene, and with a mechanism-based inhibitor mimicking the structure of the substrate, phenylacrylate, to be identified.[32, 68] Computational studies that model the energetics of forming cycloadducts between prFMN and phenylacrylic acid further support the feasibility of the mechanism.[31]

In contrast to the identity of the chemical intermediates in the FDC mechanism, which are supported by various lines of experiment, the kinetics of the FDC-catalyzed reaction have not been extensively investigated. In Chapter 2, I described pre-steady state kinetic analyses of FDC from *S. cerevisiae* reacting with phenylacrylic acid that uncovered complex kinetic behavior that most likely arises from negative cooperativity between the two active sites of the enzyme dimer.[68] In this chapter, we extend our kinetic analysis of FDC by using stopped-flow absorption

spectroscopy to examine the reaction of the enzyme with both styrene and phenylacrylate at concentrations ranging from sub-stoichiometric to several-fold molar excess. Based on our experiments, we propose a "two-stroke" mechanism for the FDC-catalyzed reaction in which conformational changes transmitted between the two subunits drive the release of styrene from the active site to complete the catalytic cycle.

3.2 Materials and Methods

3.2.1 Reagents

trans-Phenylacrylic acid and styrene were purchased from Sigma-Aldrich Co. All other materials were purchased from Sigma-Aldrich Co. or Thermo Fisher Scientific Co.

3.2.2 Expression and Purification of FDC

Expression and purification of recombinant *S. cerevisiae* holo-FDC from *E. coli* were performed as described previously.[15, 68] In short, a pET28b plasmid containing in tandem *tPAD* (not tagged) and *FDC* with a C-terminal 6x-His tag was transformed into *E. coli* BL21 DE3 star (Invitrogen). *E. coli* cultures were grown at 37 °C in LB supplemented with 50 μg/mL kanamycin. Once an OD_{600} of 0.6 – 0.8 was reached, cultures were induced with 0.2 mM IPTG and incubated at 18 °C overnight (~18 h). Cells were harvested by centrifugation and either immediately purified or stored at -20 °C.

Cell pellets were resuspended in Buffer A (50 mM potassium phosphate, 500 mM potassium chloride, 5 mM imidazole pH 7.5; 4 mL of Buffer A/1 g of cell pellet), EDTA-free protease inhibitor tablets (Roche), lysozyme (4 mg lysozyme/1 g of cell pellet), and Benzonase nuclease (Sigma-Aldrich). Cells were lysed via sonication (10 s pulses with 30 s pauses for a total of 15 min of sonication) and the resulting lysate clarified by centrifugation at 18,500 rpm at

4 °C for 45 min. The supernatant was loaded onto a HisTrap column (GE Healthcare) equilibrated with Buffer A. Due to a previous report[19] that found prolonged light exposure could inactive FDC, the HisTrap column was wrapped in foil to reduce light exposure. (However, we would like to note that this inactivation had not been observed with any of our FDC preps.) Protein purification was performed using a Bio-Rad NGC chromatography system. The protein loaded on the HisTrap column was first washed with Buffer A and then increasing percentages of Buffer B (50 mM potassium phosphate, 500 mM potassium chloride, 500 mM imidazole pH 7.5). First, a 10% Buffer B wash (55 mM imidazole) and then a 20% Buffer B wash (104 mM imidazole) were performed to remove undesired proteins. To obtain concentrated FDC, FDC was eluted with a 100% Buffer B wash (500 mM imidazole). The FDC fractions were immediately placed in a covered ice bucket to minimize light exposure. Fractions were analyzed by SDS-PAGE on a 10% gel (BioRad) and then desalted into Buffer C (50 mM potassium phosphate, 20% (v/v) glycerol pH 7.5) using PD-10 desalting columns (GE Healthcare). All purified FDC were flash-frozen and stored at -80 °C. The cofactor content of the purified holo-enzyme was evaluated by U.V.-visible spectroscopy and LC-MS and found not to vary significantly from batch to batch. The U.V.-visible and mass spectra of a typical batch of holo-enzyme is shown in Figure 3.1.
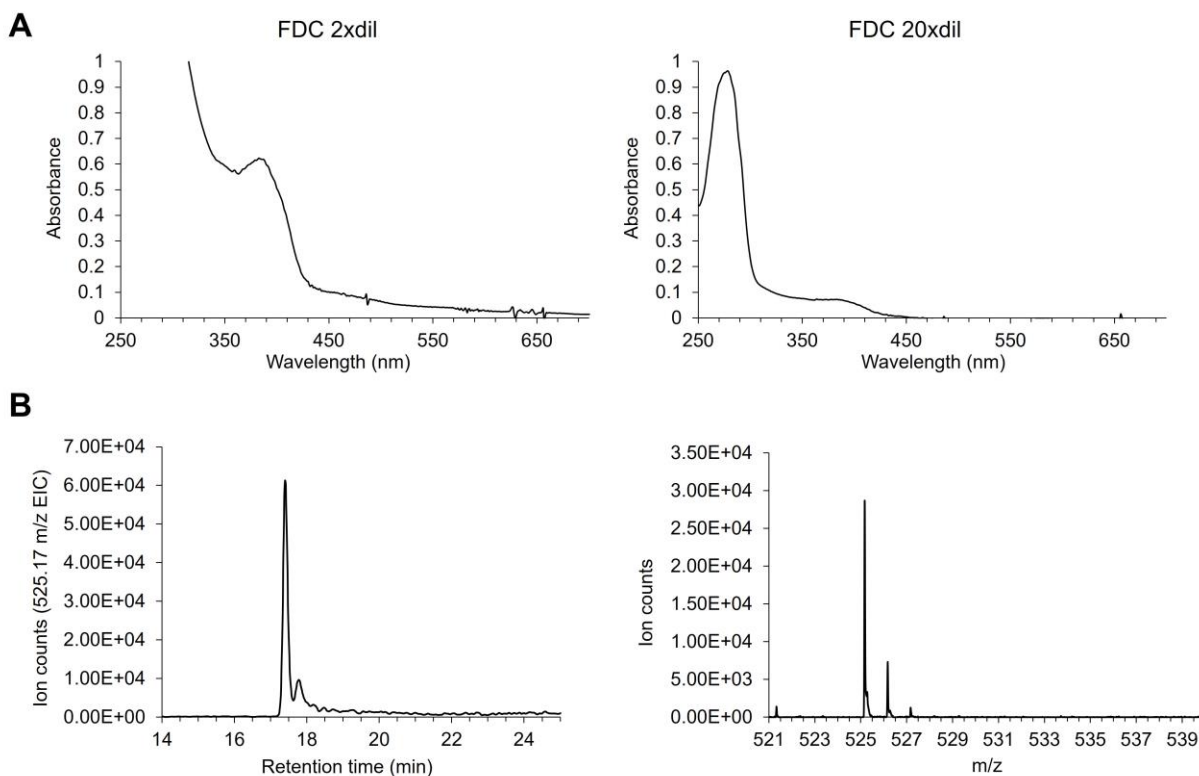
Figure 3.1: U.V.-visible spectra and LC-MS analysis of prFMN from a representative batch of holo-FDC used in stopped-flow experiments. A) U.V.-visible spectrum of a sample of purified holo-FDC diluted from a stock solution either 2-fold (to record the spectral features of the bound prFMN) or 20-fold (to record the protein peak at 280 nm). **B)** LC-MS analysis of prFMN isolated from holo-FDC. *Left*: Chromatograph of prFMN monitored by extracted ion count. *Right*: Mass spectrum (ESI) of the peak at 17.5 min showing the expected mass for prFMN.

3.2.3 Stopped-flow Absorption Spectroscopy

Experiments were performed using a Hi-Tech Scientific SF-61 DX2 double-mixing instrument (TGK Scientific) controlled by Kinetic Studios software package (TGK Scientific). Time-dependent absorption spectra were recorded using a charge coupled device whereas single wavelength measurements were recorded using a monochromator coupled with a photomultiplier tube. Experiments were performed at 4 °C and in the dark to protect against potential photodegradation of the enzyme.[19] For phenylacrylic acid experiments, both enzyme and substrate solutions were prepared in 50 mM potassium phosphate, 10% (v/v) glycerol pH 7.5. For styrene experiments, both enzyme and substrate solutions were prepared in 50 mM

potassium phosphate, 10% (v/v) glycerol, 1% DMSO pH 7.5. FDC was placed into a glass tonometer possessing an ice bath feature to cool and stabilize the enzyme.

3.2.4 Data Averaging

Stopped-flow data were typically recorded under identical experimental conditions at different timescales to obtain data with high temporal resolution on the millisecond to second timescale. Generally, 3-5 stopped-flow shots were averaged to improve the signal-to-noise ratio before fitting. This process was repeated for a variety of time ranges to improve the quality of data at all times of interest. The time dimension was binned using 100 bins for each order of magnitude and absorbance values averaged as described previously.[68]

3.3 Results

3.3.1 Reaction of FDC with Styrene

In the absence of CO_2, styrene can only react to form the prFMN cycloadduct. Therefore, we reasoned that the kinetics for this reaction should be more straightforward to interpret than for the enzyme reacting with phenylacrylate. The U.V.-visible spectral changes associated with the reaction of 180 μM holo-FDC with 1 mM styrene (final concentrations after mixing) are shown in Figure 3.2. Most noticeably, there is an increase in absorbance of the broad feature centered around 460 nm and a decrease in the sharper band centered at 380 nm. Under the conditions of the experiment, the spectral changes were essentially complete after 5 s, and the final spectrum of the styrene-reacted enzyme is essentially identical to that obtained previously when the enzyme was reacted with phenylacrylic acid (see Figure 2.3).[68] This observation is consistent with my and other Marsh laboratory previous studies that show the styrene-prFMN cycloadduct is the species that accumulates on the enzyme at equilibrium.[68]
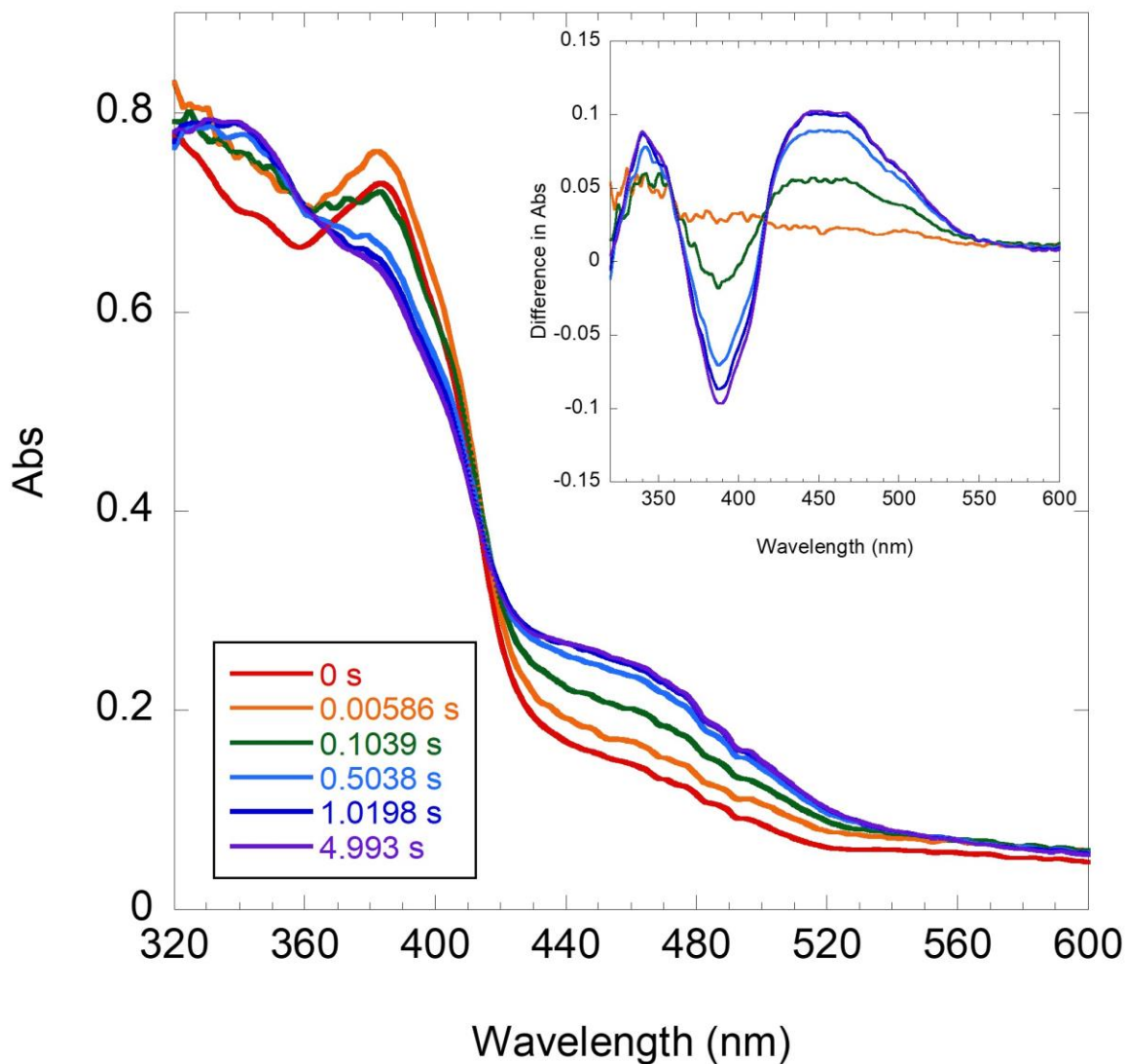
Figure 3.2: Spectral changes accompanying the reaction of FDC with styrene. Representative spectra are shown recorded at times ranging from 5 ms to 5 s after mixing. The final enzyme and substrate concentrations were 180 μM and 1 mM, respectively. The zero-time point spectrum was recorded by mixing FDC with buffer in the stopped-flow instrument. Inset: Difference spectra calculated by subtracting the zero-time point spectrum of FDC.

3.3.2 Pre-steady State Kinetics of Styrene Reaction

We used U.V.-visible stopped-flow spectroscopy to investigate the kinetics of styrene reacting with FDC. In particular, we aimed to investigate whether negative cooperativity between the two active sites of the FDC dimer (suggested by previous experiments)[68] play a role in the reaction. Therefore, we varied the styrene concentration from 1 mM to 60 μM while

keeping the FDC concentration fixed at 180 µM (concentrations after mixing, reaction at 4 °C).

The highest concentration represents a ~5-fold molar excess of substrate over enzyme, whereas

the lowest concentration is sub-stoichiometric with enzyme so that on average only one active

site in the FDC dimer should have substrate bound.

Based on the previous study (see Chapter 2), the kinetics of the reaction were monitored

at the following wavelengths: 380 nm, which monitors the consumption of prFMN; 460 nm,

which monitors the formation of the styrene-prFMN cycloadduct; and 425 nm, which also

monitors the formation of a styrene-prFMN cycloadduct but which is characterized by a

spectrum blue-shifted by ~35 nm that has a smaller extinction coefficient.[68] As discussed later,

the blue-shifted and red-shifted cycloadducts likely represent the same chemical species, but they

experience different active site environments. (We note that at all wavelengths there was a very

rapid initial decrease in absorbance that was nearly complete within the mixing time of the

spectrometer. This appears to be a mixing artifact as it was present when enzyme was shot

against plain buffer. Therefore, the first 3 ms of each reaction were excluded from the kinetic

analysis.)

The kinetics of styrene reacting with FDC are unexpectedly complicated. Three kinetic

phases are observed at each wavelength and at each styrene concentration (Figure 3.3). The

absorbance changes observed at 380 nm and 460 nm closely mirror each other (Figure 3.3A, B),

which is consistent with the conversion of the prFMN-styrene Michaelis complex (absorbance

maximum 380 nm) to the prFMN-styrene cycloadduct (absorbance maximum 460 nm). In

contrast, when the reaction was monitored at 425 nm, a somewhat different kinetic profile was

observed (Figure 3.3C). At the lower styrene concentrations, 60 and 90 µM, the absorbance

initially increases and then declines, consistent with the formation of an intermediate. However,

at higher substrate concentrations the absorbance continues to increase at longer times. This increase partially masks the decrease in absorbance seen at low concentrations, which is still evident at this wavelength even at high styrene concentrations. For the fastest phase, both the rate and amplitude appear fairly independent of styrene concentration. The next phase, however, is clearly concentration-dependent as its amplitude continues to increase with increasing styrene concentration, although the rate changes little. The slowest phase appears, again, to be concentration-independent in both rate and amplitude.

Figure 3.3: Pre-steady state kinetics of FDC reacting with styrene. FDC (180 μM) was reacted with increasing concentrations of styrene as indicated and the reaction monitored at: **A)** 380 nm, **B)** 460 nm, and **C)** 425 nm. *Note*: The absorbance traces have been offset for clarity. The data were globally fitted to a three-exponential function as described in text. **D)** The total changes in absorbance (recorded after 5 s) at the different wavelengths are plotted as a function of styrene concentration for each wavelength monitored. The dashed lines are interpolated between the data points. The concentration of styrene corresponding to 0.5 and 1.0 FDC active sites are marked above the plot.

The data were globally fitted to 3 parallel first-order reaction processes using the program

GraphPad Prism:

$$A_{(t)} = A_0 + A_1 e^{(-k_{obs1}*t)} + A_2 e^{(-k_{obs2}*t)} + A_3 e^{(-k_{obs3}*t)} \tag{3.1}$$

73

Where A_0 is the initial absorbance, and $A_{(n)}$ and $k_{obs(n)}$ for n = 1, 2, 3 are the amplitude and observed rate constant, respectively, associated with phase n.

The data could be robustly fitted by 3 apparent first-order rate constants, k_{1sty}, k_{2sty} and k_{3sty}, shared across the entire data set, with the amplitudes associated with each rate constant allowed to vary. As shown in Table 3.1–Table 3.3, the values obtained for the rate constants are: $k_{1sty} = 40$ (39 – 41) s^{-1}; $k_{2sty} = 5.9$ (5.6 – 6.1) s^{-1}; $k_{3sty} = 2.5$ (2.4 – 2.6) s^{-1} (95% confidence intervals in parentheses). The individual amplitudes associated with each rate constant varied somewhat as a function of styrene concentration, most of which we attribute to signal noise as the absorbance changes are quite small. However, the sum of the amplitudes ($A_{tot} = A_{1sty} + A_{2sty} + A_{3sty}$) exhibits a clear trend in which the signal initially increases sharply as a function of styrene concentration and then increases more gradually (Figure 3.3D). The inflection point in the curve occurs at a substrate to enzyme ratio of ~0.5 and, interestingly, even at the highest styrene concentration shows no evidence of saturation.

Table 3.1: Amplitudes and observed rate constants for reaction of styrene monitored at 380 nm. *Note*: Rate constants constrained to be shared across all wavelengths and concentrations.

[Styrene] (µM)	60	90	180	360	540	720	1000
A_0	0.1265	0.112	0.0905	0.07188	0.05526	0.03887	0.007194
95% CI	0.1263 - 0.1267	0.1118 - 0.1122	0.09027 - 0.09074	0.07165 - 0.07212	0.05502 - 0.05550	0.03863 - 0.03911	0.00693 - 0.00745
A_1	0.03379	0.03189	0.02885	0.0241	0.02146	0.02301	0.02332
95% CI	0.03307 - 0.03451	0.03114 - 0.03262	0.02803 - 0.02964	0.02326 - 0.02491	0.02063 - 0.02228	0.02223 - 0.02378	0.02254 - 0.02411
k_{1sty} (s^{-1})	39.91	39.91	39.91	39.91	39.91	39.91	39.91
95% CI	38.78 - 41.10	38.78 - 41.10	38.78 - 41.10	38.78 - 41.10	38.78 - 41.10	38.78 - 41.10	38.78 - 41.10
A_2	0.0009265	0.006912	0.02357	0.03248	0.03502	0.03166	0.01552
95% CI	-0.000920 - 0.00271	0.00512 - 0.00865	0.02182 - 0.02529	0.03056 - 0.03439	0.03286 - 0.03715	0.02919 - 0.03411	0.01171 - 0.01933
k_{2sty} (s^{-1})	5.851	5.851	5.851	5.851	5.851	5.851	5.851

95% CI	5.584 - 6.138	5.584 - 6.138	5.584 - 6.138	5.584 - 6.138	5.584 - 6.138	5.584 - 6.138	5.584 - 6.138
A$_3$	0.011	0.01059	0.008954	0.01225	0.0186	0.02702	0.06435
95% CI	0.00956 - 0.0124	0.009165 - 0.01203	0.007321 - 0.01057	0.01026 - 0.01421	0.01635 - 0.02081	0.02453 - 0.02947	0.06092 - 0.06771
k$_{3sty}$ (s^{-1})	2.479	2.479	2.479	2.479	2.479	2.479	2.479
95% CI	2.394 - 2.562	2.394 - 2.562	2.394 - 2.562	2.394 - 2.562	2.394 - 2.562	2.394 - 2.562	2.394 - 2.562
r^2	0.9976	0.9981	0.9986	0.9995	0.9997	0.9994	0.9997

Table 3.2: Amplitudes and observed rate constants for reaction of styrene monitored at 425 nm. *Note*: Rate constants constrained to be shared across all wavelengths and concentrations.

[Styrene] (μM)	60	90	180	360	540	720	1000
A$_0$	0.007637	0.01224	0.0236	0.03459	0.04122	0.04875	0.06574
95% CI	0.00739 - 0.00787	0.01200 - 0.01248	0.02336 - 0.02385	0.03435 - 0.03484	0.04097 - 0.04146	0.04850 - 0.04899	0.06551 - 0.06598
A$_1$	-0.01604	-0.01557	-0.01143	-0.01263	-0.01091	-0.01142	-0.01181
95% CI	-0.01678 - -0.01529	-0.01632 - -0.01481	-0.01224 - -0.01059	-0.01342 - -0.01182	-0.01169 - -0.01011	-0.01218 - -0.01065	-0.01253 - -0.01109
k$_{1sty}$ (s^{-1})	39.91	39.91	39.91	39.91	39.91	39.91	39.91
95% CI	38.78 - 41.10	38.78 - 41.10	38.78 - 41.10	38.78 - 41.10	38.78 - 41.10	38.78 - 41.10	38.78 - 41.10
A$_2$	-0.01204	-0.01435	-0.02877	-0.02773	-0.02945	-0.02749	-0.0152
95% CI	-0.01383 - -0.01029	-0.01613 - -0.01261	-0.03065 - -0.02697	-0.02950 - -0.02603	-0.03124 - -0.02771	-0.02927 - -0.02575	-0.01732 - -0.01306
k$_{2sty}$ (s^{-1})	5.851	5.851	5.851	5.851	5.851	5.851	5.851
95% CI	5.584 - 6.138	5.584 - 6.138	5.584 - 6.138	5.584 - 6.138	5.584 - 6.138	5.584 - 6.138	5.584 - 6.138
A$_3$	0.01738	0.01703	0.02081	0.01283	0.01041	0.005376	-0.01983
95% CI	0.01591 - 0.01891	0.01556 - 0.01857	0.01916 - 0.02258	0.01118 - 0.01457	0.008675 - 0.01222	0.003642 - 0.007172	-0.02178 - 0.01786
k$_{3sty}$ (s^{-1})	2.479	2.479	2.479	2.479	2.479	2.479	2.479
95% CI	2.394 - 2.562	2.394 - 2.562	2.394 - 2.562	2.394 - 2.562	2.394 - 2.562	2.394 - 2.562	2.394 - 2.562
r^2	0.9929	0.9934	0.9866	0.9989	0.9985	0.9981	0.9987

Table 3.3: Amplitudes and observed rate constants for reaction of styrene monitored at 460 nm. *Note*: Rate constants constrained to be shared across all wavelengths and concentrations.

[Styrene] (μM)	60	90	180	360	540	720	1000
A$_0$	0.02998	0.03844	0.05917	0.07601	0.09003	0.1042	0.1318

95% CI	0.02974 - 0.03022	0.03820 - 0.03868	0.05893 - 0.05940	0.07577 - 0.07625	0.08979 - 0.09027	0.1040 - 0.1044	0.1316 - 0.1321
A_1	-0.02343	-0.02414	-0.02174	-0.01877	-0.01623	-0.01667	-0.01591
95% CI	-0.02415 - -0.02270	-0.02488 - -0.02339	-0.02257 - -0.02088	-0.01962 - -0.01791	-0.01708 - -0.01537	-0.01746 - -0.01586	-0.01667 - -0.01515
k_{1sty} (s^{-1})	39.91	39.91	39.91	39.91	39.91	39.91	39.91
95% CI	38.78 - 41.10	38.78 - 41.10	38.78 - 41.10	38.78 - 41.10	38.78 - 41.10	38.78 - 41.10	38.78 - 41.10
A_2	-0.005825	-0.008971	-0.02776	-0.03268	-0.04	-0.03472	-0.0211
95% CI	-0.007499 - -0.004123	-0.01064 - -0.007273	-0.02943 - -0.02610	-0.03450 - -0.03085	-0.04199 - -0.03800	-0.03695 - -0.03249	-0.02445 - -0.01774
k_{2sty} (s^{-1})	5.851	5.851	5.851	5.851	5.851	5.851	5.851
95% CI	5.584 - 6.138	5.584 - 6.138	5.584 - 6.138	5.584 - 6.138	5.584 - 6.138	5.584 - 6.138	5.584 - 6.138
A_3	-0.004669	-0.005094	-0.00182	-0.008024	-0.008975	-0.01985	-0.0536
95% CI	-0.006059 - -0.003292	-0.00648 - -0.00371	-0.00341 - -0.000190	-0.00989 - -0.00611	-0.01114 - -0.006769	-0.02214 - -0.01752	-0.05664 - -0.05050
k_{3sty} (s^{-1})	2.479	2.479	2.479	2.479	2.479	2.479	2.479
95% CI	2.394 - 2.562	2.394 - 2.562	2.394 - 2.562	2.394 - 2.562	2.394 - 2.562	2.394 - 2.562	2.394 - 2.562
r^2	0.997	0.9971	0.999	0.9996	0.9997	0.9998	0.9998

3.3.3 Reaction of FDC with Phenylacrylic Acid

As described in Chapter 2, we previously investigated the pre-steady state kinetics of FDC reacting with phenylacrylic acid.[68] However, informed by the results obtained with styrene, we extended our studies to cover a wider range of substrate concentrations and, in particular, to examine the reaction at sub-stoichiometric concentrations. Accordingly, holo-FDC, 180 μM after mixing, was reacted at 4 °C with final concentrations of phenylacrylate ranging from 1 mM to 45 μM and the reaction monitored at 380 nm, 425 nm, and 460 nm over the course of 5 s, as shown in Figure 3.4.
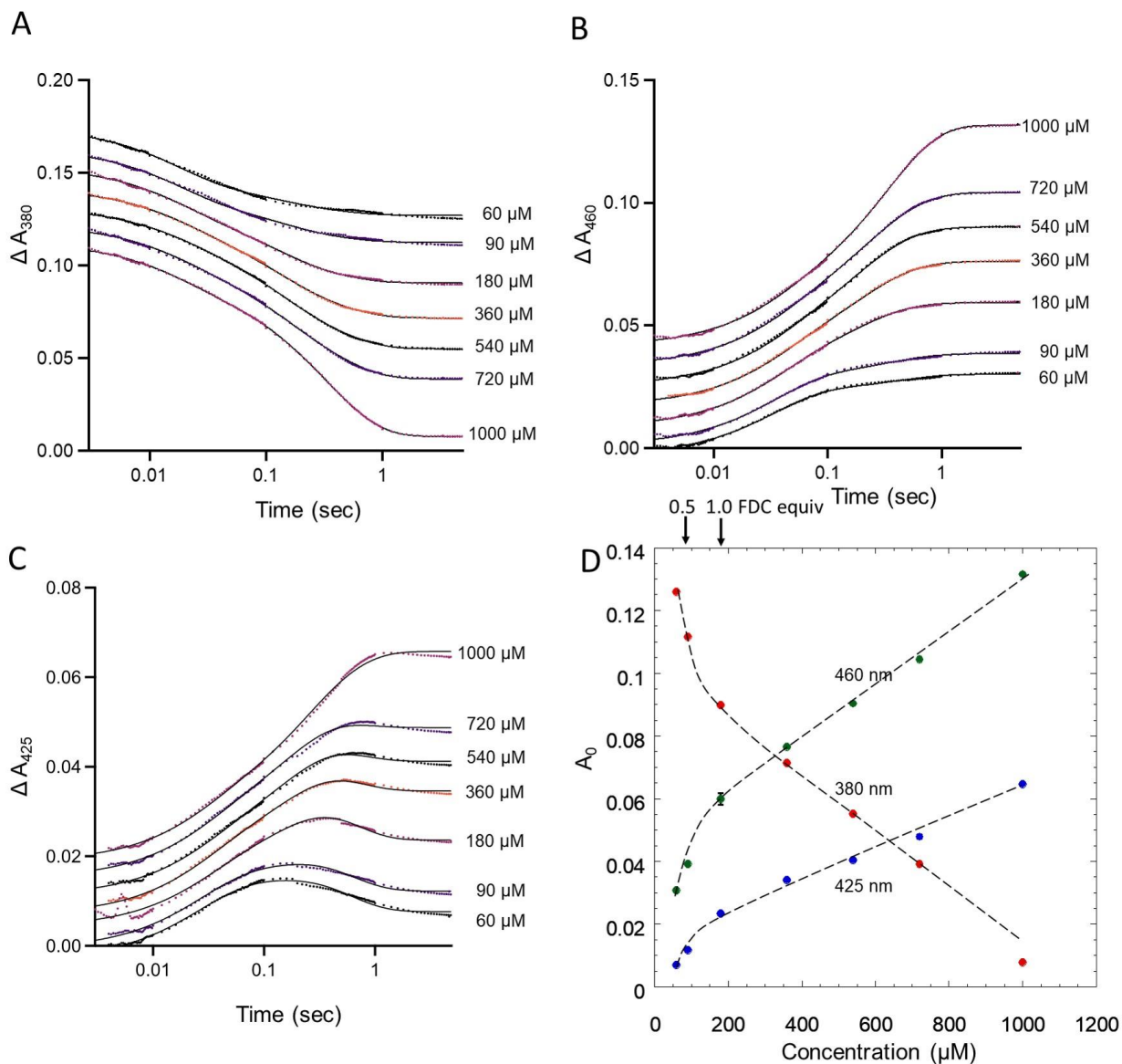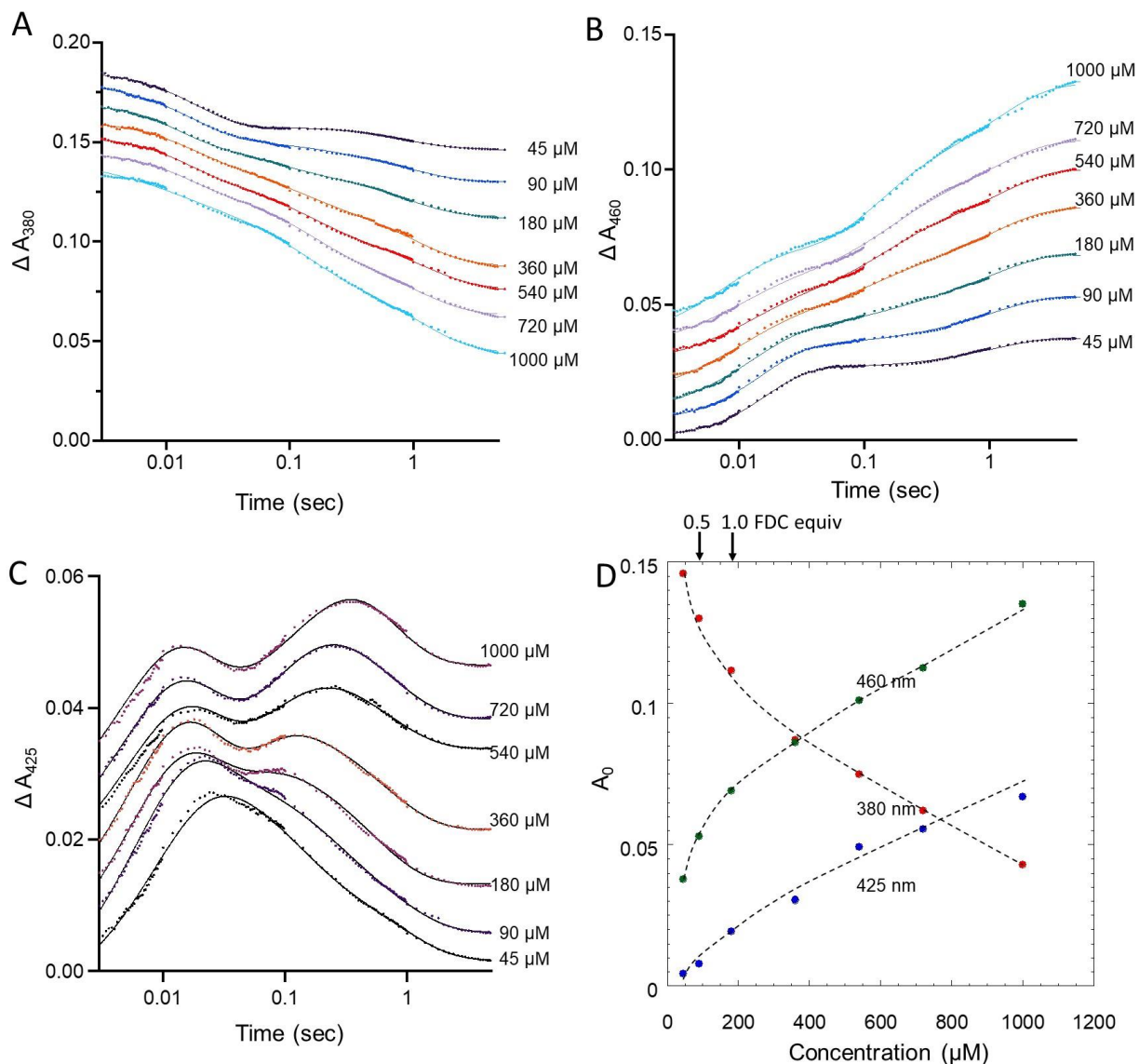
Figure 3.4: Pre-steady state kinetics of FDC reacting with phenylacrylate. FDC (180 μM) was reacted with increasing concentrations of phenylacrylate as indicated and the reaction monitored at: **A)** 380 nm, **B)** 460 nm, and **C)** 460 nm. The data are shown with traces individually fitted to a four-exponential function; however as discussed in the text it was not possible to obtain robust values for individual rate constants from fits. *Note*: The absorbance traces have been offset for clarity. **D)** The total changes of the absorbances (recorded after 5 s) at the different wavelengths are plotted as a function of phenylacrylate concentration for each wavelength monitored. The dashed lines are interpolated between the data points. The concentration of phenylacrylate corresponding to 0.5 and 1.0 FDC active sites are marked above the plot.

The absorbance changes observed with phenylacrylate as the substrate (Figure 3.4) are

similar to those seen with styrene (Figure 3.3), reflecting the fact that similar adducts are formed

with prFMN by both molecules. However, in this case the kinetic behavior is more complex. The

added complexity most likely arises because the initially formed phenylacrylate-prFMN

cycloadduct then undergoes decarboxylation to form the styrene-prFMN adduct, which previous

studies have shown is the species that accumulates on the enzyme.[68] Although it is hard to

discern from the traces monitored at 380 and 460 nm, it is clearly evident from the traces

obtained at 425 nm that the reaction exhibits four phases, the amplitudes of which are dependent

on phenylacrylate concentration (Figure 3.4). Most noticeably, the slower two phases have

amplitudes that are markedly concentration dependent and at the lowest phenylacrylate

concentrations, 45 and 90 µM, become nearly indiscernible. At the higher phenylacrylate

concentrations, it is evident that the system does not reach a steady state even after 5 s as the

absorbance continues to change; this is most noticeable at 1 mM phenylacrylate (Figure 3.4A,

B). However, at these higher concentrations and longer time scales the absorbance changes are

associated with multiple turnovers. As such, they reflect the approach of the system to chemical

equilibrium, rather than reporting on the kinetics of chemical steps in the enzyme mechanism.

The data were globally fitted to 4 parallel first-order reaction processes using the

GraphPad Prism:

$$A_{(t)} = A_0 + A_1 e^{(-k_{obs1}*t)} + A_2 e^{(-k_{obs2}*t)} + A_3 e^{(-k_{obs3}*t)} + A_4 e^{(-k_{obs4}*t)} \qquad (3.2)$$

Where A_0 is initial absorbance, and $A_{(n)}$ and $k_{obs(n)}$ for n = 1, 2, 3,4 are the amplitude and

observed rate constant, respectively, associated with phase n. The fits were constrained such that

the 4 observed first-order rate constants associated with the reactions were shared across all data

sets, whereas the amplitudes were allowed to vary.

The complexity of the kinetic behavior observed with phenylacrylate meant that it was

not possible to obtain robust fits to the data. As shown in Figure 3.4, all the traces could be

reasonably well fitted using 4 exponential functions, with residuals of $r^2 > 0.995$. But attempts to fit either individual traces, or globally fit the data, using Prism software to obtain values for the 4 rate constants resulted in values with either very wide or indeterminate confidence. Nevertheless, the approximate values for the observed rate constants could be estimated from the data as k_{1phe} ~150–200 s^{-1}; k_{2phe} ~100 s^{-1}; k_{3phe} ~8 s^{-1}; k_{4phe} ~1 s^{-1} (Table 3.4, Table 3.5, Table 3.6). The values for k_{1phe} and k_{2phe} were subject to the greatest variation in trials to fit the data, whereas the values obtained k_{3phe} for k_{4phe} and were less dependent on the initial parameters used in fitting.

The initial reaction of prFMN with phenylacrylate, k_{1phe} ~150–200 s^{-1}, occurs significantly faster than that of styrene, $k_{1sty} = 40$ s^{-1}, which may reflect the higher intrinsic reactivity of phenylacrylate towards dipolar cycloaddition. The second phase of the reaction is also rapid, k_{2phe} ~100 s^{-1}; we tentatively assign this phase to the decarboxylation of the prFMN-phenylacrylate cycloadduct to form the prFMN-styrene cycloadduct, which previous work[68] has shown is the adduct that accumulates on the enzyme. As discussed below, we propose that k_{3phe} is likely associated with product release. It is unclear what process gives rise to k_{4phe}, but in any case, this process is too slow for it to play a role in the catalytic cycle.

Table 3.4: Amplitudes and observed rate constants for reaction of phenylacrylate monitored at 380 nm. *Note*: Rate constants constrained to be shared across all wavelengths and concentrations.

[Phenylacrylate] (μM)	45	90	180	360	540	720	1000
A_0	0.146	0.1296	0.1119	0.08795	0.07716	0.06303	0.04497
95% CI	N/D	N/D	N/D	N/D	N/D	N/D	N/D
A_1	-0.03444	-0.02398	-0.01863	-0.02513	-0.02075	-0.01213	-0.0161
95% CI	N/D	N/D	N/D	N/D	N/D	N/D	N/D
k_{1phe} (s^{-1})	~ 194	~ 194	~ 194	~ 194	~ 194	~ 194	~ 194
95% CI	N/D	N/D	N/D	N/D	N/D	N/D	N/D
A_2	0.05899	0.04953	0.04153	0.04217	0.03902	0.02793	0.03064
95% CI	N/D	N/D	N/D	N/D	N/D	N/D	N/D
k_{2phe} (s^{-1})	~ 97	~ 97	~ 97	~ 97	~ 97	~ 97	~ 97
95% CI	N/D	N/D	N/D	N/D	N/D	N/D	N/D
A_3	0.000568	0.006591	0.01319	0.02032	0.02528	0.03278	0.03369

95% CI	N/D	N/D	N/D	N/D	N/D	N/D	N/D
k_{3phe} (s^{-1})	~ 7.9	~ 7.9	~ 7.9	~ 7.9	~ 7.9	~ 7.9	~ 7.9
95% CI	N/D	N/D	N/D	N/D	N/D	N/D	N/D
A$_4$	0.01203	0.01718	0.02204	0.03318	0.03177	0.03415	0.04182
95% CI	N/D	N/D	N/D	N/D	N/D	N/D	N/D
k_{4phe} (s^{-1})	~ 0.9	~ 0.9	~ 0.9	~ 0.9	~ 0.9	~ 0.9	~ 0.9
95% CI	N/D	N/D	N/D	N/D	N/D	N/D	N/D
r^2	0.9982	0.9991	0.9995	0.9991	0.9993	0.9998	0.9996

Table 3.5: Amplitudes and observed rate constants for reaction of phenylacrylate monitored at 425 nm. *Note*: Rate constants constrained to be shared across all wavelengths and concentrations.

[Phenylacrylate] (μM)	45	90	180	360	540	720	1000
A$_0$	0.001307	0.005121	0.01167	0.02011	0.03274	0.03706	0.04545
95% CI	N/D	N/D	N/D	N/D	N/D	N/D	N/D
A$_1$	-0.004963	-0.03536	-0.04665	-0.05801	-0.04793	-0.06139	-0.06683
95% CI	N/D	N/D	N/D	N/D	N/D	N/D	N/D
k_{1phe} (s^{-1})	~ 194	~ 194	~ 194	~ 194	~ 194	~ 194	~ 194
95% CI	N/D	N/D	N/D	N/D	N/D	N/D	N/D
A$_2$	-0.03362	-0.008513	0.007715	0.02215	0.01988	0.03451	0.04106
95% CI	N/D	N/D	N/D	N/D	N/D	N/D	N/D
k_{2phe} (s^{-1})	~ 97	~ 97	~ 97	~ 97	~ 97	~ 97	~ 97
95% CI	N/D	N/D	N/D	N/D	N/D	N/D	N/D
A$_3$	0.01851	0.01581	0.007976	-0.001211	-0.01017	-0.0168	-0.02159
95% CI	N/D	N/D	N/D	N/D	N/D	N/D	N/D
k_{3phe} (s^{-1})	~ 7.9	~ 7.9	~ 7.9	~ 7.9	~ 7.9	~ 7.9	~ 7.9
95% CI	N/D	N/D	N/D	N/D	N/D	N/D	N/D
A$_4$	0.01268	0.01472	0.0149	0.01609	0.01318	0.017	0.01617
95% CI	N/D	N/D	N/D	N/D	N/D	N/D	N/D
k_{4phe} (s^{-1})	~ 0.9	~ 0.9	~ 0.9	~ 0.9	~ 0.9	~ 0.9	~ 0.9
95% CI	N/D	N/D	N/D	N/D	N/D	N/D	N/D
r^2	0.9955	0.9947	0.9834	0.9694	0.9752	0.9717	0.9826

Table 3.6: Amplitudes and observed rate constants for reaction of phenylacrylate monitored at 460 nm. *Note*: Rate constants constrained to be shared across all wavelengths and concentrations.

[Phenylacrylate] (μM)	45	90	180	360	540	720	1000
A$_0$	0.03801	0.05348	0.06914	0.08583	0.1	0.1109	0.1317
95% CI	N/D	N/D	N/D	N/D	N/D	N/D	N/D
A$_1$	0.03269	0.02648	0.01054	0.002261	0.003082	-0.00991	-0.01723

95% CI	N/D	N/D	N/D	N/D	N/D	N/D	N/D
k_{1phe} (s^{-1})	~ 194	~ 194	~ 194	~ 194	~ 194	~ 194	~ 194
95% CI	N/D	N/D	N/D	N/D	N/D	N/D	N/D
A_2	-0.05631	-0.05344	-0.04093	-0.03063	-0.02499	-0.0141	-0.009911
95% CI	N/D	N/D	N/D	N/D	N/D	N/D	N/D
k_{2phe} (s^{-1})	~ 97	~ 97	~ 97	~ 97	~ 97	~ 97	~ 97
95% CI	N/D	N/D	N/D	N/D	N/D	N/D	N/D
A_3	-1.56E-05	-0.001918	-0.008164	-0.01709	-0.02467	-0.02859	-0.03301
95% CI	N/D	N/D	N/D	N/D	N/D	N/D	N/D
k_{3phe} (s^{-1})	~ 7.9	~ 7.9	~ 7.9	~ 7.9	~ 7.9	~ 7.9	~ 7.9
95% CI	N/D	N/D	N/D	N/D	N/D	N/D	N/D
A_4	-0.01163	-0.01724	-0.02152	-0.02452	-0.0265	-0.02772	-0.03616
95% CI	N/D	N/D	N/D	N/D	N/D	N/D	N/D
k_{4phe} (s^{-1})	~ 0.9	~ 0.9	~ 0.9	~ 0.9	~ 0.9	~ 0.9	~ 0.9
95% CI	N/D	N/D	N/D	N/D	N/D	N/D	N/D
r^2	0.9992	0.9992	0.9991	0.9995	0.9993	0.9988	0.9988

3.4 Discussion

The prFMN-dependent class of decarboxylases catalyze (de)carboxylation reactions at sp^2-hybridized carbon atoms in an increasingly diverse range of substrates.[23, 24, 45, 69] These range from complex natural products to simple aromatic molecules. The enzymes so far characterized catalyze reactions on aromatic rings,[22, 70] heterocyclic aromatic rings[23, 24, 45, 69, 71] and conjugated double bonds. Most intriguingly, indirect evidence suggests that prFMN-dependent enzymes may even catalyze the carboxylation of benzene to support the growth of some anaerobic bacteria.[72, 73] Although numerous enzymes have been structurally characterized,[16, 22-24, 35, 40] our understanding of the kinetics of prFMN-mediated catalysis remains poorly developed. A deeper understanding of prFMN reactivity is an important prerequisite for effectively utilizing these enzymes for biocatalysis. Our studies have focused on defining the kinetic profile of FDC because it remains the best characterized member of the prFMN-dependent decarboxylase family and the chemical steps in the mechanism are most clearly defined.

In this chapter, we investigated the pre-steady state kinetics of FDC reacting with phenylacrylate and styrene over concentrations that range from sub-stochiometric to a several fold molar excess with respect to enzyme active sites. The kinetics of both reactions are surprisingly complicated, and this complexity precludes an unambiguous interpretation of all the kinetic features. Nevertheless, we consider that the concentration-dependence of the reaction kinetics may reasonably be explained by invoking negative cooperativity[74] (half-of-the-sites reactivity) between the active sites of the FDC dimer.

The reaction with styrene provides the clearest evidence for negative cooperativity because it can only form the prFMN-styrene cycloadduct and does not react further (proton abstraction from the cycloadduct occurs orders of magnitude more slowly)[30]. Here, although only a single chemical reaction can occur, three apparent first-order rate constants are needed to adequately fit the data. The concentration-dependence of the kinetic data clearly suggests that the two active sites have different affinities for styrene. The fastest phase of the reaction, characterized by $k_{1sty} = 40$ s^{-1} dominates at low substrate concentrations. However, once the styrene:enzyme ratio exceeds 0.5, the slower phase of the reaction, characterized by $k_{2sty} = 5.9$ s^{-1}, starts to increase in amplitude and becomes prominent (Figure 3.3D).

A similar pattern of concentration-dependent kinetic behavior is seen in the reaction of phenylacrylate. In this case, the two fastest phases of the reaction, characterized by k_{1phe} ~150–200 s^{-1} and k_{2phe} ~100 s^{-1} are prominent at low substrate concentrations. We attribute these to the initial formation of the phenylacrylate-prFMN cycloadduct and its conversion to the styrene-prFMN cycloadduct at the 'fast-tight' site. Only after the phenylacrylate:enzyme ratio exceeds 0.5 does the slower phase characterized by k_{3phe} ~8 s^{-1} gain in amplitude (Figure 3.4D). Although the assignment of the various apparent rate constants to chemical processes remains somewhat

tentative, this type of concentration-dependent kinetic behavior is a hallmark of half-of-the-sites reactivity.

Crystal structures are now available for numerous UbiD-like enzymes (recently reviewed in reference[18]) which show that the different family members adopt dimeric, tetrameric, or hexameric structures. However, these structures do not provide any obvious evidence for negative cooperativity, for example by revealing asymmetry between the protein subunits. Nevertheless, it appears that domain movements are likely to be important for substrate binding and catalysis. Such movements have been captured in the open and closed structures of vanillic acid decarboxylase.[25] Similar domain-scale motions have not been documented for FDC, but smaller scale active site motions have been observed in structures of FDC complexed with various mechanism-based inhibitors that mimic intermediates in the reaction.[35] Although the various structures of FDC fail to provide evidence for cooperativity, we note that the transient and often subtle motions involved in allosteric interactions are hard to capture by crystallography.

The question that arises is does this putative negative cooperativity have any mechanistic significance? We argue that it may play a role in facilitating the release of styrene from FDC. We note that even at the lowest concentration of phenylacrylate used in these experiments (45 μM) the enzyme does not return to the resting state. Even after 5 s, we see no evidence for styrene dissociating from the active site, which would show up as an increase in absorbance at 380 nm or a decrease 460 nm as prFMN is regenerated. This observation implies that styrene remains tightly bound to the enzyme as its prFMN cycloadduct, rather than undergoing cycloelimination to complete turnover. Thus the 'fast, tight' site does not appear to be kinetically competent to perform the *complete* reaction cycle.

One explanation is that FDC is severely product-inhibited by styrene, and because these experiments require relatively high concentrations of enzyme (180 μM) the accumulation of styrene-prFMN cycloadducts is favored; whereas lower concentrations would allow styrene to diffuse from the enzyme. We consider this explanation unlikely because the K_M for phenylacrylate is 60 μM,[68] implying that the enzyme would become product-inhibited at substrate concentrations well below K_M. Also, there are no enzymes known in yeast that further metabolize styrene to prevent its build up in the cell – it is assumed to be removed by diffusion. Rather, we propose that negative cooperativity plays a key role in the catalytic cycle of FDC by providing a mechanism to eject styrene from the enzyme after decarboxylation.
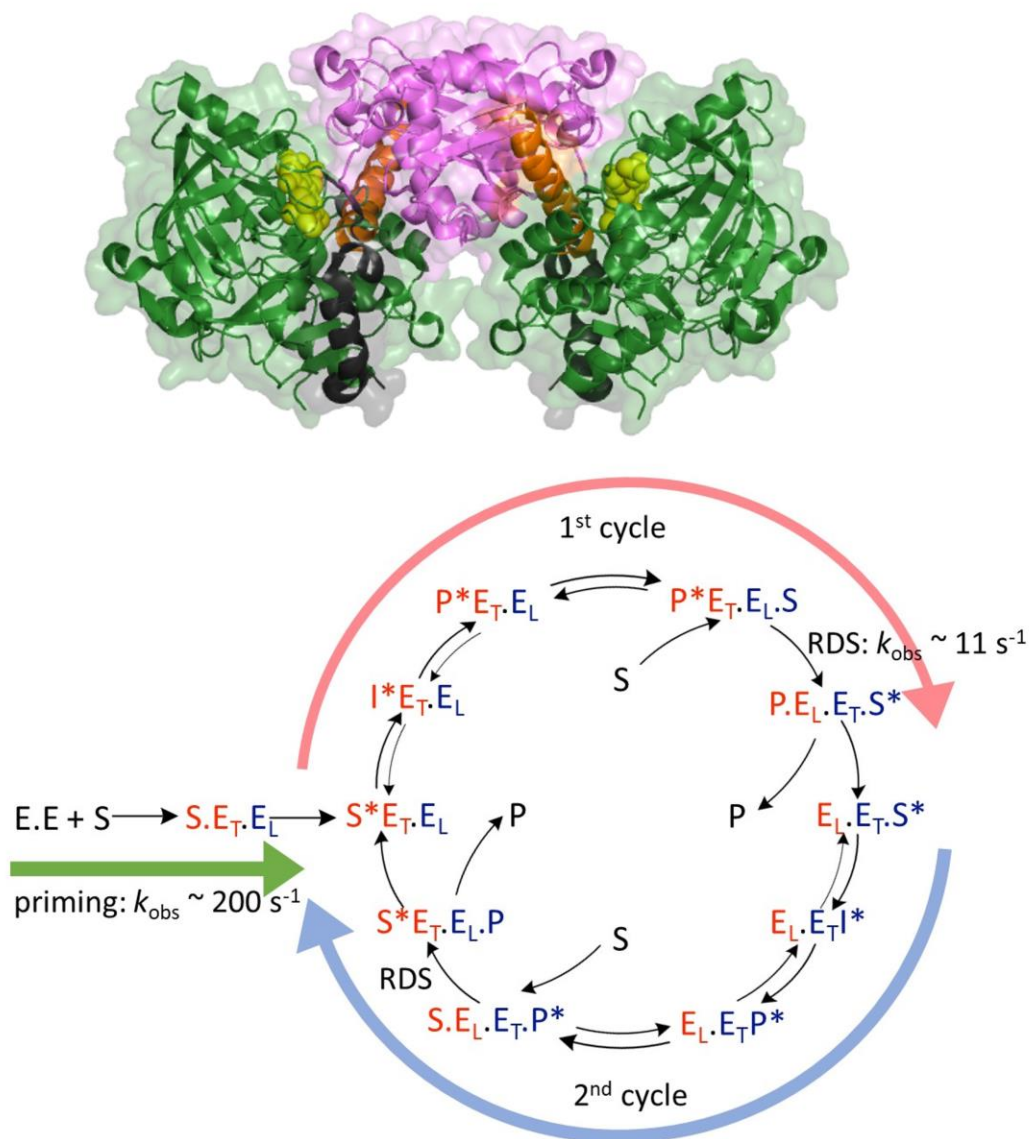
Figure 3.5: Proposed catalytic cycle for FDC-catalyzed decarboxylation incorporating negative cooperativity.
Top: The structure of the FDC dimer highlighting the domain organization (PDB: 4ZAC). The oligomerization and prFMN-binding domains are colored magenta and green, respectively; the domain-connecting helix is shown in orange and the C-terminal helix in black. prFMN is colored yellow. *Bottom*: The proposed "two-stroke" mechanism for decarboxylation. The priming phase involves the initial substrate-binding event that differentiates the two active sites, color-coded red and blue, into a tight-binding (E_T) and loose-binding (E_L) site. In the first cycle, substrate reacts with prFMN at the "red" active site; S*, I*, and P* represent covalent adducts **C**, **D**, and **E** in Figure 1.5 respectively. Reaction of substrate at the "blue" active site results in interconversion of the "T" and "L" forms of the enzyme resulting in cycloelimination of P in the rate-determining step (RDS). The second cycle proceeds analogously through reaction at the "blue" active site.

In this mechanism, outlined in Figure 3.5, substrate initially binds and undergoes

decarboxylation rapidly at the 'fast, tight' active site. Next, at higher substrate concentrations,

the substrate will bind to the 'slow, loose' active site. The effect of substrate binding at the

second active site will push the low-affinity site towards the high-affinity state, resulting in a protein conformational change that flips the 'fast, tight' site to the 'slow, loose' state and *vice versa*. This conformational change now places the prFMN-styrene cycloadduct in the low-affinity active site, causing it to undergo cycloelimination to complete the first catalytic cycle. Phenylacrylate is now in the high-affinity active site where it undergoes cycloaddition and decarboxylation to styrene. Thus, catalysis proceeds through rounds of substrate binding at one site and product release at the other that drives an alternating "two-stroke" catalytic cycle. This cycling provides a mechanism in which the energetically favorable cycloaddition and decarboxylation steps occurring at one active site are coupled to the unfavorable cycloelimination of styrene at the other active site.

In support of this mechanism, our measurements with higher concentrations of substrate show that the low-affinity active site reacts with phenylacrylate to form the phenylacrylate-prFMN cycloadduct with k_{3phe} ~8 s^{-1}, which is very similar both to the rate at which styrene reacts at the second site, $k_{2sty} = 5.9$ s^{-1} and to $k_{cat} = 11$ s^{-1} determined from steady-state kinetic analyses. In addition, various lines of evidence point to styrene release being rate-limiting in the reaction and therefore the step that primarily determines k_{cat}. These include the observation by native mass spectrometry of stable styrene-prFMN cycloadducts formed in the FDC reaction;[68] the large, normal 2° KIE = 1.15 ± 0.017 measured on V_{max}/K_M under steady state conditions for the decarboxylation of d$_7$-phenylacrylate;[30] and the negative ρ value for the reaction determined from Hammett analysis of the enzyme reported previously.[30]

We note that some aspects of the kinetics remain puzzling. Particularly unusual is the apparent lack of concentration-dependence on the rates of reaction for the various phases. The concentration-dependence of the *amplitudes* associated with k_{3phe} and k_{2sty} indicate that the 'slow,

loose' active site does not become saturated with substrate under the conditions of the experiment. (The maximum concentration of styrene in the experiment is limited by its solubility in water.) However, such behavior would normally be accompanied by a marked concentration-dependence on the *rate* of reaction as well. This suggests that a kinetic step that is independent of substrate binding is rate-limiting for this step of the reaction. This type of kinetic behavior might arise from a 'gating' motion of the protein, and indeed structural studies on several UbiD enzymes point to the importance of protein motions in catalysis. Crucially though, any such motion would have to occur *independently* of substrate binding to explain the lack of concentration-dependence on the rate of reaction.

A further unusual feature of the kinetic behavior is the amplitudes of the absorbance changes associated with the 'fast' and 'slow' active sites are quite different. *A priori* one would expect that half-of-the-sites behavior would result in the amplitudes being of similar magnitude, but it is clear from the data in Figure 3.3 and Figure 3.4 that the slower phases are associated with significantly larger absorbance changes. Again, it is currently unclear why this occurs. It is possible that the extinction coefficients associated with the two active sites may be different, and in this context, we note that the electronic spectra of flavins are very sensitive to the local environment of the protein. On the other hand, this behavior may reflect further kinetic complexity in which the internal equilibria coupling the various reaction species are different at each active site so that the prFMN adducts accumulate to different degrees.

We also note that prFMN has been observed in some FDC crystal structures with a hydroxyl group at the C1'. This inactive adduct is presumably in equilibrium with the active iminium form of prFMN. LC-MS analysis of holo-FDC used in our experiments provided no evidence for this adduct (Figure 3.1). However, the presence of such an equilibrium may

87

additionally complicate kinetic analysis, especially if the equilibrium is perturbed by substrate binding.

These unusual features of the kinetics, together with the complexity of the kinetic traces, frustrated our attempts to fit the data to a kinetic model of the FDC reaction. Extensive attempts were made to evaluate various kinetic schemes, either incorporating or omitting cooperativity, using kinetic modelling software such as Kintek Explorer. However, simple kinetic models failed to provide convincing fits to the stopped-flow traces, whereas more complex models became over-parameterized and yielded either unrealistic and/or poorly constrained values for elementary rate constants.

3.5 Conclusions

Although an increasing number of prFMN-dependent enzymes are now known, and detailed structural information available for several of them, the kinetics of prFMN-catalyzed decarboxylation remains underdeveloped. Our experiments on FDC are the first to examine the pre-steady state kinetics of a prFMN-dependent enzyme reacting with substrates under single turn-over and multiple turn-over conditions. These experiments reveal complex kinetic behavior that may be explained by negative cooperativity between the two active sites of the dimeric enzyme that results in a 'fast, tight' site and a 'slow, loose' site. We propose that interconversion between the 'fast, tight' and 'slow, loose' sites may play an important role in the mechanism by driving the release of styrene from the enzyme, which is the rate-determining step of the overall reaction. We note that all UbiD enzymes so far characterized possess either dimeric, tetrameric, or hexameric quaternary structures, with the dimer forming the basic functional unit. It is therefore possible that a similar "two-stroke" kinetic mechanism may be a general feature of the decarboxylation reactions catalyzed by this class of enzymes.

A necessary caveat to these conclusions is that the complexity of the kinetics still leaves several features of the reaction unexplained. This leaves open the possibility that mechanisms other than negative cooperativity are responsible for the multi-phasic pre-steady state kinetic behavior we observe. Additional experiments will be needed to allow the reaction mechanism to be fully elucidated and a robust kinetic model developed. Particularly, the use of slower substrates such as 4-nitrophenylacrylatic acid may allow for additional steps of the reaction to be observed and studied. In addition, known inhibitors such as FNVB could be used to test the half-of-sites reactivity model.

Chapter 4 Preliminary Study into the Isotope Effects on Ferulic Acid Decarboxylase Using Styrene and d$_8$-Styrene

4.1 Introduction

Isotope effects can provide valuable insights into reaction mechanisms and are an invaluable tool in enzymology due to the information they may potentially give about reaction transition states.[75-77] The substitution of a heavier isotope for a lighter one typically causes changes to both the equilibrium constant and rate of a chemical reaction. While substituting a heavy atom for an atom that is directly involved in bond formation or cleavage generally yields larger isotope effects (primary isotope effects), information can also be collected using a heavy atom directly bonded to or adjacently bonded to the atom involved in the bond change (secondary isotope effects). Although 2° KIEs are smaller, they can be highly informative as they can reveal information regarding changes in molecular geometry that occur in the reaction transition state.

A previous investigation performed by the Marsh laboratory observed secondary deuterium kinetic isotope effects at both the Cα and Cβ of phenylacrylic acid under steady state conditions.[30] Large normal 2° KIEs were observed for d$_7$-phenylacrylic acid (fully deuterated) in both water (2° V/K$_{(H2O)}$ = 1.15 ± 0.017) and D$_2$O (2° V/K$_{(D2O)}$ = 1.32 ± 0.035). Normal 2° KIEs were also observed for α-d$_1$-phenylacrylic acid and for β,2,3,4,5,6-d$_6$-phenylacrylic acid (deuterated at Cβ and the aryl ring), although these KIEs were solvent dependent. No 2° KIE was measured for α-d$_1$-phenylacrylic acid in water (2° V/K$_{(H2O)}$ = 0.99 ± 0.02) while a normal 2° KIE was observed in D$_2$O (2° V/K$_{(D2O)}$ = 1.12 ± 0.03). β,2,3,4,5,6-d$_6$-Phenylacrylic acid exhibited the

opposite phenomenon with a normal 2° KIE in water (2° V/K$_{(H2O)}$ = 1.10 ± 0.016) and no effect

detected in D$_2$O (2° V/K$_{(D2O)}$ = 1.01 ± 0.027). While complicated by the solvent dependence, the

normal 2° KIEs measured at both Cα and Cβ indicate a change from tetrahedral to planar

geometry at these atoms that occurs in the rate-determining step of the reaction. These data

coupled with solvent isotope effect and linear free-energy studies provided strong support for the

rate-determining step of the FDC reaction being the cycloelimination of the styrene-prFMN

cycloadduct to generate styrene and the iminium prFMN species. Furthermore, the

cycloelimination step being rate-limiting provided a feasible explanation for the solvent

dependence of the 2° KIEs. During the formation of the styrene-prFMN cycloadduct in water,

the α-carbon of the substrate receives a proton from E285. However, in D$_2$O, E285 would

exchange its proton for a deuterium from the solvent. This would result in the α-carbon of the

styrene-prFMN cycloadduct already possessing a deuterium. In the case of β,2,3,4,5,6-d$_6$-

phenylacrylic acid in D$_2$O, a cryptic 2° KIE at the Cα position could mask the 2° KIE at the Cβ

position, resulting in no observed 2° KIE. In contrast, for α-d$_1$-phenylacrylic acid in D$_2$O, the α-

carbon would possess two deuterium atoms and thus, the 2° KIE would be more evident.

Additionally, this would explain the larger 2° KIEs observed when d$_7$-phenylacrylic acid was

used.

The pre-steady state kinetic studies described in Chapter 2 and Chapter 3 of this

dissertation have revealed that FDC exhibits complicated kinetic behavior and likely possesses

half-of-sites reactivity. Nevertheless, I was interested to see if isotope effects could similarly be

observed under pre-steady state conditions. Measuring such isotope effects in the pre-steady state

regime could provide additional information on the individual transition states of steps in the

mechanism rather than just the transition state of the rate-limiting step. In this chapter, I describe

a preliminary investigation that indicates that secondary isotope effects can be observed under pre-steady state conditions. Since only one concentration of substrate was used, the data should be treated as a glimpse into the isotope effects for FDC. However, the observation of an inverse 2° equilibrium isotope effect being present during styrene-prFMN cycloadduct formation in this study suggests that a more detailed analysis on the substrate concentration-dependence of the isotope effect could yield important mechanistic insights.

4.2 Materials and Methods

4.2.1 Reagents

Styrene and d_8-styrene were purchased from Sigma-Aldrich Co. All other materials were purchased from Sigma-Aldrich Co. or Thermo Fisher Scientific Co.

4.2.2 Expression and Purification of FDC

Expression and purification of recombinant *S. cerevisiae* holo-FDC from *E. coli* were performed as described previously.[15, 68] In short, a pET28b plasmid containing in tandem *tPAD* (not tagged) and *FDC* with a C-terminal 6x-His tag was transformed into *E. coli* BL21 DE3 star (Invitrogen). *E. coli* cultures were grown at 37 °C in LB supplemented with 50 μg/mL kanamycin. Once an OD_{600} of 0.6 – 0.8 was reached, cultures were induced with 0.2 mM IPTG and incubated at 18 °C overnight (~18 h). Cells were harvested by centrifugation and either immediately purified or stored at -20 °C.

Cell pellets were resuspended in Buffer A (50 mM potassium phosphate, 500 mM potassium chloride, 5 mM imidazole pH 7.5; 4 mL of Buffer A/1 g of cell pellet), EDTA-free protease inhibitor tablets (Roche), lysozyme (4 mg lysozyme/1 g of cell pellet), and Benzonase nuclease (Sigma-Aldrich). Cells were lysed via sonication (10 s pulses with 30 s pauses for a

total of 15 min of sonication) and the resulting lysate clarified by centrifugation at 18,500 rpm at 4 °C for 45 min. The supernatant was loaded onto a HisTrap column (GE Healthcare) equilibrated with Buffer A. Due to a previous report[19] that found prolonged light exposure could inactive FDC, the HisTrap column was wrapped in foil to reduce light exposure. (However, we would like to note that this inactivation had not been observed with any of our FDC preps.) Protein purification was performed using a Bio-Rad NGC chromatography system. The protein loaded on the HisTrap column was first washed with Buffer A and then increasing percentages of Buffer B (50 mM potassium phosphate, 500 mM potassium chloride, 500 mM imidazole pH 7.5). First, a 10% Buffer B wash (55 mM imidazole) and then a 20% Buffer B wash (104 mM imidazole) were performed to remove undesired proteins. To obtain concentrated FDC, FDC was eluted with a 100% Buffer B wash (500 mM imidazole). The FDC fractions were immediately placed in a covered ice bucket to minimize light exposure. Fractions were analyzed by SDS-PAGE on a 10% gel (BioRad) and then desalted into Buffer C (50 mM potassium phosphate, 20% (v/v) glycerol pH 7.5) using PD-10 desalting columns (GE Healthcare). All purified FDC were flash-frozen and stored at -80 °C.

4.2.3 Stopped-flow Absorption Spectroscopy

Experiments were performed using a Hi-Tech Scientific SF-61 DX2 double-mixing instrument (TGK Scientific) controlled by Kinetic Studios software package (TGK Scientific). A monochromator was used to collect single-wavelength absorbance traces. Concentrated FDC and all substrate solutions were prepared in 50 mM potassium phosphate, 10% (v/v) glycerol, 1% (v/v) DMSO pH 7.5. FDC was placed in a glass tonometer with an ice bath feature to stabilize the enzyme. Experiments were performed at 4 °C and in the dark to protect against potential photodegradation.[19] Reactions with styrene and d_8-styrene were performed in triplicate in which

at least 5 measurements were made at each wavelength of interest. To ensure that measurements were made under as closely similar conditions as possible, a set of traces were first recorded for the reaction of styrene with FDC. Then, the substrate line was thoroughly washed with reaction buffer and a set of traces were recorded for the reaction of d_8-styrene with the same solution of FDC. The substrate solutions were alternated in this manner several times, while maintaining the same batch of FDC. This procedure minimized potential differences in amplitudes and rates due to loss of enzyme activity or changes in temperature during the experiment. All reactions were followed for the same period of time allowing for averages over the triplicates to be taken and used for data analysis.

4.3 Results and Discussion

Based on the previous study in Chapter 3, a low styrene:enzyme ratio of 1:3 was chosen to study the reaction in a single active site. Further, fully deuterated styrene (d_8-styrene) was chosen due to the Marsh laboratory's previous study[30] reporting larger 2° KIEs when both Cα and Cβ of phenylacrylic acid were deuterated compared to when only one position was deuterated. The reaction of 188 μM FDC with 60 μM styrene (final concentrations after mixing) were monitored at 425 nm and 460 nm to observe the formation of the styrene-prFMN cycloadduct. As previously noted in Chapter 2 and Chapter 3, a very fast initial decrease in absorbance was observed at all wavelengths with a k_{obs} >1000 s^{-1} (Figure 4.1). This phase was also observed with enzyme shot against buffer. Therefore, this phase was determined to be a mixing artifact.
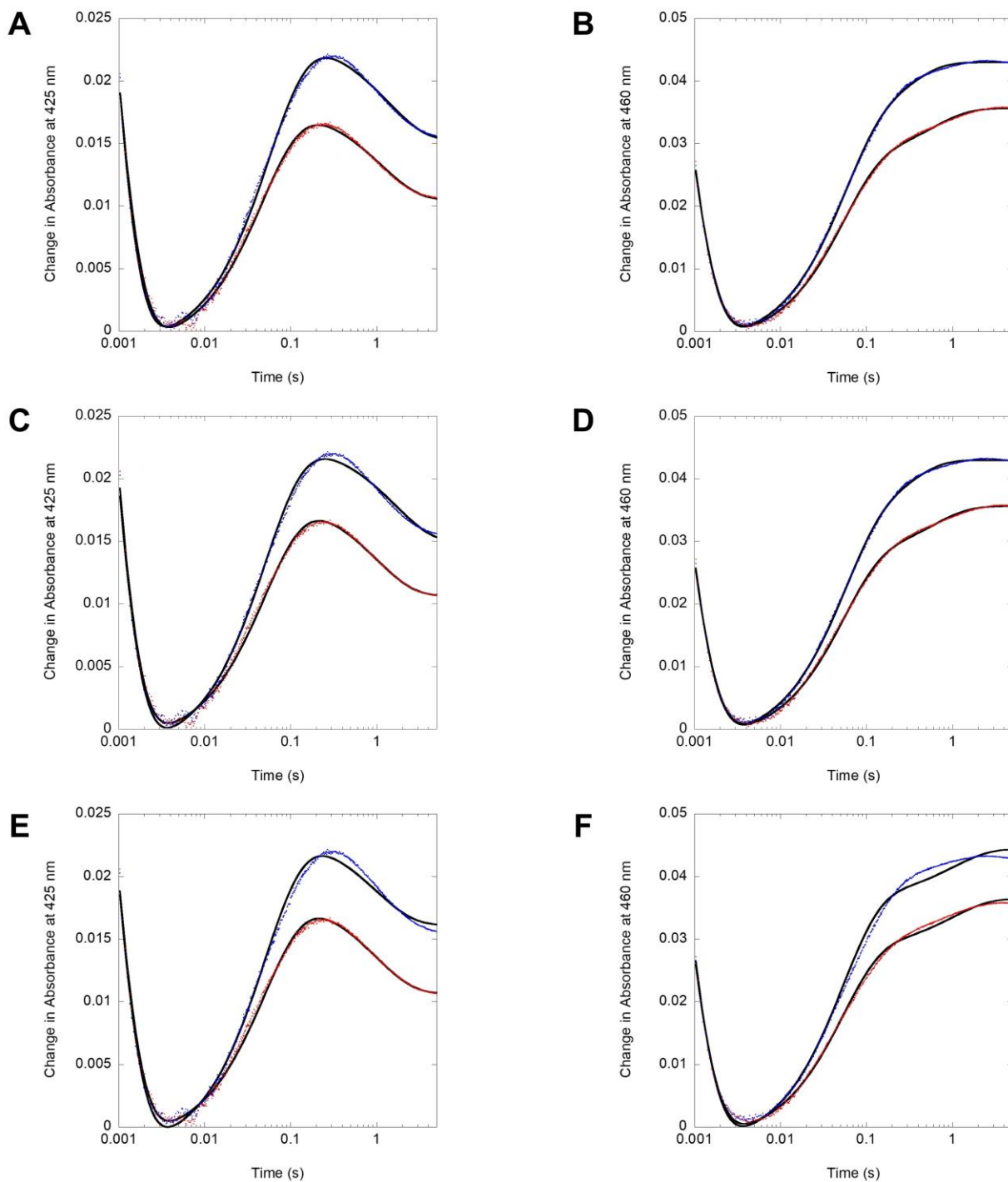
Figure 4.1: Pre-steady state kinetics of 188 μM FDC reacting with 60 μM styrene and 60 μM d8-styrene. A) Reaction of FDC with styrene (red) and with d8-styrene (blue) monitored at 425 nm. Both traces were fitted to a three-exponential equation in which all observed rate constants and amplitudes were allowed to float. **B)** Reaction of FDC with styrene (red) and with d8-styrene (blue) monitored at 460 nm. Both traces were fitted to a three-exponential equation in which all observed rate constants and amplitudes were allowed to float. **C)** Reaction of FDC with styrene (red) and with d8-styrene (blue) monitored at 425 nm. Both traces were fitted to a three-exponential equation in which the second observed rate constant (k_{obs2}) was fixed to 19 s^{-1} while all other variables were allowed to float. **D)** Reaction of FDC with styrene (red) and with d8-styrene (blue) monitored at 460 nm. Both traces were

fitted to a three-exponential equation in which the second observed rate constant (k_{obs2}) was fixed to 19 s^{-1} while all other variables were allowed to float. **E)** Reaction of FDC with styrene (red) and with d$_8$-styrene (blue) monitored at 425 nm. Both traces were fitted to a three-exponential equation in which all three observed rate constants (k_{obs1}, k_{obs2}, and k_{obs3}) were fixed to 1600 s^{-1}, 19 s^{-1}, and 1 s^{-1}, respectively. The associated amplitudes were allowed to float. **F)** Reaction of FDC with styrene (red) and with d$_8$-styrene (blue) monitored at 460 nm. Both traces were fitted to a three-exponential equation in which all three observed rate constants (k_{obs1}, k_{obs2}, and k_{obs3}) were fixed to 1600 s^{-1}, 19 s^{-1}, and 1 s^{-1}, respectively. The associated amplitudes were allowed to float.

The FDC reaction with styrene exhibited the expected kinetic behaviors at 425 nm and 460 nm. The data were fitted to a series of three first-order reaction processes in KaleidaGraph:

$$A_{(t)} = A_0 + A_1 e^{-(k_{obs1}*t)} + A_2 e^{-(k_{obs2}*t)} + A_3 e^{-(k_{obs3}*t)} \tag{4.1}$$

Where A_0 is the initial absorbance, and $A_{(n)}$ and $k_{obs(n)}$ for n = 1, 2, 3 are the amplitude and observed rate constant, respectively, associated with phase n. The values of the best fits (Figure 4.1A,B) are shown in Table 4.1 and Table 4.2. At 425 nm, the initial very fast phase is followed by an increase in absorbance with a $k_{obs2,H}$ of 20.5 ± 0.2 s^{-1} and then a final, smaller absorbance decrease with a $k_{obs3,H}$ of 0.88 ± 0.02 s^{-1} (Figure 4.1A). At 460 nm, both the second and third phases are characterized with increases in absorbance, although the absorbance change for the third phase is quite small (Figure 4.1B). The second phase occurs with a $k_{obs2,H}$ of 19.0 ± 0.1 s^{-1} while the third phase occurs with a $k_{obs3,H}$ of 1.73 ± 0.04 s^{-1}.

Table 4.1: Amplitudes, observed rate constants, and calculated 2° IEs for single wavelength traces at 425 nm.

	A₁	k_{obs1}	A₂	k_{obs2}	A₃	k_{obs3}	A₀	R²
Styrene	0.104 ± 0.003	1599 ± 23	-0.01936 ± 0.00006	20.5 ± 0.2	0.00750 ± 0.00005	0.88 ± 0.02	0.22351 ± 0.00005	0.997
d₈-Styrene	0.126 ± 0.005	1792 ± 31	-0.02486 ± 0.00007	17.3 ± 0.1	0.00830 ± 0.00007	0.74 ± 0.02	0.22427 ± 0.00007	0.998
2° IE			0.778 ± 0.003	1.19 ± 0.01	0.90 ± 0.01	1.20 ± 0.04	0.9966 ± 0.0004	

Table 4.2: Amplitudes, observed rate constants, and calculated 2° IEs for single wavelength traces at 460 nm.

	A_1	k_{obs1}	A_2	k_{obs2}	A_3	k_{obs3}	A_0	R^2
Styrene	0.139 ± 0.003	1600 ± 21	-0.0287 ± 0.0001	19.0 ± 0.1	-0.0085 ± 0.0001	1.73 ± 0.04	0.17564 ± 0.00004	0.9993
d$_8$-Styrene	0.132 ± 0.003	1550 ± 18	-0.0335 ± 0.0003	19.0 ± 0.2	-0.0114 ± 0.0003	3.7 ± 0.09	0.18299 ± 0.00003	0.9996
2° IE			0.857 ± 0.007	1.00 ± 0.01	0.75 ± 0.02	0.47 ± 0.02	0.9598 ± 0.0002	

The reaction of FDC with 60 μM d$_8$-styrene overall exhibits the same three phases at both wavelengths of interest as the protiated substrate (Figure 4.1A,B). Further, the data could be fitted well to Equation 4.1 with the best fits (Figure 4.1A,B) shown in Table 4.1 and Table 4.2. However, there are notable differences with the deuterated substrate that become especially apparent when the single wavelength traces are overlayed. At both 425 nm and 460 nm, the second phase in the reaction with d$_8$-styrene has a larger amplitude. At 425 nm, this results in an inverse 2° equilibrium isotope effect of 0.778 ± 0.003. Similarly, the 2° equilibrium isotope effect at 460 nm is inverse and determined to be 0.857 ± 0.007. At both wavelengths, the second phase should correlate with the formation of the styrene-prFMN cycloadduct and thus, the calculated 2° equilibrium isotope effect should be the same. Therefore, while the methods allow for good precision to be determined, the different calculated values of the 2° equilibrium isotope effect indicate there is a systematic experimental error. Nevertheless, the inverse nature of the 2° equilibrium isotope effects for this phase indicate that the equilibrium of this reaction shifts with d$_8$-styrene to favor the Michaelis complex. This makes sense since heavy isotopes prefer stiffer bonds and the formation of the styrene-prFMN cycloadduct involves the rehybridization from sp^2 to sp^3 for both the Cα and Cβ of styrene. Thus, these 2° equilibrium isotope effects are consistent

with the cycloaddition reaction between FDC and its substrate to form the styrene-prFMN cycloadduct.

An inverse 2° equilibrium isotope effect is also present in the third phase for both wavelengths. At 425 nm, where the third phase is more readily apparent due to the change in direction of the amplitude, the calculated 2° equilibrium isotope effect is 0.75 ± 0.02. In comparison, the 2° equilibrium isotope effect at 460 nm is 0.90 ± 0.01. As discussed earlier, inverse 2° equilibrium isotope effects are consistent with styrene-prFMN cycloadduct formation. While the substrate concentration is only a third of the enzyme concentration, it is possible that the second active site may have substrate bound and that the third phase represents the formation of the styrene-prFMN cycloadduct in this active site. This would also explain the absorbance increase of the third phase at 460 nm, but the reasoning for the absorbance decrease at 425 nm is less clear. A possible explanation is that reaction in the second active site results in a change in the environment of one or both active sites, which could affect the extinction coefficient for the styrene-prFMN cycloadduct(s). However, it is unlikely that the third phase represents the transient formation of the single-tethered prFMN adduct (Figure 1.5, intermediate **D**) in the first active site as this reaction occurs much slower.[30] In addition, the 2° equilibrium isotope effect for this reaction would likely be normal since both Cα and Cβ undergo rehybridization from sp^3 to sp^2. A more extensive study involving additional substrate concentrations (and potentially including high concentrations of bicarbonate) could help to elucidate this third phase.

Similarly, while 2° KIEs are observed, the data cannot be confidently interpreted until additional experiments are performed. For the second phase, the observed rate constants exhibit a normal 2° KIE of 1.19 ± 0.01 at 425 nm but are at unity ($k_{obs,2,H}/k_{obs,2,D} = 1.00 \pm 0.01$) at 460 nm. Since the second phase should represent the same reaction step at both wavelengths, the 2° KIE

should be the same. In addition, a normal 2° KIE suggests a rehybridization from sp^3 to sp^2, which is the opposite of what occurs in the cycloaddition reaction. The 2° KIEs of the third phase are also conflicting. At 425 nm, an inverse 2° KIE of 0.47 ± 0.02 is calculated which is out of the range for a 2° isotope effect. In contrast, a normal 2° KIE of 1.20 ± 0.04 is calculated at 460 nm. While an inverse 2° KIE is consistent with the formation of the styrene-prFMN cycloadduct, the conflicting 2° KIEs of the third phase do not allow for much interpretation.

A possible explanation for the conflicting 2° KIEs is that these are the result of artifacts during the fitting process. To test the robustness of the fits, all the single wavelength traces were fitted to Equation 4.1 in which the value of k_{obs2} was fixed at 19 s^{-1} (Figure 4.1C,D). The value of k_{obs2} was chosen due to the similar values obtained at both wavelengths and for both substrates. For 460 nm, the fits were nearly identical compared to the fits in which all parameters were allowed to float (Figure 4.1A,B) with the fits for styrene possessing a χ^2 of 6.5×10^{-5} and a R^2 value of 0.9993 and the fits for d_8-styrene possessing a χ^2 of 5.5×10^{-5} and a R^2 value of 0.9996. For 425 nm, the fits were also very similar to the fits obtained with all parameters allowed to float. Specifically, the fit for styrene had a χ^2 of 5.3×10^{-5} and a R^2 value of 0.997 and compared well to the unconstrained fit, which possessed a χ^2 of 4.6×10^{-5} and the same R^2 value. The fit for d_8-styrene was slightly worse with a χ^2 of 8.2×10^{-5} and a R^2 of 0.997 compared to the unconstrained fit with a χ^2 of 6.1×10^{-5} and a R^2 of 0.998. This is also reflected in the noticeable premature end of the second phase and the under- and over-estimation of the third phase for d_8-styrene (Figure 4.1C).

Fitting the traces to Equation 4.1 in which all three observed rate constants were fixed ($k_{obs1} = 1600$ s^{-1}, $k_{obs2} = 19$ s^{-1}, and $k_{obs3} = 1$ s^{-1}) resulted in noticeably worse fits (Figure 4.1E,F). For styrene at 425 nm, the fit matched well with a slightly larger χ^2 of 5.4×10^{-5} (compared to $\chi^2 =$

4.6x10^{-5} for the unconstrained fit) but again, the R^2 value did not change. The fit for d$_8$-styrene at 425 nm is worse with the second phase being overestimated and the third phase being under- and overestimated. This is reflected in the much larger χ^2 value for this fit (1.4x10^{-3}) even though the R^2 value barely changed (0.996). At 460 nm, the χ^2 values for both styrene substrates increased by about 2 orders of magnitude (1.5x10^{-3} for styrene and 5.8x10^{-3} for d$_8$-styrene) compared to the χ^2 values of the unconstrained fits (6.5x10^{-5} for styrene and 5.5x10^{-5} for d$_8$-styrene). The R^2 values also decreased with the fit for styrene possessing a R^2 of 0.998 (unconstrained fit R^2 = 0.9993) and the fit for d$_8$-styrene possessing a R^2 of 0.996 (unconstrained fit R^2 = 0.9996). The deficiencies of the fit are particularly noticeable for the d$_8$-styrene trace in which the second phase is overestimated and third phase is both under- and overestimated.

Taken all together, the unconstrained fits provide a good estimation of the observed rate constant of the second phase at both wavelengths and this phase appears to not possess a 2° KIE. However, the constrained fits suggest that a small additional phase may be present between the second and third phase due to the inability to describe the full absorbance increase at both wavelengths with a single observed rate constant (Figure 4.1C,D,E,F). This is supported by the styrene concentration series data presented in Chapter 3 in which the data were globally fitted to three phases that occurred after the initial mixing artifact. In contrast, the data presented in this chapter were only fitted to two phases after the initial mixing artifact since the data could be reasonably described without adding another phase (Figure 4.1A,B). This additional phase may also allow for a better estimation of the observed rate constant for the final phase at both wavelengths and for both substrates. A more extensive concentration study will be vital for analyzing this phase.

4.4 Conclusions

This chapter describes a preliminary investigation into the isotope effects on the pre-steady state kinetic behavior of FDC forming the styrene-prFMN cycloadduct using styrene and its fully deuterated version, d_8-styrene. The reactions were monitored at 425 nm and 460 nm to monitor the formation of the styrene-prFMN cycloadduct. In addition, due to FDC exhibiting kinetic behavior that matches well with a half-of-sites reactivity model, a low concentration of substrate (60 µM) was used compared to enzyme (188 µM) in an attempt to have the reaction occur in only one active site of the homodimer. While low substrate concentration coupled with the properties of the prFMN and its adducts resulted in small absorbance changes, there were notable differences in the kinetic phases between the protiated and deuterated substrates. Specifically, an inverse 2° equilibrium isotope effect is observed for the second phase at both wavelengths. This is consistent with the formation of the styrene-prFMN cycloadduct, which should be represented by the second phase. An inverse 2° equilibrium isotope effect is also seen for the third phase at both wavelengths but the explanation for this is not clear. 2° KIEs for individual phases were inconsistent between wavelengths, preventing any analysis. Fixing the observed rate constant values for the second phase did not greatly affect the fits, whereas fixing all observed rate constants generally yielded poorer fits that better described the styrene data than the d_8-styrene data. However, the inability to describe the full absorbance increase at 425 nm and 460 nm with a single observed rate constant suggests the presence of an additional phase between the second and third phase. Nevertheless, before an in-depth analysis can be performed, a more extensive concentration range study needs to be performed as well as a concentration range study using phenylacrylic acid and d_7-phenylacrylic acid.

Chapter 5 Conclusions and Future Directions

5.1 Introduction

The discovery of the prFMN in 2015 has enabled scientists to study the UbiD family of decarboxylases *in vitro*. There are more than 100 proposed UbiD family members, spanning all three domains of the microbial world.[2] These family members are involved in both primary and secondary metabolism as well as the degradation of toxic compounds to protect their host. This suggests that the UbiD family has ancient origins and highlights the importance of understanding how this family performs catalysis utilizing the prFMN cofactor. Currently, FDC is the most well-understood UbiD family member. In this last chapter, I will review the results and conclusions of my work on FDC as well as propose future directions for the study of FDC.

5.2 The Styrene-prFMN Cycloadduct Builds up At Chemical Equilibrium

At the start of my work on FDC, the existence of the prFMN cofactor had only been known for ~2 years and the 1,3-dipolar cycloaddition mechanism for FDC decarboxylation was still under scrutiny. Not only was 1,3-dipolar cycloaddition chemistry unprecedented in Nature, but the only evidence for this chemistry was produced with inhibitors. Therefore, I endeavored to study the reaction intermediates of FDC using substrates.

In collaboration with the Ruotolo lab and a previous Marsh laboratory graduate student Dr. Kyle Ferguson, the reaction of FDC with both phenylacrylic acid and styrene was successfully studied using native MS. With both substrates, peaks of the correct *m/z* to be the proposed styrene-prFMN cycloadduct, complexed with either a proton or K^+ ion, were observed.

These peaks were confirmed to be derived from the reaction of substrate with the prFMN of FDC using fully deuterated versions of the substrates. Due to the protocol for native MS, the FDC reaction could only be studied at chemical equilibrium. Nevertheless, these data indicate that the styrene-prFMN cycloadduct builds up on the enzyme at equilibrium. This observation is further supported by the significant population (30%) of AnFDC crystals containing the styrene-prFMN cycloadduct which were obtained by the Leys group by incubating AnFDC crystals with phenylacrylic acid and then flash-cooling.[35] In addition, I was able to obtain the absorbance spectrum of the styrene-prFMN cycloadduct, revealing a wide major absorbance band at ~450 nm as well as a minor band at ~340 nm.

5.3 FDC Displays Half-of-sites Reactivity

Due to the k_{cat} for FDC, it became apparent that further investigation into reaction intermediates would require data collection on at least a millisecond timescale. This coupled with the rich U.V.-visible spectral properties of flavins led to the decision to use stopped-flow absorption spectroscopy to analyze the pre-steady state kinetics of the FDC reaction. I attempted to further slow the reaction of FDC using a sub-optimal pH of 7.5 (optimal pH is 6.5) as well as a temperature of 4 °C. Nevertheless, under these conditions, FDC still has a k_{cat} of 11.3 s^{-1}.

The absorption spectrum of FDC reacting with phenylacrylic acid and styrene are similar with a loss of the 380 nm band that represents the iminium prFMN species and the increase in a broad absorbance band at ~460 nm. The latter peak matches well with the spectrum of the styrene-prFMN cycloadduct, further supporting our observations that this intermediate accumulates on the enzyme at equilibrium. Notably, the reaction of FDC with phenylacrylic acid appears to approach equilibrium within 1 s, whereas reaction with styrene equilibrates within 5 s. The data presented in this dissertation, together with the data reported by others,[30, 35] strongly

supports the hypothesis that cycloelimination of the styrene-prFMN cycloadduct is the rate-determining step of the FDC reaction.

Due to the similar spectral changes for the forward and reverse reaction, the same wavelengths were chosen for pre-steady state single-wavelength kinetic studies of the reactions. These data reveal that FDC exhibits surprisingly complex kinetic behavior that we are currently unable to completely model. Nevertheless, the kinetic behavior can be tentatively explained by half-of-sites reactivity, a form of negative cooperativity between the two monomers of the FDC homodimer. The reaction of FDC with styrene, which could only progress to the styrene-prFMN cycloadduct intermediate, displays three kinetic phases when monitored at 380 nm, 425 nm, or 460 nm and can be globally fitted to a three-exponential function. In comparison, the reaction of FDC with phenylacrylic acid consistently shows four kinetic phases when monitored at these wavelengths and, in Chapter 2, was successfully globally fitted to a half-of-sites reactivity model described by four observed rate constants.

Although this particular model is no longer supported due to the newer data in Chapter 3, the concentration independence of the faster phases coupled with the clear concentration dependence of the slower phases for both phenylacrylic acid and styrene could be explained by a half-of-sites reactivity model in which one active site of the FDC dimer is in a "fast, tight-binding" state and the other active site is in a "slow, loose-binding" state. The faster, concentration-independent phases represent the formation and breakdown of the styrene-prFMN cycloadduct in the "fast, tight" active site. In contrast, the slower, concentration-dependent phase(s) are likely representing the formation (and breakdown in the case of phenylacrylic acid) of this same cycloadduct intermediate in the "slow, loose" active site, which is only seen at higher substrate concentrations. Importantly, during the reaction with either substrate, there is no

sign of the iminium species of prFMN re-forming which would be indicated by an increase in absorbance at 380 nm, even at the lowest substrate to enzyme ratio (1:4). This implies that the "fast, tight" active site is unable to perform the cycloelimination step at an appreciable rate.

Through the structural studies of other UbiD enzymes such as HudA and VdcCD, it has been shown that the conserved UbiD protein fold can perform notable domain motions that change the relative distance of the prFMN-binding domain and the oligomerization domain via a hinge motion performed by a conserved α-helix.[18, 67] Importantly, the active site of all UbiD enzymes is located at the interface of these two domains. Moreover, for VdcCD, domain motion is proposed to be necessary for catalysis to initiate the reaction between substrate and the prFMN cofactor, as well to exert consistent strain on the reaction intermediates to ensure full catalysis occurs and no dead-end adducts are formed.[25] Therefore, it is reasonable to hypothesize that FDC can undergo similar domain motions and that these domain motions are involved in catalysis.

The observation that cycloelimination does not appear to occur in FDC under single-turnover conditions, combined with the knowledge that this reaction step is likely rate-limiting, could be explained by the need for FDC to undergo a domain motion that provides the energy required to overcome the high activation energy barrier for cycloelimination. Specifically, we propose that substrate binding in the "slow, loose" active site (which would only occur with high substrate concentrations) results in communication between the two active sites that yields the "slow, loose" active site transitioning into the "fast, tight" state, while the "fast, tight" active site that has been stalled at cycloelimination transitions into the "slow, loose" state. The styrene-prFMN cycloadduct is now in a low affinity active site due to the latter transition from "fast, tight" to the "slow, loose" state. This low affinity environment of the new "slow, loose" active site allows for the cycloelimination step to occur, producing styrene which can dissociate from

105

the enzyme as well as regenerating the iminium prFMN for the next round of catalysis. Cycloelimination in this "slow, loose" active site may also be assisted by the energetically favorable reaction progression (up to cycloelimination) occurring in the *new* "fast, tight" active site, which has bound phenylacrylic acid. Regardless, the new "fast, tight" active site will perform the catalytic reaction until the cycloelimination step. At this point, the same process of phenylacrylic acid binding in the current "slow, loose" active site resulting in transition of the active sites' states occurs, thus producing a catalytic cycle.

Additional studies are needed to test the validity of this "two-stroke" catalytic cycle model. Mutagenesis studies could be used to test the need for communication between FDC monomers for catalysis by producing FDC variants that do not oligomerize or by mixing an inactive FDC variant with wild-type FDC to generate dimers that only have one functional active site. However, the latter would require oligomerization of FDC dimers to be reversible which has not been studied. Investigating the temperature and pH-dependence of the FDC reaction under pre-steady state conditions may allow for better characterization of the multiple phases observed as certain steps in the mechanism may be sensitive to these factors. Characterizing the active site variants E285D and E285Q (*S. cerevisiae* numbering) reacting with phenylacrylic acid under pre-steady state conditions might provide information on the protonation step of the single-tethered adduct, which is the step that precedes the formation of the styrene-prFMN cycloadduct. Previous studies on these variants from AnFDC reported that the aspartic acid substitution significantly lowered the observed k_{cat}, whereas the glutamine variant was inactive and thus allowed for the single-tethered adduct to be spectrally and structurally characterized.[19, 35] However, U.V.-visible spectra and MS analyses revealed that the E285Q variant had low cofactor incorporation and both variants contained a mixture of iminium prFMN and prFMN

radical. In comparison, the U.V.-visible spectra of the corresponding *S. cerevisiae* variants revealed both contained a mixture of FMN and iminium prFMN, although this is likely not due to the amino acid substitutions since the wildtype preparation also bound a notable amount of FMN.[19] (I would like to note that this high FMN content has not been observed in my FDC preparations). Nevertheless, the *S. cerevisiae* variants may also have incomplete cofactor maturation (indicated by the presence of the prFMN radical) like their *A. niger* counterparts.

The above discussion highlights another important area for continued study: the oxidative maturation of prFMN in FDC (and the UbiD family as a whole). While numerous prFMN species can exist bound by the enzyme and in solution,[36, 39] the exact mechanism for oxidative maturation is not fully understood yet. This has hindered investigations into UbiD, in which the prFMN only oxidizes to the radical species,[21] and may prevent the study of future family members. Since both facultative anaerobes and obligate anaerobic microbes possess UbiD family members, prFMN oxidative maturation likely occurs through different mechanisms based on available oxidizing agents. Furthermore, almost all the currently characterized UbiD family members form a notable amount of prFMN radical, suggesting that either the fully oxidized iminium species is not as heavily favored at equilibrium as expected or that oxidation from the radical species to the iminium species is extremely difficult. Lastly, determination of the extinction coefficient for the iminium prFMN species in FDC would greatly benefit kinetic studies by simplifying the determination of the concentration of active enzyme.

5.4 FDC Displays Equilibrium Isotope Effects Under Pre-Steady State Conditions

After observing the complex kinetic behavior of FDC, I became interested in the transition states of the enzyme reaction. Since secondary isotope effects provide insight into the transition state and a previous study performed by the Marsh laboratory observed secondary

kinetic isotope effects under steady state conditions[30], I hypothesized that secondary isotope effects could be observed under pre-steady state conditions. From my preliminary investigation with styrene and d_8-styrene in Chapter 4, there appears to be a 2° equilibrium isotope effect for the first kinetic phase of the reaction at both 425 nm and 460 nm. While the calculated 2° equilibrium isotope effect value may be inaccurate due to the overall small changes in absorbance that occur in the FDC reaction, the 2° equilibrium isotope effect was consistently observed over three trials. The 2° equilibrium isotope effect is inverse, suggesting that the equilibrium between the Michaelis complex and the styrene-prFMN cycloadduct shifts to favor the Michaelis complex when the substrate is deuterated. This is reasonable since the conversion of the Michaelis complex to the styrene-prFMN cycloadduct requires the α=β bond of the substrate to transition from sp^2-hybridization to sp^3-hybridization and heavy-labelled substrates will prefer stiffer bonds.

However, it is important to note that this study is preliminary and more experiments are required before definitive conclusions can be drawn. Investigating the reaction with styrene that is singly deuterated at either Cα or Cβ would help to verify the observed inverse 2° equilibrium isotope effect of the first kinetic phase. In addition, monitoring the reaction using various concentrations of protiated and deuterated styrene substrates could provide more insight into the formation of the styrene-prFMN cycloadduct. Further, as more information on the kinetic behavior of FDC is established, the forward decarboxylation reaction with phenylacrylic acid could be studied for primary isotope effects (decarboxylation step using a heavy-labeled carboxyl group) as well as secondary isotope effects (cycloadduct formation and breakdown using singly and fully deuterated substrates).

5.5 Looking to the Future

The need to eliminate reliance on non-renewable fossil fuels has encouraged exploration to identify alternative methods for synthesizing the petrochemical styrene which is widely used in the polymer industry. FDC has attracted notable interest in this search due to its ability to produce styrene from phenylacrylic acid under ambient conditions, allowing for an eco-friendly alternative. In 2011, the first microbial system to generate styrene from glucose was designed.[78] This was achieved by over-expressing recombinant phenylalanine ammonia lyase (PAL) and recombinant FDC in the phenylalanine over-producing *E. coli* strain NST74. Styrene titers reached 260 mg/L after 29 h (post-induction), likely limited due to styrene toxicity (~300 mg/L). Excitingly, earlier this year, a new *E. coli* system improved styrene yield to ~24 g/L, nearly a 100-fold improvement.[79] In this system, two *E. coli* BL21(DE3) strains were mixed at resting phase: one strain over-expressed recombinant PAL and the other over-expressed native EcUbiX and recombinant AnFDC. Styrene was generated by addition of phenylalanine to the consortium with total conversions ranging from 88-98% within 4 h. Not only was this a significant acceleration in the rate of styrene production but the authors were able to overcome styrene toxicity using this system. Furthermore, the system could generate styrene from the protein-rich biomasses casamino acids, spirulina algae (acid-treated), and pumpkin seed powder (acid-treated) with conversions of 82%, 93%, and 83%, respectively. Thus, the system accepts a wide range of phenylalanine sources and is not inhibited by other biomass components which allows for various feedstocks to be utilized such as food waste. Lastly, the authors noted that lyophilization of the cells allowed for storage up to 9 months without change in activity and that the lyophilized cells could be added directly to media for styrene production. Together, these studies demonstrate not only the clear feasibility of an FDC-based system for the eco-friendly

109

industrial production of styrene but also that further improvements to the system will likely be achievable in the near future.

FDC is also capable of carboxylating styrene using pressurized CO_2 or high concentrations of bicarbonate, which can be used for CO_2 fixation as well as production of carboxylic acids under mild conditions. Although the decarboxylation reaction is heavily favored, by coupling the FDC-catalyzed carboxylation reaction to the energetically favorable reduction of phenylacrylate to 3-phenyl-2-propenol, near-total styrene carboxylation was achieved. In 2020, the Leys laboratory developed a system in which 3-phenyl-2-propenol (the alcohol form of phenylacrylic acid) could be generated from styrene and potassium bicarbonate with a conversion of 95%.[80] This was accomplished by adding purified AnFDC (or lyophilized cell-free extracts containing AnFDC) to resting *E. coli* cells over-expressing carboxylic acid reductase (CAR) and containing endogenous alcohol dehydrogenase (EcADH). CAR performs the thermodynamically favorable reduction of phenylacrylic acid to 3-phenyl-2-propenal using NADPH and ATP. EcADH then reduces 3-phenyl-2-propenal to the primary alcohol 3-phenyl-2-propenol. Importantly, optimal conversion was achieved at stoichiometric molar ratios of styrene and potassium bicarbonate instead of requiring high bicarbonate concentrations. *In vitro*, utilizing purified enzymes, the authors were also able to convert styrene to 3-phenylacrylamide (14% conversion, NADPH-independent CAR amidation) and to a secondary amine (93% conversion, using cyclopropylamine and an imine reductase).

Further, the rational design and directed evolution of FDC has increased the already broad range of substrates for decarboxylation. Wild-type FDC can decarboxylate phenylacrylic acids as well as linear conjugated compounds such as sorbic acid (and most recently 2,4,6-octatrienoic acid)[81]. The active site variant I327S of AnFDC improved or gained decarboxylase

activity against a variety of mono- and bicyclic (hetero)aromatic carboxylic acids including benzofuran-2-carboxylic acid (>99% conversion), 2-naphthoic acid (7%), and pyrrole-2-carboxylic acid (60% conversion).[80] The authors also demonstrated that benzofuran-2-carboxylic acid could be converted to its alcohol, amide, or secondary amine form using the AnFDC-CAR-EcADH system or the purified enzymes discussed in the previous paragraph. Directed evolution studies have created FDC variants that can produce isobutene from 3-methylcrotonic acid[82] and butadiene from *cis,cis*-muconic acid in which the FDC variant performs two consecutive decarboxylation steps.[83] The latter conversion allowed for the creation of a whole-cell *E. coli* system capable of producing butadiene from glucose with a total yield of ~2 g/L. Thus, the potential applications for FDC as part of a "green" industrial production system for various valuable compounds are only just beginning to be explored.

Lastly, the UbiD family could be a source for additional biocatalysts due to the variety of carboxylic acid compounds its family members react with. While FDC is currently the most versatile member, studies on AroY,[22] HmfF,[23] PhdA,[45] and HudA[24] have all shown levels of substrate promiscuity which could be enhanced through directed evolution or rational design. In addition, protein complexes containing UbiD-like enzymes are proposed to carboxylate benzene[72, 84] and naphthalene[85, 86] as an activation step in the degradation of these toxic, unreactive compounds by soil-dwelling microbes. Taken together, these studies indicate that scientists have just started tapping into the potential of the UbiD family and the prFMN cofactor. Nevertheless, in order to efficiently modify the UbiD family for our needs, the mechanisms of these reactions need to be investigated. Currently, the quinoid-based mechanism of the AroY-catalyzed decarboxylation is based on DFT calculations and the nature of the substrates involved. Similarly, the electrophilic aromatic substitution mechanism for HudA was proposed from an

inhibitor-prFMN adduct and DFT calculations. Mechanistic studies will provide valuable insight into how other UbiD enzymes catalyze their reactions. Once we have this understanding, as in the case of FDC, we will be better able to utilize the UbiD family as industrial biocatalysts.

References

1.   Cox, G. B.; Young, I. G.; McCann, L. M.; Gibson, F., Biosynthesis of Ubiquinone in *Escherichia coli* K-12: Location of Genes Affecting the Metabolism of 3-Octaprenyl-4-hydroxybenzoic Acid and 2-Octaprenylphenol. *Journal of Bacteriology* **1969,** *99*, 450-458.

2.   Lupa, B.; Lyon, D.; Gibbs, M. D.; Reeves, R. A.; Wiegel, J., Distribution of genes encoding the microbial non-oxidative reversible hydroxyarylic acid decarboxylases/phenol carboxylases. *Genomics* **2005,** *86* (3), 342-351.

3.   Leppik, R. A.; Young, I. G.; Gibson, F., Membrane-associated reactions in ubiquinone biosynthesis in Escherichia coli. 3-octaprenyl-4-hydroxybenzoate carboxy-lyase. *Biochimica et Biophysica Acta (BBA) - Biomembranes* **1976,** *436* (4), 800-810.

4.   Meganathan, R., Ubiquinone biosynthesis in microorganisms. *FEMS Microbiology Letters* **2001,** *203* (2), 131-139.

5.   Zhang, H.; Javor, G. T., Regulation of the isofunctional genes ubiD and ubiX of the ubiquinone biosynthetic pathway of Escherichia coli. *FEMS Microbiology Letters* **2003,** *223* (1), 67-72.

6.   Clausen, M.; Lamb, C. J.; Megnet, R.; Doerner, P. W., PAD1 encodes phenylacrylic acid decarboxylase which confers resistance to cinnamic acid in Saccharomyces cerevisiae. *Gene* **1994,** *142* (1), 107-112.

7.   Gulmezian, M.; Hyman, K. R.; Marbois, B. N.; Clarke, C. F.; Javor, G. T., The role of UbiX in Escherichia coli coenzyme Q biosynthesis. *Archives of Biochemistry and Biophysics* **2007,** *467* (2), 144-153.

8.   Mukai, N.; Masaki, K.; Fujii, T.; Kawamukai, M.; Iefuji, H., PAD1 and FDC1 are essential for the decarboxylation of phenylacrylic acids in Saccharomyces cerevisiae. *Journal of Bioscience and Bioengineering* **2010,** *109* (6), 564-569.

9.   Rangarajan, E. S.; Li, Y.; Iannuzzi, P.; Tocilj, A.; Hung, L.-W.; Matte, A.; Cygler, M., Crystal structure of a dodecameric FMN-dependent UbiX-like decarboxylase (Pad1) from Escherichia coli O157: H7. *Protein Science* **2004,** *13* (11), 3006-3016.

10.   Blaesse, M.; Kupke, T.; Huber, R.; Steinbacher, S., Crystal structure of the peptidyl-cysteine decarboxylase EpiD complexed with a pentapeptide substrate. *The EMBO Journal* **2000,** *19* (23), 6299-6310.

11.   Blaesse, M.; Kupke, T.; Huber, R.; Steinbacher, S., Structure of MrsD, an FAD-binding protein of the HFCD family. *Acta Crystallographica Section D* **2003,** *59* (8), 1414-1421.

12.   Kopec, J.; Schnell, R.; Schneider, G., Structure of PA4019, a putative aromatic acid decarboxylase from Pseudomonas aeruginosa. *Acta Crystallographica Section F* **2011,** *67* (10), 1184-1188.

13.   Bhuiya, M. W.; Lee, S. G.; Jez, J. M.; Yu, O., Structure and Mechanism of Ferulic Acid Decarboxylase (FDC1) from Saccharomyces cerevisiae. *Appl Environ Microbiol* **2015,** *81* (12), 4216-23.

14.   Jacewicz, A.; Izumi, A.; Brunner, K.; Schnell, R.; Schneider, G., Structural Insights into the UbiD Protein Family from the Crystal Structure of PA0254 from Pseudomonas aeruginosa. *PLoS ONE* **2013,** *8*, e63161.

15.   Lin, F.; Ferguson, K. L.; Boyer, D. R.; Lin, X. N.; Marsh, E. N. G., Isofunctional Enzymes PAD1 and UbiX Catalyze Formation of a Novel Cofactor Required by Ferulic Acid Decarboxylase and 4-Hydroxy-3-polyprenylbenzoic Acid Decarboxylase. *ACS Chemical Biology* **2015,** *10* (4), 1137-1144.

16.   Payne, K. A. P.; White, M. D.; Fisher, K.; Khara, B.; Bailey, S. S.; Parker, D.; Rattray, N. J. W.; Trivedi, D. K.; Goodacre, R.; Beveridge, R.; Barran, P.; Rigby, S. E. J.; Scrutton, N. S.; Hay, S.; Leys, D., New cofactor supports α,β-unsaturated acid decarboxylation via 1,3-dipolar cycloaddition. *Nature* **2015,** *522* (7557), 497-501.

17.   White, M. D.; Payne, K. A. P.; Fisher, K.; Marshall, S. A.; Parker, D.; Rattray, N. J. W.; Trivedi, D. K.; Goodacre, R.; Rigby, S. E. J.; Scrutton, N. S.; Hay, S.; Leys, D., UbiX is a flavin prenyltransferase required for bacterial ubiquinone biosynthesis. *Nature* **2015,** *522* (7557), 502-506.

18.   Roberts, G. W.; Leys, D., Structural insights into UbiD reversible decarboxylation. *Current Opinion in Structural Biology* **2022,** *75*.

19.   Bailey, S. S.; Payne, K. A. P.; Fisher, K.; Marshall, S. A.; Cliff, M. J.; Spiess, R.; Parker, D. A.; Rigby, S. E. J.; Leys, D., The role of conserved residues in Fdc decarboxylase in prenylated flavin mononucleotide oxidative maturation, cofactor isomerization, and catalysis. *Journal of Biological Chemistry* **2018,** *293* (7), 2272-2287.

20.   Mergelsberg, M.; Willistein, M.; Meyer, H.; Stärk, H. J.; Bechtel, D. F.; Pierik, A. J.; Boll, M., Phthaloyl-coenzyme A decarboxylase from Thauera chlorobenzoica: the prenylated flavin-, K+-and Fe2+-dependent key enzyme of anaerobic phthalate degradation. *Environmental microbiology* **2017,** *19* (9), 3734-3744.

21.   Marshall, S. A.; Fisher, K.; Cheallaigh, A. N.; White, M. D.; Payne, K. A.; Parker, D.; Rigby, S. E.; Leys, D., Oxidative maturation and structural characterization of prenylated FMN binding by UbiD, a decarboxylase involved in bacterial ubiquinone biosynthesis. *Journal of Biological Chemistry* **2017,** *292* (11), 4623-4637.

22.   Payer, S. E.; Marshall, S. A.; Bärland, N.; Sheng, X.; Reiter, T.; Dordic, A.; Steinkellner, G.; Wuensch, C.; Kaltwasser, S.; Fisher, K.; Rigby, S. E. J.; Macheroux, P.; Vonck, J.; Gruber, K.; Faber, K.; Himo, F.; Leys, D.; Pavkov-Keller, T.; Glueck, S. M., Regioselective para-Carboxylation of Catechols with a Prenylated Flavin Dependent Decarboxylase. *Angewandte Chemie International Edition* **2017,** *56* (44), 13893-13897.

23.   Payne, K. A. P.; Marshall, S. A.; Fisher, K.; Cliff, M. J.; Cannas, D. M.; Yan, C. Y.; Heyes, D. J.; Parker, D. A.; Larrosa, I.; Leys, D., Enzymatic Carboxylation of 2-Furoic Acid Yields 2,5-Furandicarboxylic Acid (FDCA). *Acs Catalysis* **2019,** *9* (4), 2854-2865.

24.   Payne, K. A. P.; Marshall, S. A.; Fisher, K.; Rigby, S. E. J.; Cliff, M. J.; Spiess, R.; Cannas, D. M.; Larrosa, I.; Hay, S.; Leys, D., Structure and Mechanism of Pseudomonas aeruginosa PA0254/HudA, a prFMN-Dependent Pyrrole-2-carboxylic Acid Decarboxylase Linked to Virulence. *Acs Catalysis* **2021,** *11* (5), 2865-2878.

25.   Marshall, S. A.; Payne, K. A. P.; Fisher, K.; Titchiner, G. R.; Levy, C.; Hay, S.; Leys, D., UbiD domain dynamics underpins aromatic decarboxylation. *Nature Communications* **2021,** *12* (1).

26.   Gahloth, D.; Fisher, K.; Payne, K. A. P.; Cliff, M.; Levy, C.; Leys, D., Structural and biochemical characterization of the prenylated flavin mononucleotide-dependent indole-3-carboxylic acid decarboxylase. *Journal of Biological Chemistry* **2022,** *298* (4).

114

27.	Beveridge, R.; Migas, L. G.; Payne, K. A.; Scrutton, N. S.; Leys, D.; Barran, P. E., Mass spectrometry locates local and allosteric conformational changes that occur on cofactor binding. *Nature Communications* **2016,** *7* (1), 12163.

28.	Baunach, M.; Hertweck, C., Natural 1,3-Dipolar Cycloadditions. *Angewandte Chemie International Edition* **2015,** *54* (43), 12550-12552.

29.	Li, T.; Huo, L.; Pulley, C.; Liu, A., Decarboxylation mechanisms in biological system. *Bioorganic Chemistry* **2012,** *43*, 2-14.

30.	Ferguson, K. L.; Arunrattanamook, N.; Marsh, E. N. G., Mechanism of the Novel Prenylated Flavin-Containing Enzyme Ferulic Acid Decarboxylase Probed by Isotope Effects and Linear Free-Energy Relationships. *Biochemistry* **2016,** *55* (20), 2857-2863.

31.	Tian, G.; Liu, Y., Mechanistic insights into the catalytic reaction of ferulic acid decarboxylase from Aspergillus niger: a QM/MM study. *Physical Chemistry Chemical Physics* **2017,** *19* (11), 7733-7742.

32.	Ferguson, K. L.; Eschweiler, J. D.; Ruotolo, B. T.; Marsh, E. N. G., Evidence for a 1,3-Dipolar Cyclo-addition Mechanism in the Decarboxylation of Phenylacrylic Acids Catalyzed by Ferulic Acid Decarboxylase. *Journal of the American Chemical Society* **2017,** *139* (32), 10972-10975.

33.	Eckstein, J. W.; Hastings, J. W.; Ghisla, S., Mechanism of bacterial bioluminescence: 4a,5-Dihydroflavin analogs as models for luciferase hydroperoxide intermediates and the effect of substituents at the 8-position of flavin on luciferase kinetics. *Biochemistry* **1993,** *32* (2), 404-411.

34.	Nanni Jr, E. J.; Sawyer, D. T.; Ball, S. S.; Bruice, T. C., Redox chemistry of N5-ethyl-3-methyllumiflavinium cation and N5-ethyl-4a-hydroperoxy-3-methyllumiflavin in dimethylformamide. Evidence for the formation of the N5-ethyl-4a-hydroperoxy-3-methyllumiflavin anion via radical-radical coupling with superoxide ion. *Journal of the American Chemical Society* **1981,** *103* (10), 2797-2802.

35.	Bailey, S. S.; Payne, K. A. P.; Saaret, A.; Marshall, S. A.; Gostimskaya, I.; Kosov, I.; Fisher, K.; Hay, S.; Leys, D., Enzymatic control of cycloadduct conformation ensures reversible 1,3-dipolar cycloaddition in a prFMN-dependent decarboxylase. *Nature Chemistry* **2019,** *11* (11), 1049-1057.

36.	Wang, P.-H.; Khusnutdinova, A. N.; Luo, F.; Xiao, J.; Nemr, K.; Flick, R.; Brown, G.; Mahadevan, R.; Edwards, E. A.; Yakunin, A. F., Biosynthesis and Activity of Prenylated FMN Cofactors. *Cell Chemical Biology* **2018,** *25* (5), 560-570.e6.

37.	Arunrattanamook, N.; Marsh, E. N. G., Kinetic Characterization of Prenyl-Flavin Synthase from Saccharomyces cerevisiae. *Biochemistry* **2018,** *57* (5), 696-700.

38.	Marshall, S. A.; Payne, K. A. P.; Fisher, K.; White, M. D.; A, N. C.; Balaikaite, A.; Rigby, S. E. J.; Leys, D., The UbiX flavin prenyltransferase reaction mechanism resembles class I terpene cyclase chemistry. *Nat Commun* **2019,** *10* (1), 2357.

39.	Balaikaite, A.; Chisanga, M.; Fisher, K.; Heyes, D. J.; Spiess, R.; Leys, D., Ferulic Acid Decarboxylase Controls Oxidative Maturation of the Prenylated Flavin Mononucleotide Cofactor. *ACS Chemical Biology* **2020,** *15* (9), 2466-2475.

40.	Annaval, T.; Han, L.; Rudolf, J. D.; Xie, G.; Yang, D.; Chang, C.-Y.; Ma, M.; Crnovcic, I.; Miller, M. D.; Soman, J.; Xu, W.; Phillips, G. N.; Shen, B., Biochemical and Structural Characterization of TtnD, a Prenylated FMN-Dependent Decarboxylase from the Tautomycetin Biosynthetic Pathway. *ACS Chemical Biology* **2018,** *13* (9), 2728-2738.

41.   Junghare, M.; Spiteller, D.; Schink, B., Enzymes involved in the anaerobic degradation of ortho-phthalate by the nitrate-reducing bacterium Azoarcus sp. strain PA01. *Environmental microbiology* **2016,** *18* (9), 3175-3188.

42.   Ebenau-Jehle, C.; Mergelsberg, M.; Fischer, S.; Brüls, T.; Jehmlich, N.; von Bergen, M.; Boll, M., An unusual strategy for the anoxic biodegradation of phthalate. *The ISME Journal* **2017,** *11* (1), 224-236.

43.   Koopman, F.; Wierckx, N.; de Winde, J. H.; Ruijssenaars, H. J., Identification and characterization of the furfural and 5-(hydroxymethyl) furfural degradation pathways of Cupriavidus basilensis HMF14. *Proceedings of the National Academy of Sciences* **2010,** *107* (11), 4919-4924.

44.   Costa, K. C.; Moskatel, L. S.; Meirelles, L. A.; Newman, D. K., PhdA catalyzes the first step of phenazine-1-carboxylic acid degradation in Mycobacterium fortuitum. *Journal of bacteriology* **2018,** *200* (10), e00763-17.

45.   Datar, P. M.; Marsh, E. N. G., Decarboxylation of Aromatic Carboxylic Acids by the Prenylated-FMN-dependent Enzyme Phenazine-1-carboxylic Acid Decarboxylase. *Acs Catalysis* **2021,** *11* (18), 11723-11732.

46.   Chow, K. T.; Pope, M. K.; Davies, J., Characterization of a vanillic acid non-oxidative decarboxylation gene cluster from Streptomyces sp. D7. *Microbiology* **1999,** *145* (9), 2393-2403.

47.   Miller, B. G.; Wolfenden, R., Catalytic Proficiency: The Unusual Case of OMP Decarboxylase. *Annual Review of Biochemistry* **2002,** *71* (1), 847-885.

48.   Wolfenden, R., Benchmark Reaction Rates, the Stability of Biological Molecules in Water, and the Evolution of Catalytic Power in Enzymes. *Annual Review of Biochemistry* **2011,** *80* (1), 645-667.

49.   Belcher, J.; McLean, K. J.; Matthews, S.; Woodward, L. S.; Fisher, K.; Rigby, S. E. J.; Nelson, D. R.; Potts, D.; Baynham, M. T.; Parker, D. A.; Leys, D.; Munro, A. W., Structure and Biochemical Properties of the Alkene Producing Cytochrome P450 OleTJE (CYP152L1) from the Jeotgalicoccus sp. 8456 Bacterium. *Journal of Biological Chemistry* **2014,** *289* (10), 6535-6550.

50.   Cleland, W. W., Mechanisms of Enzymatic Oxidative Decarboxylation. *Accounts of Chemical Research* **1999,** *32* (10), 862-868.

51.   Jordan, F.; Patel, H., Catalysis in Enzymatic Decarboxylations: Comparison of Selected Cofactor-Dependent and Cofactor-Independent Examples. *ACS Catalysis* **2013,** *3* (7), 1601-1617.

52.   Keasling, J. D., Manufacturing Molecules Through Metabolic Engineering. *Science* **2010,** *330* (6009), 1355-1358.

53.   Kourist, R.; Guterl, J.-K.; Miyamoto, K.; Sieber, V., Enzymatic Decarboxylation—An Emerging Reaction for Chemicals Production from Renewable Resources. *ChemCatChem* **2014,** *6* (3), 689-701.

54.   McKenna, R.; Thompson, B.; Pugh, S.; Nielsen, D. R., Rational and combinatorial approaches to engineering styrene production by Saccharomyces cerevisiae. *Microbial Cell Factories* **2014,** *13* (1), 123.

55.   Somerville, C.; Youngs, H.; Taylor, C.; Davis, S. C.; Long, S. P., Feedstocks for Lignocellulosic Biofuels. *Science* **2010,** *329* (5993), 790-792.

56.   Leys, D., Flavin metamorphosis: cofactor transformation through prenylation. *Current Opinion in Chemical Biology* **2018,** *47*, 117-125.

57.   Leys, D.; Scrutton, N. S., Sweating the assets of flavin cofactors: new insight of chemical versatility from knowledge of structure and mechanism. *Current Opinion in Structural Biology* **2016,** *41*, 19-26.

58.   Piano, V.; Palfey, B. A.; Mattevi, A., Flavins as Covalent Catalysts: New Mechanisms Emerge. *Trends in Biochemical Sciences* **2017,** *42* (6), 457-469.

59.   Bentinger, M.; Tekle, M.; Dallner, G., Coenzyme Q – Biosynthesis and functions. *Biochemical and Biophysical Research Communications* **2010,** *396* (1), 74-79.

60.   Pindur, U.; Schneider, G. H., Pericyclic key reactions in biological systems and biomimetic syntheses. *Chemical Society Reviews* **1994,** *23* (6), 409-415.

61.   Ruotolo, B. T.; Benesch, J. L. P.; Sandercock, A. M.; Hyung, S.-J.; Robinson, C. V., Ion mobility–mass spectrometry analysis of large protein complexes. *Nature Protocols* **2008,** *3* (7), 1139-1152.

62.   Henry, E. R.; Hofrichter, J., [8] Singular value decomposition: Application to analysis of experimental data. In *Methods in Enzymology*, Academic Press: 1992; Vol. 210, pp 129-192.

63.   Ghisla, S.; Hartmann, U.; Hemmerich, P.; Müller, F., Studien in der Flavin-Reihe, XVIII. Die reduktive Alkylierung des Flavinkerns2); Struktur und Reaktivität von Dihydroflavinen. *Justus Liebigs Annalen der Chemie* **1973,** *1973* (8), 1388-1415.

64.   Ghisla, S.; Massey, V.; Lhoste, J.-M.; Mayhew, S. G., Fluorescence and optical characteristics of reduced flavines and flavoproteins. *Biochemistry* **1974,** *13* (3), 589-597.

65.   Johnson, E. F.; Hinz, W.; Atreya, C. E.; Maley, F.; Anderson, K. S., Mechanistic characterization of Toxoplasma gondii thymidylate synthase (TS-DHFR)-dihydrofolate reductase. Evidence for a TS intermediate and TS half-sites reactivity. *J Biol Chem* **2002,** *277* (45), 43126-36.

66.   Lee, A. L.; Sapienza, P. J., Thermodynamic and NMR Assessment of Ligand Cooperativity and Intersubunit Communication in Symmetric Dimers: Application to Thymidylate Synthase. *Front Mol Biosci* **2018,** *5*, 47.

67.   Bloor, S.; Michurin, I.; Titchiner, G. R.; Leys, D., Prenylated flavins: structures and mechanisms. *Febs Journal* **2022**.

68.   Kaneshiro, A. K.; Koebke, K. J.; Zhao, C.; Ferguson, K. L.; Ballou, D. P.; Palfey, B. A.; Ruotolo, B. T.; Marsh, E. N. G., Kinetic Analysis of Transient Intermediates in the Mechanism of Prenyl-Flavin-Dependent Ferulic Acid Decarboxylase. *Biochemistry* **2021,** *60* (2), 125-134.

69.   Kawanabe, K.; Aono, R.; Kino, K., 2,5-Furandicarboxylic acid production from furfural by sequential biocatalytic reactions. *J. Biosci. Bioeng.* **2021,** *123*, 18-24.

70.   Boll, M.; Geiger, R.; Junghare, M.; Schink, B., Microbial degradation of phthalates: biochemistry and environmental implications. *Environmental Microbiology Reports* **2020,** *12* (1), 3-15.

71.   Payer, S. E.; Faber, K.; Glueck, S. M., Non-Oxidative Enzymatic (De)Carboxylation of (Hetero)Aromatics and Acrylic Acid Derivatives. *Advanced Synthesis & Catalysis* **2019,** *361* (11), 2402-2420.

72.   Abu Laban, N.; Selesi, D.; Rattei, T.; Tischler, P.; Meckenstock, R. U., Identification of enzymes involved in anaerobic benzene degradation by a strictly anaerobic iron-reducing enrichment culture. *Environmental Microbiology* **2010,** *12* (10), 2783-2796.

73.   Meckenstock, R. U.; Boll, M.; Mouttaki, H.; Koelschbach, J. S.; Tarouco, P. C.; Weyrauch, P.; Dong, X. Y.; Himmelberg, A. M., Anaerobic Degradation of Benzene and

Polycyclic Aromatic Hydrocarbons. *Journal of Molecular Microbiology and Biotechnology* **2016,** *26* (1-3), 92-118.

74.   Wielgus-Kutrowska, B.; Grycuk, T.; Bzowska, A., Part-of-the-sites binding and reactivity in the homooligomeric enzymes - facts and artifacts. *Archives of Biochemistry and Biophysics* **2018,** *642*, 31-45.

75.   Cleland, W., [13] Isotope effects: Determination of enzyme transition state structure. *Methods in enzymology* **1995,** *249*, 341-373.

76.   Cook, P., Mechanism from isotope effects. *Isotopes in environmental and health studies* **1998,** *34* (1-2), 3-17.

77.   Cleland, W., The use of isotope effects to determine enzyme mechanisms. *Archives of biochemistry and biophysics* **2005,** *433* (1), 2-12.

78.   McKenna, R.; Nielsen, D. R., Styrene biosynthesis from glucose by engineered E. coli. *Metabolic engineering* **2011,** *13* (5), 544-554.

79.   Messiha, H. L.; Scrutton, N. S.; Leys, D., High-titer Bio-Styrene Production Afforded by Whole-cell Cascade Biotransformation. *ChemCatChem* **2023**.

80.   Aleku, G. A.; Saaret, A.; Bradshaw-Allen, R. T.; Derrington, S. R.; Titchiner, G. R.; Gostimskaya, I.; Gahloth, D.; Parker, D. A.; Hay, S.; Leys, D., Enzymatic C–H activation of aromatic compounds through CO2 fixation. *Nature chemical biology* **2020,** *16* (11), 1255-1260.

81.   Messiha, H. L.; Payne, K. A. P.; Scrutton, N. S.; Leys, D., A Biological Route to Conjugated Alkenes: Microbial Production of Hepta-1,3,5-triene. *ACS Synthetic Biology* **2021,** *10* (2), 228-235.

82.   Saaret, A.; Villiers, B.; Stricher, F.; Anissimova, M.; Cadillon, M.; Spiess, R.; Hay, S.; Leys, D., Directed evolution of prenylated FMN-dependent Fdc supports efficient in vivo isobutene production. *Nature Communications* **2021,** *12* (1), 5300.

83.   Mori, Y.; Noda, S.; Shirai, T.; Kondo, A., Direct 1,3-butadiene biosynthesis in Escherichia coli via a tailored ferulic acid decarboxylase mutant. *Nature Communications* **2021,** *12* (1), 2195.

84.   Luo, F.; Gitiafroz, R.; Devine, C. E.; Gong, Y.; Hug, L. A.; Raskin, L.; Edwards, E. A., Metatranscriptome of an anaerobic benzene-degrading, nitrate-reducing enrichment culture reveals involvement of carboxylation in benzene ring activation. *Applied and environmental microbiology* **2014,** *80* (14), 4095-4107.

85.   Bergmann, F. D.; Selesi, D.; Meckenstock, R. U., Identification of new enzymes potentially involved in anaerobic naphthalene degradation by the sulfate-reducing enrichment culture N47. *Archives of microbiology* **2011,** *193*, 241-250.

86.   Heker, I.; Haberhauer, G.; Meckenstock, R. U., Naphthalene Carboxylation in the Sulfate-Reducing Enrichment Culture N47 Is Proposed to Proceed via 1,3-Dipolar Cycloaddition to the Cofactor Prenylated Flavin Mononucleotide. *Applied and Environmental Microbiology* **2023,** *0* (0), e01927-22.